Strong Coupling Theory for Tunneling and Vibrational Relaxation in Driven Bistable Systems

M. Thorwart

Institut für Physik, Universität Augsburg, Universitätsstr. 1, 86135 Augsburg, Germany; and Delft University of Technology, Lorentzweg 1, 2628 CJ Delft, The Netherlands

M. Grifoni

Delft University of Technology, Lorentzweg 1, 2628 CJ Delft, The Netherlands

and

P. Hänggi

Institut für Physik, Universität Augsburg, Universitätsstr. 1, 86135 Augsburg, Germany

CONTENTS

I. *Introduction.* A. Experiments. B. Prior theoretical approaches.
II. *The driven dissipative bistable system.*
III. *The reduced density matrix in the discrete variable representation DVR.* A. The Feynman–Vernon influence functional. B. Real-time paths in the DVR basis. C. The population of the left well. D. An example: The symmetric double-doublet system.
IV. *The generalized non-interacting cluster approximation.*
V. *The generalized master equation in the discrete variable representation.* A. General derivation. B. The leading order approximation. C. Comparison with numerical *ab-initio* path integral simulations.
VI. *The quantum relaxation rate.* A. Markovian approximation. B. The quantum relaxation rate.
VII. *Results: Quantum relaxation rate and asymptotic populations.* A. Absence of external driving. B. The influence of external (time-dependent) driving forces. C. Dependence on the bath parameters.
VIII. *Conclusions and outlook.*
Appendixes. A. Scaling to dimensionless quantities. B. The bath correlation function. C. Numerical iteration scheme for solving the generalized master equation. D. Example: A single path subject to dissipation. E. Harmonic well approximation. F. Flow to weak damping.

I. INTRODUCTION

The sensitivity of tunneling to the influence of the environment has been in the focus of intense research over the last years [1–5]. A popular model for the investigation of tunneling processes is a double-well potential with an energy barrier that separates two energetically degenerate minima. In an idealized system, the barrier can be coherently traversed by a quantum mechanical particle (*coherent tunneling*). A real physical system, however, experiences the influence of the surrounding "outer world." This coupling disturbs the coherent tunneling process and it constitutes the origin of decoherence and dissipation in the quantum system. To model the dissipative influence, the environment is commonly described as an ensemble of harmonic oscillators (*heat bath*, *reservoir*) being at thermal equilibrium at temperature T. A bilinear coupling between the quantum system and the bath mimics phenomenologically the interaction of the system with the "rest of the world." By this method, the quantum mechanical analogue of the generalized Langevin equation can be derived.

The spectrum of the uncoupled symmetric bistable potential consists of a ladder of doublets being pairs of energetically nearly degenerate energy eigenstates. The degeneracy is lifted by the tunneling splittings within the single doublets. The doublets themselves are separated by large interdoublet energy gaps which are of the order of the related characteristic system frequency scale, the latter are generally orders of magnitude larger than the tunneling splittings.

By now, two different situations have been in the center of detailed investigations on the dissipative tunneling dynamics in a bistable potential: (i) On the one hand, one considers the regime of low temperatures, i.e., $k_{\mathrm{B}}T$ is of the order of the energy splitting of the lowest tunneling doublet. A common approach to simplify the *spatially continuous* dynamics consists then in restricting the problem to the two lowest energy eigenstates, being the solely significantly thermally populated states in this deep quantum regime. Coupling the two-level system to a bosonic bath of harmonic oscillators leads to the prominent *spin-boson problem* [1, 3, 5]. (ii) On the other hand, the starting point is classical rate theory. *Semiclassical* tunneling corrections to the relaxation rate are calculated by use of various instanton techniques [2]. This formalism is applicable when the quantized energy levels lie very dense below the barrier, i.e., in cases when the energy barrier is large compared to the characteristic level splitting of the quantum system. Moreover, a *local equilibrium* is required, restricting this approach only to time-*in*dependent systems. By complex-time path integral techniques, the free energy is calculated in a semiclassical steepest-descent method. This leads to the dissipative bounce solution which in turn determines the semiclassical decay rate.

Modern experimental developments have paved the way to study the influence of time-dependent external driving forces like a laser beam or an rf-field. Such time-dependent driving fields have most interesting implications for quantum systems like, for instance, the effect of *coherent destruction of tunneling* [6, 7], the effect of *quantum stochastic resonance* [8–16], or the occurrence of *quantum steps in hysteresis loops* [13, 17], to name but a few (for recent reviews, see [4, 5, 14, 18]). Such driving fields may also be used to control and reduce decoherence in open quantum systems [19, 20].

The present work deals with tunneling processes in a time-dependent bistable potential in a temperature regime where the two-level approximation (*spin-boson regime*) is invalid. Likewise, the (possibly) strong time-dependent external fields prevent the use of *semiclassical* methods. Our analysis therefore bridges those two well established limiting regimes in quantum rate theory.

With this objective in mind, we release the restriction of the bistable potential to its two lowest energy eigenstates and extend the model to include more energy eigenstates which are populated at higher temperatures. This implies an interesting consequence: Since the energy splittings of the higher doublets are larger, tunneling becomes more favorable via the higher doublets. However, for the temperature being too large, tunneling is again hampered due to the decoherent influence of the environment. This interplay among tunneling, vibrational relaxation (i.e., transitions *between* the doublets), and thermal effects leads to a rich and complex dynamics.

The specific problem we tackle is the following: Let us consider a quantum particle which is initially localized in one of the two wells of a double-well potential. What is then the *rate* with which the probability of finding the particle in this well decays in the presence of an Ohmic-like environment? In addition, what are the asymptotic well populations? An additional manipulation of the potential barrier, i.e., a static bias or a time-dependent harmonic driving, may be applied. In this work, we provide an analytic method to solve this non-trivial problem—also in the presence of a time-dependent driving field—in a very general manner. We restrict ourselves neither to a large semiclassical potential barrier, nor to a weak system-bath interaction, nor to weak driving fields. Our analysis is based on the real-time path integral technique which uses the Feynman–Vernon formulation as a starting basis. By treating the bath induced correlations between quantum paths within a generalized non-interacting cluster approximation, a generalized master equation for the diagonal elements of the reduced density matrix is derived. It turns out that the approximation is appropriate in the regime of moderate temperature and/or moderate system-bath coupling. A further simplification of the integro-differential equation leads to a Markovian approximated master equation whose rate coefficients are obtained in the form of closed analytical expressions. By comparing the results of the full generalized master equation versus the Markovian approximated master equation and versus the numerical quasiadiabatic propagator path integral algorithm [21], we conclude that the analytical approximation permits correct predictions for the decay process out of the initially populated potential well. The rate governing the long-time dynamics of the decay is obtained as the *smallest eigenvalue* of the matrix of the (time averaged) rate coefficients. The dependence of this quantum relaxation rate and of the asymptotic population of the metastable well on the various physical parameters is investigated in detail.

We stress that the developed method is *not* restricted to this specific problem but can be applied to many different other physical situations where a potential with a discrete energy spectrum can be assumed. A short summary of this present work has been published in Ref. [22].

Before we proceed, we motivate that the stated problem is not of formal academic nature but, in contrast, has several applications to real physical systems. For that purpose, we have collected numerous experimental works in the following Section I.A. In the subsequent Section I.B we briefly review the few existing theoretical works and discuss some of their shortcomings and inconsistencies which we attempt to overcome by our techniques. The rest of the paper is organized as follows: In Section II our specific model is introduced. The succeeding Section III is devoted to the derivation of the dissipative real-time path integral which is cast in the discrete variable representation (DVR), i.e., the eigenbasis of that system operator which couples to the reservoir. The example of the double-doublet system illustrates this transformation in Section III.D. In Section IV we introduce an approximation to the so far exact real-time path integral expressions. This approximative treatment of the bath induced path correlations allows for the derivation of a generalized master equation (GME). This is shown in Section V, where also the lowest order expressions for the integral kernels of the GME are given. In Section VI we extract the leading rate for the decay out of one of the two potential wells. This is possible if one applies an additional Markovian approximation to the GME. A detailed study of the dependence of the quantum relaxation rate on the various model parameter is put forward in Section VII. Moreover, an investigation of the asymptotic well population is presented. Finally, our conclusions together with an outlook are presented in Section VIII.

A. *Experiments*

Several experiments where dissipative multilevel systems are involved have been performed in many different physical systems. We report on four timely examples to motivate the importance and the need for a consistent and general theory for the above stated problem.

The first set of experiments deals with quantum tunneling of magnetization in nanomagnets [23]. A macroscopic sample of molecular magnets consists of a large number (typically 10^4–10^{11}) of chemically identical magnetic clusters of the same magnetic size. They are regularly arranged on a

crystal lattice. The single molecules have usually a large spin quantum number, typically $S \simeq 10$. Experiments (see below) indicate a strong uniaxial magnetocrystalline anisotropy. It favors a doubly degenerate spin alignment along the c-axis of the crystal, $m_S = \pm S$, and generates an energy barrier for the reversal of magnetization. This implies two-fold degenerate excited states corresponding to the spin-projections $m_s = \pm(S-1), \pm(S-2), \ldots, 0$ in a double-well potential [24]. At sufficiently low temperatures, the spins can tunnel through the anisotropy barrier. Two such materials are currently studied in detail: The first is referred to as Mn_{12}-acetate. It possesses a tunneling barrier of $\Delta U/k_B \simeq 62$K (k_B denotes the Boltzmann constant). Resonant tunneling of magnetization reveals itself as quantum steps in hysteresis loops which go along with maxima in the relaxation rate for specific values of an external magnetic field [25]. The second candidate is known as Fe_8 and has the advantage that the anisotropy barrier is approximately three times smaller than in Mn_{12} ($\Delta U/k_B \simeq 22$K). This property enhances the observed effect by several orders of magnitude as compared to the case with Mn_{12}. For the Fe_8 samples several experiments on quantum tunneling of magnetization have been reported as well [26, 27]. Especially interesting for us are the measurements by Wernsdorfer *et al.* [27]; those are performed at non-adiabatic driving fields and at temperatures where many doublets contribute to the dynamics.

A second class of experiments addresses tunneling of the magnetic flux in superconducting quantum interference devices (SQUIDs) [28–36]. The dynamics of the total flux threaded through the SQUID (or the phase difference across a current biased Josephson junction) obeys a collective motion of a macroscopic number of quasiparticles. The classical equation of motion for the flux dynamics maps to that of a particle moving dissipatively in a (symmetric) double-well potential. Its lowest left (right) well corresponds to one of the two fluxoid states 0 (1) of the SQUID. For sufficiently low temperature, the transition between these states occurs via tunneling through the potential barrier. Measurements of the relaxation of a fluxoid state initially prepared in an rf-SQUID have addressed two different physical situations: The results in Ref. [29] have been interpreted as *incoherent tunneling* in a *macroscopic two-state system* and those in Ref. [30] have been explained as *resonant tunneling* between two quasi-degenerate localized states in different fluxoid wells. The rate of tunneling out of the metastable well vs the applied external flux exhibits a series of local maxima. These occur at those values of the external flux where the adiabatic energy levels of the biased SQUID potential form avoided level crossings. By applying a resonant time-dependent external rf-field, Han *et al.* [31] created a population inversion between the two adjacent fluxoid wells. Furthermore, Silvestrini *et al.* [32] reported the observation of energy level quantization in underdamped Josephson junctions *above* the crossover temperature which separates the classical from the quantum regime. Han *et al.* [33] recently presented evidence for transitions between the fluxoid wells due to cascaded, two-photon processes. In the latest work of this group, Friedman *et al.* [34] report on the realization of a quantum superposition of macroscopic states in an rf-SQUID. Similar observations were recently made by the group of Mooij [35, 36] where symmetric and antisymmetric quantum superpositions of macroscopic states of a dc-SQUID have been created.

Another set of experiments concerns the tunneling dynamics of substitutional defects in solids [37]. For instance, in a crystalline environment tunneling arises from defect ions which do not fit properly in the sites offered by the host lattice. The symmetry of the host crystal determines a complicated potential energy landscape with several degenerate minima for the defect ion. Golding *et al.* [38] studied the relaxation rates of individual microscopic defects in a mesoscopic disordered Bi-metal. Since the sample dimensions were comparable to the phase-breaking length for quantum transport [4] at low temperatures, the sample's conductance was highly sensitive to the positions of the scattering centers. Their observations were found to be consistent with predictions of the dissipative two-level system [1–3] at low temperatures. However, measurements at higher temperatures [39] have indicated the failure of the two-level theory [40]. Furthermore, the study of thermally assisted tunneling of atomic hydrogen and deuterium in boron-doped crystalline silicon reveals [41] that the relaxation rate calculated by a path integral centroid formalism differs from experimental measurements by

two orders of magnitude. Finally, Enss and Hunklinger [42] have pointed out several discrepancies between predictions of a semiclassical tunneling model, where the two wells are approximated by harmonic oscillators (*harmonic-well approximation*, see also Appendix E), and experimental measurements at low temperatures. They proposed an improved approach by taking into account elastic interactions among the tunneling systems to resolve these discrepancies.

The last class of experiments concerns systems in chemical physics with the goal of controlling of chemical reactions [43–45]. The hydrogen pair transfer in the hydrogen-bonded cyclic dimers of numerous carboxylic acids is used as a prototype system to study the relation between quantum tunneling and chemical kinetics. The measurements show that the free hydrogen-bonded dimers possess two energetically degenerate equilibrium configurations. They correspond to the two minima of a double-well potential. Both quantum tunneling and vibrational excitation are important for the transfer of the hydrogen pair. This has been studied experimentally in detail in Refs. [43]. A specific control scheme ("Hydrogen-Subway") has been proposed [44, 45] to steer intramolecular hydrogen transfer reactions in malonaldehyde by ultrashort laser pulses. The conventionally proposed method for the transfer consists in applying a laser pulse that lifts an initially localized wavepacket in the reactant region *over* the barrier thus allowing propagation towards the final product configuration. The new approach in Ref. [45] is to drive the wave packet not over but *through* the barrier. This is achieved by exciting higher lying doublets where tunneling occurs on a much shorter time-scale than in the lower doublets. The advantage of this new proposal is that it requires laser intensities which are considerably smaller than those used in the conventional approach.

B. *Prior Theoretical Approaches*

Previous theoretical works dealing with dissipative spatially continuous quantum systems, being driven or undriven, naturally fall into two classes: Approaches that are more of a numerical or analytical flavor, respectively.

In Ref. [7], the harmonically driven double-well potential has been investigated numerically in the presence of dissipation. For that purpose, a master equation for the reduced density matrix has been derived on the basis of the standard Born–Markov assumption [46]. Subsequently, an analytical Floquet approach is used to derive the master equation. In doing so, an improved master equation has been obtained in Ref. [47]. Here, the Floquet theory is applied on the level of the Schrödinger equation and the Born–Markov approximation is made for the quasienergy spectrum. In both cases, the system-bath coupling is treated perturbatively. This restricts the method to the *weak-coupling regime*. The same regime of a weak system-bath coupling was treated by Naundorf *et al.* [45]. Also, standard Redfield (i.e., weak-coupling) techniques have been applied to derive a master equation. The specific shape of a laser pulse is determined in order to control hydrogen tunneling in a dissipative environment [45]. In the strong coupling regime, the harmonically driven double-well potential has been studied in the context of quantum hysteresis and quantum stochastic resonance [11]. In this work, the system has been iterated numerically using the tensor multiplication scheme within the quasiadiabatic propagator path integral technique developed by Makri and Makarov [21].

More analytical oriented works in the context of dissipative multilevel bistable systems have been performed by several groups [48–56].

The starting point in Refs. [48, 49] is a multilevel system with interdoublet transition terms (vibrational relaxation) which are *not* strictly derived from a *continuous* double-well potential; these are constructed phenomenologically. This leads to the assumption that the vibrational coupling occurs only between vibrational states located inside the same well.

The group of Silbey [48] considered a *static* multilevel system. Additionally, only tunneling states differing by one quantum of vibrational excitation are assumed to be connected. Finally, it is assumed that the vibrational coupling within each well is the same for both wells. This *a priori* excludes the case with a static asymmetry of the potential.

The group of Morillo and Cukier [49] started out from a similar Hamiltonian like in Ref. [48]. They restricted the model further and included only the *two doublets* with the lowest energy, i.e., the so-called *double-doublet system*. The authors for the first time included a time-dependent driving which couples to a phenomenologically constructed dipole operator of the multilevel system. The system-bath interaction is treated perturbatively within a generalized Redfield approach.

In a sequence of articles [50], Dekker analyzed the real-time dynamics of a quantum particle in the dissipative static double-well potential *ab initio* by means of a multisite spin-hopping model. He derives the reduced quantum Liouville equation for the particle, thereby not restricting the dynamics to the lowest doublet only. The interdoublet vibrational dynamics is approximated by coarse-graining the density matrix elements on a time scale of many vibrational periods. It is further assumed that the localized states in the wells are approximated by the eigenfunctions of a harmonic oscillator (*harmonic-well approximation*). This latter assumption can be justified as long as the barrier height is large compared to the interdoublet energy gap. In this parameter regime, however, the application of the standard semiclassical rate theory [2] is appropriate, and even simpler to apply. In the deep quantum regime with low to intermediate barrier heights, this assumption increasingly becomes invalid and leads to considerable deviations of the approximated wave functions from the exact ones (cf. also Appendix E). Also, the eigenenergies of the harmonic potential are considerably different from the exact ones for a shallow energy barrier.

A related problem has been investigated in a series of theoretical works by Ovchinnikov and co-workers [51–56] by applying *semiclassical* techniques. In Ref. [51] Larkin and Ovchinnikov developed a method to calculate the decay rate of metastable voltage states of Josephson junctions. They constructed a kinetic equation for the probabilities of population of many energy levels. The transition probabilities are determined for a cubic potential in semiclassical approximation for *weak* system-bath coupling. This procedure assumes a decay into the continuum via quantum tunneling or thermal hopping. However, within confining potentials such as a double-well this assumption may be not justified. The effect of time-dependent driving is included within an approximation. The low temperature case where tunneling prevails is considered in Ref. [52] for vortices moving in a washboard potential being weakly coupled to the environment. Also quasiclassical conditions have been assumed. The problem of divergent expressions for the decay rate at avoided level crossings is cured in Ref. [53] where a *two-level approximation* at the avoided level crossings is invoked. The authors treat the problem within the harmonic well (i.e., quasiclassical) approximation for a constant spectral density of the bath modes, and for a weak system-bath coupling. The semiclassical expressions of Ref. [51] are applied to Josephson junctions (i) in Ref. [54] to calculate numerically the decay rate of the zero-voltage state for non-stationary conditions, and (ii) in Ref. [55] to study the influence of temperature for resonant macroscopic quantum tunneling. Finally, the theory is adapted to SQUIDs in Ref. [56] to explain the experimental findings of Ref. [30]. However, the theoretical results follow qualitatively those obtained from the standard WKB-approximation. The calculated decay rate differs from the experimental results by two-to-four orders of magnitude for small static potential asymmetries, i.e., with still large barriers, where the semiclassical treatment should yield rather good agreement. In contrast, for large bias asymmetries, one of the two barrier heights becomes rather small so that the semiclassical approximation is expected to yield worse results. The agreement with the experimental data turned out to be of the same order of magnitude. This inconsistency may be mainly traced back to the fact that the semiclassical treatment is not appropriate for a system in the deep quantum regime when only two to six levels lie below the energy barrier.

In summary, *no* analytic treatment exists in the prior literature where tunneling and vibrational relaxation is investigated consistently in the regime where a finite number of discrete energy eigenstates rules the dissipative dynamics. This is so even for the situation that no time-dependent driving acts upon the system. While standard Redfield theory for a weak system-bath coupling is used frequently, the theory for the strong coupling regime for static as well as for driven multilevel systems is still

in its infancy. The main objective of this work is to fill this gap in deriving analytical schemes that cover the physics in this prominent regime of a moderate-to-strong system-bath coupling.

II. THE DRIVEN DISSIPATIVE BISTABLE SYSTEM

We consider a quantum particle with mass $\mathcal{M}$, position operator $\mathbf{q}$, and momentum operator $\mathbf{p}$ moving in a one-dimensional double-well potential $V_0(\mathbf{q})$ which may include a static asymmetry. The potential experiences a time-dependent external force, $s\sin(\Omega t)$, with field strength s and frequency Ω. It is described by the Hamiltonian

$$\mathbf{H}_{\rm S}(t) = \mathbf{H}_0 - \mathbf{q}\, s\sin\Omega t = \frac{\mathbf{p}^2}{2\mathcal{M}} + V_0(\mathbf{q}) - \mathbf{q}\, s\sin\Omega t, \tag{1}$$

with

$$V_0(\mathbf{q}) = \frac{\mathcal{M}^2\omega_0^4}{64\Delta U}\mathbf{q}^4 - \frac{\mathcal{M}\omega_0^2}{4}\mathbf{q}^2 - \mathbf{q}\varepsilon \tag{2}$$

being the asymmetric double-well potential. The quantity ε denotes the static bias force. In absence of the asymmetry ($\varepsilon = 0$), ΔU denotes the barrier height, and ω_0 is the angular frequency of classical oscillations around the well minima.

The energy spectrum of $\mathbf{H}_0$ follows from the time-independent Schrödinger equation with a static double-well potential $V_0(\mathbf{q})$, i.e., $\mathbf{H}_0|n\rangle = \mathcal{E}_n|n\rangle,\ n = 1, 2, \ldots$.

In absence of a static bias ($\varepsilon = 0$) and for energies well below the barrier, the spectrum consists of a ladder of pairs of energy eigenstates (*doublets*). The energy gaps within each doublet generally are several orders of magnitude smaller than the inter-doublet energy gaps and are responsible for the *tunneling dynamics* between the two wells. The large energy gaps are of the order of the harmonic oscillator energy gap $\hbar\omega_0$ associated with each well. For energies above the barrier, the energy gaps are also of the order of $\hbar\omega_0$. Transitions between those largely separated energy eigenstates are termed *vibrational relaxation*. In the presence of a static tilt ($\varepsilon \neq 0$), no general statement can be made. Spectra with typical avoided level crossings can occur as well as such with almost equally separated energy levels; cf. Fig. 6a in Section VII.B.1.

Following the common approach [1–4, 57] to model the influence of the environment by an ensemble of harmonic oscillators, the bath Hamiltonian $\mathbf{H}_{\rm B}$ (including the interaction with the system) is given by

$$\mathbf{H}_{\rm B} = \sum_{j=1}^{\mathcal{N}} \frac{1}{2}\left[\frac{\mathbf{p}_j^2}{m_j} + m_j\omega_j^2\left(\mathbf{x}_j - \frac{c_j}{m_j\omega_j^2}\mathbf{q}\right)^2\right]. \tag{3}$$

The whole system is thus described by the Hamiltonian $\mathbf{H}(t) = \mathbf{H}_{\rm S}(t) + \mathbf{H}_{\rm B}$. In the case of a thermal equilibrium bath, its influence on the system is fully characterized by the spectral density

$$J(\omega) = \frac{\pi}{2}\sum_{j=1}^{\mathcal{N}} \frac{c_j^2}{m_j\omega_j}\delta(\omega - \omega_j). \tag{4}$$

With the number $\mathcal{N}$ of harmonic oscillators approaching infinity, we arrive at a continuous spectral density. Throughout this work, we choose an Ohmic spectral density with an exponential cut-off, i.e.,

$$J(\omega) = \eta\omega\exp(-\omega/\omega_c). \tag{5}$$

Here, $\eta = \mathcal{M}\gamma$, with γ being the strength of the coupling to the heat bath. Moreover, $\omega_c \gg (\omega_0, \Omega, \gamma)$ denotes a cut-off frequency being the largest frequency in the model.

We choose a factorizing initial condition of Feynman–Vernon form [57]. This means that at time $t = t_0$, the full density operator $\mathbf{W}(t_0)$ is given as a product of the initially prepared system density operator $\boldsymbol{\rho}_{\mathrm{S}}(t_0)$ and the canonical bath density operator at temperature $T = 1/k_{\mathrm{B}}\beta$, i.e.,

$$\mathbf{W}(t_0) = \boldsymbol{\rho}_{\mathrm{S}}(t_0) Z_{\mathrm{B}}^{-1} \exp\bigl(-\beta \mathbf{H}_{\mathrm{B}}^0\bigr), \tag{6}$$

where $Z_{\mathrm{B}} = \mathrm{tr}\exp(-\beta \mathbf{H}_{\mathrm{B}}^0)$ and $\mathbf{H}_{\mathrm{B}}^0 = \sum_{j=1}^{\mathcal{N}} (1/2)[\mathbf{p}_j^2/m_j + m_j \omega_j^2 \mathbf{x}_j^2]$.

In order to describe the dynamics of the system of interest we focus on the time evolution of the reduced density matrix. In position representation it reads

$$\begin{aligned} \rho(q_f, q_f'; t) &= \mathrm{tr}_{\mathrm{res}} \langle q_f \Pi_j x_j | \mathbf{U}(t, t_0) \mathbf{W}(t_0) \mathbf{U}^{-1}(t, t_0) | q_f' \Pi_j x_j' \rangle, \\ \mathbf{U}(t, t_0) &= \mathcal{T} \exp\left\{ -i/\hbar \int_{t_0}^{t} \mathbf{H}(t')\, dt' \right\}. \end{aligned} \tag{7}$$

Here, $\mathcal{T}$ denotes the time ordering operator, $\mathbf{W}(t_0)$ is the full density operator at the initial time t_0, and $\mathrm{tr}_{\mathrm{res}}$ indicates the partial trace over the harmonic bath oscillators x_j.

III. THE REDUCED DENSITY MATRIX IN THE DISCRETE VARIABLE REPRESENTATION DVR

A. *The Feynman–Vernon Influence Functional*

Due to our assumption of a factorizing initial condition in Eq. (6), the partial trace over the bath can be performed and the reduced density operator be recast according to Feynman and Vernon [57] as

$$\rho(q_f, q_f', t) = \int dq_0 \int dq_0'\; G(q_f, q_f', t; q_0, q_0', t_0) \rho_{\mathrm{S}}(q_0, q_0', t_0), \tag{8}$$

with the propagator G given by

$$G(q_f, q_f', t; q_0, q_0', t_0) = \int_{q(t_0)=q_0}^{q(t)=q_f} \mathcal{D}q \int_{q'(t_0)=q_0'}^{q'(t)=q_{\mathrm{f}}'} \mathcal{D}q'\, \mathcal{A}[q] \mathcal{A}^*[q'] \mathcal{F}_{\mathrm{FV}}[q, q']. \tag{9}$$

Here, $\mathcal{A}[q] = \exp\{i S_{\mathrm{S}}[q]/\hbar\}$ denotes the bare system amplitude, with $S_{\mathrm{S}}[q]$ being the classical action functional of the system variable q along a path $q(t)$. $\mathcal{F}_{\mathrm{FV}}[q, q'] = \exp(-\phi_{\mathrm{FV}}[q, q']/\hbar)$ denotes the Feynman–Vernon influence functional. For our purpose, it is convenient to write the influence phase $\phi_{\mathrm{FV}}[q, q']$ in terms of relative coordinates $\xi(t') = q(t') - q'(t')$ and center of mass coordinates $\chi(t') = q(t') + q'(t')$, respectively; it reads

$$\begin{aligned} \phi_{\mathrm{FV}}[\chi, \xi] = &\int_{t_0}^{t} dt' \int_{t_0}^{t'} dt'' \{\dot{\xi}(t') S(t' - t'') \dot{\xi}(t'') + i \dot{\xi}(t') R(t' - t'') \dot{\chi}(t'')\} \\ &+ \xi(t) \int_{t_0}^{t} dt' \{\dot{\xi}(t') S(t - t') + i \dot{\chi}(t') R(t - t')\} + \xi(t_0) \Bigg\{ \xi(t) S(t - t_0) \\ &- \int_{t_0}^{t} dt' \dot{\xi}(t') S(t' - t_0) \Bigg\} + i \chi(t_0) \Bigg\{ \xi(t) R(t - t_0) - \int_{t_0}^{t} dt' \dot{\xi}(t') R(t' - t_0) \Bigg\}. \end{aligned} \tag{10}$$

Herein, $S(t)$ and $R(t)$ denote the real and imaginary part, respectively, of the bath correlation function $Q(t)$, i.e., [3]

$$Q(t) = S(t) + i\,R(t) = \frac{1}{\pi}\int_0^\infty d\omega \frac{J(\omega)}{\omega^2}\left\{ \coth\frac{\hbar\omega\beta}{2}(1-\cos\omega t) + i\sin\omega t \right\}. \tag{11}$$

We evaluate in the following the reduced density matrix explicitly. It turns out that this is conveniently performed in the *discrete* eigenbasis of the position operator $\mathbf{q}$. This representation is the so-termed *discrete variable representation (DVR)* [58]. The reason for this basis transformation is that only then can the influence phase, Eq. (10), be evaluated at the eigenvalues q_μ of $\mathbf{q}$. This is shown in the subsequent section.

B. *Real-Time Paths in the DVR Basis*

The time-independent double-well potential $V_0(\mathbf{q})$, Eq. (2), possesses a discrete energy spectrum. The interesting temperature regime for us is that in which only a finite and small number of energy eigenstates is thermally significantly populated. A quantum mechanical description would not be necessary if the temperature is very large compared to the natural energy scale of the system. We assume furthermore that the time-dependent driving does not excite arbitrary high lying energy eigenstates of the static problem. Then, it is appropriate to consider only the M-dimensional Hilbert space spanned by the M lowest lying energy eigenstates of the static potential. The problem of a spatially continuous double-well potential is then reduced to a problem of a finite dimensional M-level system (MLS). The case of $M = 2$ (with ε and s being sufficiently small) is the well-known (driven) spin-boson problem [1, 3, 5], while $M = 4$ constitutes, for instance, the double-doublet system [49]. This reduction has been shown to be sensible for the case of the parametrically driven dissipative quantum harmonic oscillator [59]. There, the spatially continuous potential is appropriately described by a discrete M-level system with $M = 3$ to $M = 6$.

Next we perform a basis transformation to the so-called *discrete variable representation* (DVR) [58]. The new basis is chosen as the eigenbasis of that operator which couples the bare system to the harmonic bath. In our case this is the position operator $\mathbf{q}$. We define the DVR basis $\{|q_\mu\rangle\}$ according to

$$\langle q_\mu|\mathbf{q}|q_\nu\rangle = q_\mu\delta_{\mu\nu}, \qquad \mu,\nu = 1,\ldots,M. \tag{12}$$

This basis follows from the energy eigenbasis $\{|m\rangle\}$ by inserting the identity $\mathbb{I} = \sum_{m=1}^M |m\rangle\langle m|$ yielding $|q_\mu\rangle = \sum_{m=1}^M \langle m|q_\mu\rangle|m\rangle$. This step allows us to transform the description of the dynamics as transitions between energy eigenstates to a hopping among the M discrete position eigenvalues q_μ of the spatial grid. While for the static symmetric case, $\varepsilon = 0$, the position eigenvalues q_μ are located symmetrically on the q-axis with respect to $q = 0$, this is no longer the case in the presence of a static bias $\varepsilon \neq 0$.

To describe the dynamics in the DVR basis, we define a quantum mechanical path $q(t')$ along which the system evolves in time. It starts out at time $t' = t_0$ in the state $q(t' = t_0) = q_{\mu_0}$ and evolves via $\tilde{N}$ jumps between the M discrete states into the final state $q(t' = t_{\tilde{N}}) = q_{\mu_{\tilde{N}}}$. The full time interval is split into $\tilde{N}$ short time intervals such that the jumps happen at times $t' = t_j$. The intermediate states are labeled by q_{μ_j}, where $\mu_j = 1,\ldots,M$ is the quantum state index, and $j = 1,\ldots,\tilde{N}-1$ denotes the time index. The full path is assumed to be a sequence of constant path segments according to

$$q(t') = -q_{\mu_0}\Theta(t'-t_1) + \sum_{j=1}^{\tilde{N}-1} q_{\mu_j}[\Theta(t'-t_j) - \Theta(t'-t_{j+1})] + q_{\mu_{\tilde{N}}}\Theta(t'-t_{\tilde{N}}), \tag{13}$$

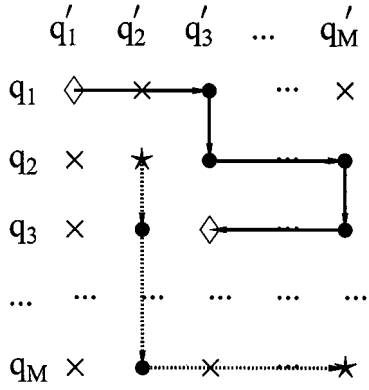

FIG. 1. The M^2 states of the reduced density matrix of an M-level system. Shown are two examples of paths that travel between two diagonal states of the density matrix (see text). One path (solid line) connects the diagonal states $\diamond$ and the other (dashed line) travels between the diagonal states $\star$. The intermittently visited off-diagonal states are marked by $\bullet$.

where $\Theta(t)$ is the Heaviside function. Thus, upon switching to the center-of-mass and relative coordinates $\chi(t') = q(t') + q'(t')$ and $\xi(t') = q(t') - q'(t')$, respectively (cf. Eq. (14) and Eq. (15) below), the double path integral over the M-state paths $q(t')$ and $q'(t')$ in Eq. (9) is visualized as an integral over a *single* path that jumps between the M^2 states of the reduced density matrix in the (q, q')-plane. The total number N of jumps is given by the sum of the number of jumps for the paths q and q', i.e., $N = \tilde{N} + \tilde{N}'$.

Figure 1 illustrates this idea for a general M-state system described by its $M \times M$ density matrix. Two paths are depicted: one (full line) starts in the diagonal state $(q_1, q_1' = q_1)$ and jumps in $\tilde{N}' = 3$ horizontal jumps and in $\tilde{N} = 2$ vertical jumps to the final diagonal state $(q_3, q_3' = q_3)$. It visits four intermediate off-diagonal states (filled circles). The second path (dashed line) starts in the diagonal state $(q_2, q_2' = q_2)$ and travels via two intermediate states to the final diagonal state $(q_M, q_M' = q_M)$.

The paths in the relative and center of mass coordinates read

$$\begin{aligned}\xi(t') &= q(t') - q'(t') \\ &= -\xi_{\mu_0\nu_0}\Theta(t' - t_1) + \sum_{j=1}^{N-1} \xi_{\mu_j\nu_j}[\Theta(t' - t_j) - \Theta(t' - t_{j+1})] + \xi_{\mu_N\nu_N}\Theta(t' - t_N),\end{aligned} \tag{14}$$

and

$$\begin{aligned}\chi(t') &= q(t') + q'(t') \\ &= -\chi_{\mu_0\nu_0}\Theta(t' - t_1) + \sum_{j=1}^{N-1} \chi_{\mu_j\nu_j}[\Theta(t' - t_j) - \Theta(t' - t_{j+1})] + \chi_{\mu_N\nu_N}\Theta(t' - t_N).\end{aligned} \tag{15}$$

Herein, the path weights are given as

$$\xi_{\mu_j\nu_j} \equiv q_{\mu_j} - q'_{\nu_j} \tag{16}$$

and

$$\chi_{\mu_j\nu_j} \equiv q_{\mu_j} - q'_{\nu_j}. \tag{17}$$

In this discrete notation, the index μ refers to the path q and the index ν to the primed path q'. The time intervals in which the system is in a diagonal state of the reduced density matrix are called

sojourns. They are characterized by $\xi(t') = 0$ and $\chi(t') \neq 0$. The time spans in which the system is in an off-diagonal state are called *clusters*. The clusters are characterized by $\xi(t') \neq 0$ and $\chi(t') \neq 0$. This is different from the spin-boson problem [1, 3, 5] where the off-diagonal states (*blips*) are characterized by $\xi(t') \neq 0$ and $\chi(t') = 0$. Upon determining the derivatives of the paths with respect to the time variable t', we find

$$\dot{\xi}(t') = \sum_{j=1}^{N} \xi_j \delta(t' - t_j) \tag{18}$$

and

$$\dot{\chi}(t') = \sum_{j=1}^{N} \chi_j \delta(t' - t_j). \tag{19}$$

Thereby, we have introduced new paths weights according to

$$\xi_j \equiv \xi_{\mu_j \nu_j} - \xi_{\mu_{j-1} \nu_{j-1}} \tag{20}$$

and

$$\chi_j \equiv \chi_{\mu_j \nu_j} - \chi_{\mu_{j-1} \nu_{j-1}}, \tag{21}$$

with $j = 1, \ldots, N$. For $j = 0$, we define $\xi_0 \equiv \xi_{\mu_0 \nu_0}$ and $\chi_0 \equiv \chi_{\mu_0 \nu_0}$. Hence, a path with N transitions at times $t_1, t_2, \ldots, t_N$ can be parametrized by two sets of path weights $\{\chi_0, \chi_1, \chi_2, \ldots, \chi_N\}$ and $\{\xi_0, \xi_1, \xi_2, \ldots, \xi_N\}$. In the influence functional the paths are coupled. The situation mimics the case of interacting electrical charges. Thus, the paths weights in Eqs. (20), (21) are termed *charges*. In the discrete notation, the real-time path integral expression (8) assumes the form

$$\rho_{\mu_N \nu_N}(t) = \langle q_{\nu_N} | \boldsymbol{\rho}(t) | q_{\nu_N} \rangle = \sum_{\mu_0 \nu_0} \int_{\xi(t_0)=\xi_0}^{\xi(t)=\xi_N} \mathcal{D}\xi \int_{\chi(t_0)=\chi_0}^{\chi(t)=\chi_N} \mathcal{D}\chi \, \mathcal{B}[\chi, \xi] \mathcal{F}_{\mathrm{FV}}[\chi, \xi] \rho_{\mu_0 \nu_0}. \tag{22}$$

Here, $\mathcal{B}[\chi, \xi] = \mathcal{A}[q]\mathcal{A}^*[q']$, and the influence phase takes on the form

$$\phi_{\mathrm{FV}}[\chi, \xi] = -\sum_{l=1}^{N} \sum_{j=0}^{l-1} \xi_l S(t_l - t_j) \xi_j - i \sum_{l=1}^{N} \sum_{j=0}^{l-1} \xi_l R(t_l - t_j) \chi_j. \tag{23}$$

C. *The Population of the Left Well*

Since we are interested in the decay of the population of one (metastable) well of the bistable potential, say the left well, we define the quantity of interest to be the sum of the populations of those L DVR-states $|q_\mu\rangle$, $\mu = 1, \ldots, L$, which belong to the *negative position eigenvalues* q_μ, i.e., those which are located to the left from the zero. This yields

$$P_{\mathrm{left}}(t) = \sum_{\mu=1}^{L} \rho_{\mu\mu}(t). \tag{24}$$

In absence of a static bias, i.e., $\varepsilon = 0$ in Eq. (1), the energy eigenfunctions occur in pairs of symmetric and antisymmetric wave functions. This implies a choice for an even number M of states. Then, half of the position eigenvalues is on the left side and the other half is on the right side of the

position point of reflection symmetry, being at $q = 0$ for $V_0(\mathbf{q})$ in Eq. (2). The consequence is that for the population $P_{\text{left}}(t)$ of the left well, usually $L = M/2$ DVR-states are relevant. However, in the case of a finite static asymmetry, no such general statement can be made.

To determine $P_{\text{left}}(t)$ in Eq. (24) we focus on the case that the final state (μ_N, ν_N) of the system will be a diagonal state, i.e.,

$$\nu_N = \mu_N. \tag{25}$$

Since then $q(t) = q'(t)$, it follows that $\xi(t) \equiv 0$ in Eq. (14).

The initially localized wave packet is assumed to be *a superposition of energy eigenstates*. The transformation to the DVR-basis generates an initial system density matrix $\rho_{\mu_0\nu_0}$ which generally is non-diagonal, i.e.,

$$\nu_0 \neq \mu_0. \tag{26}$$

Accordingly, we keep the general initial conditions $\rho_{\mu_0\nu_0} \neq 0$ in Eq. (22).

We proceed to the explicit evaluation of the path integral in Eq. (22) with the boundary conditions given in Eqs. (25) and (26).

To determine the transition amplitudes of the bare system we consider a discrete path starting in a general initial state that ends in a diagonal state. It is described by a sequence of pairs of state labels

$$(\mu_0, \nu_0) \to (\mu_1, \nu_1) \to (\mu_2, \nu_2) \to \cdots \to (\mu_N, \nu_N) = (\mu_N, \mu_N). \tag{27}$$

The first symbol of each pair belongs to the horizontal direction and labels the rows of the reduced density matrix. The second symbol corresponds to the vertical direction and labels the columns. This implies that for a horizontal jump the first index remains constant, i.e., $(\mu_j, \nu_j) \to (\mu_{j+1}, \nu_{j+1}) = (\mu_j, \nu_{j+1})$, while for a vertical jump the second index is unchanged meaning $(\mu_j, \nu_j) \to (\mu_{j+1}, \nu_{j+1}) = (\mu_{j+1}, \nu_j)$.

We are interested in the probability amplitude of finding the system in state (μ_{j+1}, ν_{j+1}) after a time $\Delta t = t_{j+1} - t_j$ having started from (μ_j, ν_j). This quantity is given by the time evolution operator of the bare system. We find for a vertical jump, i.e., $\nu_{j+1} = \nu_j$, the amplitude $\langle q_{\mu_{j+1}}| \exp\{-i\mathbf{H}_0\Delta t/\hbar\}|q_{\mu_j}\rangle$ and for a horizontal jump, i.e., $\mu_{j+1} = \mu_j$, $\langle q_{\nu_{j+1}}| \exp\{+i\mathbf{H}_0\Delta t/\hbar\}|q_{\nu_j}\rangle$, respectively. The relevant part of the system Hamiltonian $\mathbf{H}_{\text{S}}(t)$ in Eq. (1) is the time-independent part $\mathbf{H}_0$ since we are interested in the cases $q_{\mu_{j+1}} \neq q_{\mu_j}$ and $q_{\nu_{j+1}} \neq q_{\nu_j}$. Taking into account the exponential operator up to linear order in the argument, i.e., $\exp\{\pm i\mathbf{H}_0\Delta t/\hbar\} \approx \mathbb{I} \pm i\mathbf{H}_0\Delta t/\hbar$, and using the orthogonality relation $\langle q_l \mid q_m\rangle = \delta_{lm}$, the result for the transition probability amplitude per unit time Δt is obtained as $\pm i\,\Delta_j/2$. Here, the factor of $1/2$ is extracted to have the same convention as in the spin-boson-problem. The factors Δ_j for a horizontal jump are defined according to

$$\Delta_j = \Delta_{\nu_{j+1}\nu_j} \equiv \frac{2}{\hbar}\langle q_{\nu_{j+1}}|\mathbf{H}_0|q_{\nu_j}\rangle, \tag{28}$$

and for a vertical jump

$$\Delta_j = \Delta_{\mu_{j+1}\mu_j} \equiv \frac{2}{\hbar}\langle q_{\mu_{j+1}}|\mathbf{H}_0|q_{\mu_j}\rangle, \tag{29}$$

respectively. The $+$ $(-)$ sign belongs to a horizontal (vertical) transition in the reduced density matrix. The different signs for horizontal and vertical direction reflect the fact that the bare transition amplitude $\mathcal{A}[q]$ belongs to the vertical direction, while the complex conjugate transition amplitude $\mathcal{A}^*[q']$ belongs to the horizontal direction of the reduced density matrix.

The amplitude to stay in the jth off-diagonal state lasting from t_j to t_{j+1} depends on the time-dependent diagonal elements of the bare system Hamiltonian in the DVR-basis. It is given by the so-called *bias factor* $\exp(i\int_{t_j}^{t_{j+1}} dt'[E_{\mu_j}(t') - E_{\nu_j}(t')])$, where

$$E_{\mu_j}(t') = \frac{1}{\hbar}\langle q_{\mu_j}|\mathbf{H}_{\rm S}(t')|q_{\mu_j}\rangle = \frac{1}{\hbar}\big(F_{\mu_j} - q_{\mu_j} s\sin\Omega t'\big) \tag{30}$$

with $F_{\mu_j} \equiv \langle q_{\mu_j}|\mathbf{H}_0|q_{\mu_j}\rangle$. For the entire evolution from t_0 to t_N, N of these factors are multiplied, yielding the overall contribution $\exp\{i\sum_{j=0}^{N-1}\int_{t_j}^{t_{j+1}} dt'[E_{\mu_j}(t') - E_{\nu_j}(t')]\}$. This defines the transition probability amplitudes of the bare system in a unique way.

The functional integration over all *continuous* paths in Eq. (22) turns into a *discrete* sum over all possible path configurations $\{\mu_j \nu_j\}$ in the DVR basis and an integration over all intermediate times $\{t_j\}$. In formal terms this implies

$$\int \mathcal{D}\xi \int \mathcal{D}\chi \curvearrowright \int \mathcal{D}\{t_j\} \sum_{\{\mu_j \nu_j\}}, \tag{31}$$

where we have introduced a compact notation according to

$$\int_{t_0}^{t} \mathcal{D}\{t_j\} \equiv \int_{t_0}^{t} dt_N \int_{t_0}^{t_N} dt_{N-1} \cdots \int_{t_0}^{t_3} dt_2 \int_{t_0}^{t_2} dt_1 \tag{32}$$

for the time ordered integration over the N transition times t_j in Eq. (22).

Collecting all parts we obtain the dissipative real-time path integral for the diagonal elements of the reduced density matrix of an M-level system in the DVR-basis, i.e.,

$$\begin{aligned}\rho_{\mu_N\mu_N}(t) &= \langle q_{\mu_N}|\boldsymbol{\rho}(t)|q_{\mu_N}\rangle \\ &= \sum_{\mu_0,\nu_0=1}^{M} \rho_{\mu_0\nu_0} \sum_{N=1}^{\infty} \int_{t_0}^{t} \mathcal{D}\{t_j\} \sum_{\{\mu_j\nu_j\}} \exp\left\{ i\sum_{j=0}^{N-1}\int_{t_j}^{t_{j+1}} dt'\big[E_{\mu_j}(t') - E_{\nu_j}(t')\big]\right\} \\ &\quad \times \prod_{j=0}^{N-1}(-1)^{\delta_j}\left(\frac{i}{2}\right)^N \Delta_j \exp\left\{ \sum_{l=1}^{N}\sum_{j=0}^{l-1}\xi_l S(t_l - t_j)\xi_j + i\sum_{l=1}^{N}\sum_{j=0}^{l-1}\xi_l R(t_l - t_j)\chi_j\right\}. \end{aligned} \tag{33}$$

In this expression, the sum over all possible path configurations $\{\mu_j \nu_j\}$ in the spirit of Eq. (27) has to be performed with $\delta_j = 0(1)$ for a horizontal (vertical) jump.

Several comments on this quite comprehensive path integral expression are apposite: First, the path integral in Eq. (33) is given in its most general form and is formally *exact* because no approximations, neither on the form of the system Hamiltonian nor on the type of the system-bath interaction, are made. This method could be applied to *any* problem where a potential with a discrete spectrum is given, and where the coupling to the heat bath is mediated via the position operator. The main ingredients are the matrix elements of the system Hamiltonian, being represented in the DVR-basis, and the position eigenvalues via the paths weights. No specific requirements on the shape of the external driving have been made; even a stochastic driving force (such as multiplicative noise) can be included.

In the case of only two levels, i.e., $M = 2$, Eq. (33) reduces to the well-known expression for the (driven) spin-boson problem [1, 3, 5]. There, the problem simplifies due to the fact that the path weights during the time evolution take on only two values, corresponding to the two states localized

in the left and in the right well of the potential. This means that the path flips between a sojourn and a blip at each jump. This implies that the spin-boson path integral assumes the form of a power series in the tunneling splitting $\Delta_1^{\mathcal{E}} \equiv \mathcal{E}_2 - \mathcal{E}_1$ of the two lowest levels. This is not necessarily the case for a general M-level system where a path can travel around, visiting many off-diagonal states, before ending in a diagonal state. Certainly, such a path becomes less likely the longer it remains off-diagonal. This is due to damping.

The path integral is not tractable in its most general form without assuming further approximations. Such an approximation is developed in the following Section IV. However, to gain insight into the physics behind the formal expression (33), we introduce in Section III.D the example of the so-termed *double-doublet system* and discuss the transformation to the DVR-basis. It refers to the case where two doublets in a symmetric double-well potential, Eq. (2), are localized below the barrier, i.e., the case $M = 4$.

D. *An Example: The Symmetric Double-Doublet System*

We illustrate the general method with the example of two doublets below the barrier in the double-well potential, Eq. (2). Choosing $M = 4$ generates the first non-trivial extension to the familiar spin-boson problem.

For the sake of simplicity, but without loss of generality, we consider the symmetric potential; i.e., we set $\varepsilon = 0$ in Eq. (1). For the isolated system the energy spectrum follows from the time-independent Schrödinger equation as $\mathbf{H}_0|n\rangle = \mathcal{E}_n|n\rangle$, $n = 1, 2, \ldots$. The two lowest doublets $\hbar\Delta_1^{\mathcal{E}} = \mathcal{E}_2 - \mathcal{E}_1$ and $\hbar\Delta_2^{\mathcal{E}} = \mathcal{E}_4 - \mathcal{E}_3$ are separated by the energy gap $\hbar\bar{\omega}_0 = \frac{1}{2}(\mathcal{E}_4 + \mathcal{E}_3) - \frac{1}{2}(\mathcal{E}_2 + \mathcal{E}_1) \gg \hbar\Delta_i^{\mathcal{E}}$. The interdoublet frequency $\bar{\omega}_0$ is of the order of the classical oscillation frequency ω_0 and becomes equal to it in the limit of high barriers when the two intrawell oscillators approach harmonic oscillator potentials. With the objective of the decay of a localized state in mind, we start from the so-called *localized basis*. It is this basis which is favorably used to describe the tunneling dynamics. It follows from the energy eigenbasis by a unitary transformation according to

$$\begin{aligned} |L_1\rangle &= \frac{1}{\sqrt{2}}(|1\rangle - |2\rangle), \qquad |R_1\rangle = \frac{1}{\sqrt{2}}(|1\rangle + |2\rangle), \\ |L_2\rangle &= \frac{1}{\sqrt{2}}(|3\rangle - |4\rangle), \qquad |R_2\rangle = \frac{1}{\sqrt{2}}(|3\rangle + |4\rangle). \end{aligned} \tag{34}$$

These states are localized in the left ($|L_j\rangle$) and in the right ($|R_j\rangle$) well with lower ($j = 1$) and higher ($j = 2$) energy, respectively. The localized states are depicted in Fig. 2a in position space. Shown is the double-well potential (thick solid line) for a barrier height of $E_B = \Delta U/\hbar\omega_0 = 1.4$ (we use in the figures dimensionless quantities according to the standard scaling defined in the Appendix A, Eq. (A1)). The energy eigenvalues $\mathcal{E}_1, \ldots, \mathcal{E}_4$ are marked by thin solid horizontal lines. The wave functions $\langle q \mid L_1\rangle$ (solid line) and $\langle q \mid L_2\rangle$ (dashed-dotted line) are localized in the left well, and the wave functions $\langle q \mid R_1\rangle$ (dashed line) and $\langle q \mid R_2\rangle$ (long dashed line) are localized in the right well. In the literature [50], these localized states in Eq. (34) are sometimes approximated by the eigenstates of harmonic potentials shifted to the position of the well minima, cf. Appendix E. This approximation is justified for large barrier heights where, however, semiclassical techniques [2] to determine the quantum relaxation rate are already applicable. By use of basic algebra, the matrix for the bare system Hamiltonian of the double-doublet system in the localized basis is calculated to be

$$\mathbf{H}_{\mathrm{DDS}}^{\mathrm{loc}} = \sum_{i=1,2} -\frac{\hbar\Delta_i^{\mathcal{E}}}{2}(|R_i\rangle\langle L_i| + |L_i\rangle\langle R_i|) + \hbar\bar{\omega}_0(|R_2\rangle\langle R_2| + |L_2\rangle\langle L_2|), \tag{35}$$

with frequencies $\Delta_i^{\mathcal{E}}$ and $\bar{\omega}_0$ defined above. The position operator in this localized representation

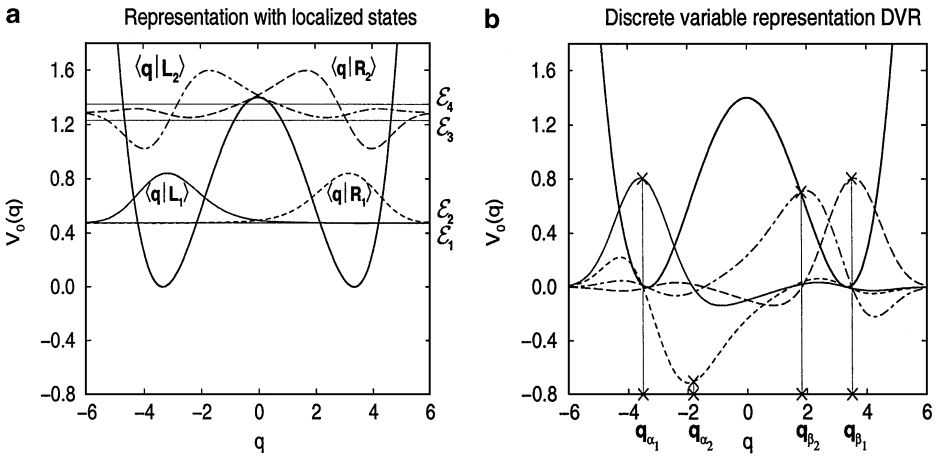

FIG. 2. (a) The first four localized states $\langle q \mid L_1\rangle, \ldots, \langle q \mid R_2\rangle$ of the static symmetric double-well potential, Eq. (2) with $\varepsilon = s = 0$, are shown in position space. They are defined according to Eq. (34). The barrier height is chosen to be $E_B = \Delta U/\hbar\omega_0 = 1.4$ (we use here and in the following figure captions dimensionless quantities according to the standard scaling defined in Eq. (A1)). The energy eigenvalues $\mathcal{E}_1, \ldots, \mathcal{E}_4$ are marked by thin solid horizontal lines. (b) The corresponding four DVR-states are shown, i.e., $\langle q \mid \alpha_1\rangle$ (solid line), $\langle q \mid \alpha_2\rangle$ (dashed line), $\langle q \mid \beta_2\rangle$ (dashed-dotted line), and $\langle q \mid \beta_1\rangle$ (long-dashed line). On the q-axis, the exact eigenvalues q_μ are marked by crosses.

then reads

$$\mathbf{q}^{\mathrm{loc}} = \sum_{i,j=1,2} a_{ij}(|R_i\rangle\langle R_j| - |L_i\rangle\langle L_j|) + b(|L_1\rangle\langle R_2| + |R_2\rangle\langle L_1| - |R_1\rangle\langle L_2| - |L_2\rangle\langle R_1|), \quad (36)$$

where $a_{11} = \langle 1|\mathbf{q}|2\rangle$, $a_{22} = \langle 3|\mathbf{q}|4\rangle$, $a_{12} = a_{21} = (\langle 1|\mathbf{q}|4\rangle + \langle 2|\mathbf{q}|3\rangle)/2$ and $b = (\langle 1|\mathbf{q}|4\rangle - \langle 2|\mathbf{q}|3\rangle)/2 \ll a_{ij}$. Note that, in clear contrast to the spin-boson case $M = 2$, the position operator in the localized basis is *nondiagonal*. Since the energies in the Hamiltonian are of different orders of magnitude, i.e., $\hbar\Delta_1^{\mathcal{E}} \ll \hbar\Delta_2^{\mathcal{E}} \ll \hbar\bar{\omega}_0$, the general time evolution of an initial state proceeds on different time scales. The coherent dynamics exhibits transitions between the wells due to *tunneling*. It occurs in the lower doublet on a time scale $(\Delta_1^{\mathcal{E}})^{-1}$ and in the upper doublet on a much shorter time scale $(\Delta_2^{\mathcal{E}})^{-1}$, being still long compared to the time scale $\bar{\omega}_0^{-1}$ of the interdoublet dynamics. The coupling to the heat bath is mediated by the position operator while the interdoublet transitions are responsible for vibrational relaxation.

For the following analytical treatment, we simplify the approach by setting $b = 0$ in Eq. (36). This is for the sake of an illustrative purpose only and has no impact on the path integral formalism introduced above. For specific results, the diagonalization of the position operator is performed numerically on the computer with $b \neq 0$. By means of ordinary diagonalization performed for the matrix in Eq. (36) the DVR-states read

$$\begin{aligned} |\alpha_1\rangle &= v(|L_1\rangle - u|L_2\rangle), \qquad |\beta_1\rangle = v(|R_1\rangle - u|R_2\rangle), \\ |\alpha_2\rangle &= v(u|L_1\rangle - |L_2\rangle), \qquad |\beta_2\rangle = v(u|R_1\rangle - |R_2\rangle), \end{aligned} \quad (37)$$

with $|\alpha_j\rangle$ ($|\beta_j\rangle$) being localized in the left (right) well, respectively. Here, $v = 1/\sqrt{1+u^2}$ and $u = (a_{11} + q_{\alpha_1})/a_{12} = -(a_{22} + q_{\alpha_2})/a_{12}$, and $q_{\alpha_i} = -q_{\beta_i}$ denote the position eigenvalues:

$$q_{\alpha_{1,2}} = \left[-(a_{11} + a_{22}) \mp \sqrt{(a_{11} - a_{22})^2 + 4a_{12}^2}\right]/2. \quad (38)$$

The four DVR-states are depicted in Fig. 2b for a barrier height of $E_{\rm B} = \Delta U/\hbar\omega_0 = 1.4$, i.e., $\langle q \mid \alpha_1\rangle$ (solid line), $\langle q \mid \alpha_2\rangle$ (dashed line), $\langle q \mid \beta_2\rangle$ (dashed-dotted line), and $\langle q \mid \beta_1\rangle$ (long-dashed line). On the q-axis, the exact eigenvalues q_μ are marked by crosses (the eigenvalues are obtained by numerical diagonalization of the position operator in Eq. (36)). As expected, the DVR-states are localized around their corresponding position eigenvalue q_μ.

It is suggestive to call transitions between the left and right well, i.e., between $|\alpha_i\rangle$ and $|\beta_j\rangle$ as *DVR-tunneling*. These are characterized by the effective tunneling matrix elements

$$\begin{aligned} \Delta_{\alpha_1\beta_1} \equiv v^2\big(\Delta_1^{\mathcal{E}} + u^2\Delta_2^{\mathcal{E}}\big), \qquad \Delta_{\alpha_2\beta_2} \equiv v^2\big(u^2\Delta_1^{\mathcal{E}} + \Delta_2^{\mathcal{E}}\big), \\ \Delta_{\alpha_1\beta_2} = \Delta_{\alpha_2\beta_1} \equiv v^2u\big(\Delta_1^{\mathcal{E}} - \Delta_2^{\mathcal{E}}\big), \end{aligned} \tag{39}$$

which constitute a *linear combination* of the bare tunneling splittings $\Delta_1^{\mathcal{E}}$ and $\Delta_2^{\mathcal{E}}$. On the other hand, transitions within one well, i. e., between $|\alpha_i\rangle$ and $|\alpha_j\rangle$ and between $|\beta_i\rangle$ and $|\beta_j\rangle$, may be termed *DVR-vibrational relaxation*. Those can be characterized by the transition matrix elements

$$\Delta_{\alpha_1\alpha_2} = \Delta_{\alpha_2\alpha_1} = \Delta_{\beta_1\beta_2} = \Delta_{\beta_2\beta_1} \equiv \Delta_{\rm R} = 2v^2u\bar{\omega}_0. \tag{40}$$

Due to parity symmetry, they assume equal values. The Hamiltonian of the double-doublet system in the DVR-basis can thus be written as

$$\mathbf{H}_{\rm DDS}^{\rm DVR} = -\sum_{i,j=1,2}\frac{1}{2}\hbar\,\Delta_{\alpha_i\beta_j}(|\alpha_i\rangle\langle\beta_j| + |\beta_j\rangle\langle\alpha_i|) - \frac{1}{2}\hbar\,\Delta_{\rm R}\mathbf{R} + \sum_{i=1,2}\hbar\left(F_{\alpha_i}|\alpha_i\rangle\langle\alpha_i| + F_{\beta_i}|\beta_i\rangle\langle\beta_i|\right), \tag{41}$$

with $F_{\alpha_1} = F_{\beta_1} = u^2v^2\bar{\omega}_0$, $F_{\alpha_2} = F_{\beta_2} = v^2\bar{\omega}_0$. The operator $\mathbf{R}$ accounts for DVR-vibrational relaxation, i.e., $\mathbf{R} = |\alpha_1\rangle\langle\alpha_2| + |\alpha_2\rangle\langle\alpha_1| + |\beta_1\rangle\langle\beta_2| + |\beta_2\rangle\langle\beta_1|$. Thereby, the time-independent problem is fully characterized. The time-dependent driving $s(t) = s\,\sin(\Omega t)$ couples to the position operator $\mathbf{q}$. The total system Hamiltonian in the DVR-basis thus reads

$$\mathbf{H}_{\rm S}^{\rm DVR}(t) = \mathbf{H}_{\rm DDS}^{\rm DVR} - s\,\sin(\Omega t)\sum_{i=1,2} q_{\alpha_i}(|\alpha_i\rangle\langle\alpha_i| - |\beta_i\rangle\langle\beta_i|). \tag{42}$$

Note that in the DVR-basis the time-dependence enters only in the diagonal elements of the Hamiltonian. So far, we have provided all required parameters for the path integral formalism developed in the previous Section III.C, namely the matrix elements in Eq. (41) of the Hamiltonian in the DVR-basis, and the position operator eigenvalues in Eq. (38). In the following section, we return to the dissipative real-time path integral formalism and develop a suitable approximation scheme to the exact expression in Eq. (33).

IV. THE GENERALIZED NON-INTERACTING CLUSTER APPROXIMATION

In the context of dissipative real-time path integrals, a common strategy of approximative treatment is as follows: It concerns the treatment of the interactions between different paths which are induced by the coupling to the heat bath and which are described by the influence functional. The working idea behind the strategy [1, 3] is to neglect some of those correlations in order to get tractable expressions. One possible approximation within the spin-boson problem ($M = 2$) is the so-termed *non-interacting blip approximation (NIBA)* [1]. There, the interactions between off-diagonal states (blips) are neglected. In the NIBA the sojourn-blip interactions are disregarded except neighboring ones, and even those are treated approximately. Within the NIBA, the influence phase simplifies

drastically and the path integral series in Eq. (33) reduces to terms which are of lowest order in the level splitting $\Delta_1^{\mathcal{E}}$. The NIBA can be justified in the case of Ohmic damping for high enough temperatures and/or large dissipation strengths. In this regime, the average blip length is small compared to the average sojourn length, and the blip-blip and the blip-sojourn interactions can consequently be neglected. In fact, for finite temperatures and Ohmic damping, long blips are exponentially suppressed by the intrablip interactions. The NIBA fails for systems with asymmetry when the friction becomes weak; however, it becomes a systematic weak-damping approximation down to zero temperature for the case of a symmetric spin-boson system [1–5].

Improved approximations take into account some of the correlations between the blips. One such step of an improved approximation has been denoted as the *interacting blip chain approximation (IBCA)* [60]. There, the interactions of all nearest-neighbor blip pairs and the full interactions of the nearest-neighbor sojourn-blip pairs are taken into account in addition. This improved approximation confirms the validity of the NIBA in the stated parameter regime. It is valid also in an extended parameter regime where the NIBA already breaks down.

The NIBA is applicable for a spin-boson system; i.e., a system with two tight binding sites. It has been generalized to the case with arbitrary many tight binding sites by Egger *et al.* [61]. In their work only tunneling transitions between *nearest-neighbor sites* are considered. The multisite paths along the discrete states of the reduced density matrix result in a sequence of *sojourns* (time intervals with the system being in a diagonal state) and *clusters* (time intervals with the system being in an off-diagonal state). It turns out that the corresponding path weights of the clusters sum up to zero. Consequently, the clusters can be considered as neutral objects. This suggests to neglect all interactions between the clusters yielding the *non-interacting cluster approximation (NICA)*. In the time-*in*dependent problem considered in Ref. [61], the time-integrations over the sojourn times in the path integral appear as convolutions. This feature makes the expression solvable by means of Laplace transforms.

Motivated by the NICA, we here generalize it to the case with many levels by observing that the multilevel problem can be mapped onto the multisite one when tunneling between non-nearest neighbor sites is also considered. Moreover, we generalize the approach in Ref. [61] by taking into account a time-dependent system Hamiltonian, together with a general initial reduced density matrix.

The key argument in Ref. [61] refers to the overall neutrality of a cluster because the cumulative charge is zero. This is also the case for a general multi-level path integral in Eq. (33). To show this, we consider a general cluster at a diagonal state ($\mu_k,\ \nu_k = \mu_k$) at time t_k. It subsequently travels around among arbitrary many off-diagonal states and re-enters at time t_l a diagonal state ($\mu_l,\ \nu_l = \mu_l$). The cumulative charge W_{cl} of this cluster is the sum over all individual path weights defined in Eq. (20), i.e.,

$$
\begin{aligned}
W_{\mathrm{cl}} &= \sum_{j=k+1}^{l} \xi_j \\
&= \left(q_{\mu_l} - q_{\nu_l} - q_{\mu_{l-1}} + q_{\nu_{l-1}}\right) + \left(q_{\mu_{l-1}} - q_{\nu_{l-1}} - q_{\mu_{l-2}} + q_{\nu_{l-2}}\right) \\
&\quad + \cdots + \left(q_{\mu_{k+2}} - q_{\nu_{k+2}} - q_{\mu_{k+1}} + q_{\nu_{k+1}}\right) + \left(q_{\mu_{k+1}} - q_{\nu_{k+1}} - q_{\mu_k} + q_{\nu_k}\right) \\
&= q_{\mu_l} - q_{\nu_l} - q_{\mu_k} + q_{\nu_k} \\
&= 0,
\end{aligned}
\tag{43}
$$

because $\nu_k = \mu_k$ and $\nu_l = \mu_l$. In this language, any path is just a sequence of sojourns and clusters, where the ξ-charges within each cluster sum up to zero.

In general, the influence functional in Eq. (23) couples the χ-charges *inside* each cluster with the ξ-charges *inside* all other clusters. Similarly, all ξ-charges are coupled to each other. These interactions consequently render the path summation intractable.

Since the entire cluster can be seen as a neutral object which is only weakly interacting with all other clusters which are themselves neutral, it is suggestive to *neglect all the intercluster interactions* in the influence phase in Eq. (33). However, all the *intra*cluster interactions, as well as all interactions of a cluster with the preceding sojourn, are fully taken into account (see below). For a path starting in an off-diagonal state, we call that part of a path which precedes the first sojourn a *semi-cluster*. Within our approximative description, we neglect the interaction of this semi-cluster with all the later clusters but take into account the correlation of the first sojourn with the preceding semi-cluster. This "coarse-graining" is performed for general transitions. We call this the *generalized non-interacting cluster approximation (gNICA)*.

Before we exploit the consequences of this approximation, we discuss its regime of validity. The gNICA is justified when the average cluster length is small compared to the average sojourn length. This is fulfilled for high temperatures and/or strong damping. Far excursions from the diagonal state are damped exponentially; see Eq. (10) for the influence phase. As such, the gNICA becomes *exact* in the limit of high temperatures.

For the case of the spin-boson-system at low temperature T, small friction γ, and no bias ($\mathcal{E} = 0$), the interblip correlations are only of second order in the coupling strength γ while the *intra*blip ones are of linear order in γ. Hence, the gNICA is a good approximation down to zero temperature [3]. However, with $M > 2$, lowest-order contributions to interblip correlations arise due to the non-zero diagonal elements F_ν in Eq. (41). This yields a rough condition of validity for the gNICA; it reads $\hbar\Delta^{\mathcal{E}}_{\max} < k_{\mathrm{B}}T$ or $\Delta^{\mathcal{E}}_{\max} \lesssim \gamma$, where $\Delta^{\mathcal{E}}_{\max} = \max\{\Delta^{\mathcal{E}}_1, \Delta^{\mathcal{E}}_2, \ldots\}$. On the other hand, an upper limit for the allowed values of the damping constant can be extracted by the following argumentation: The damping leads to a level broadening of the unperturbed eigenenergies. This is seen best in the form in Eq. (10) for the influence phase. The damping could be viewed as an additional contribution to the bare system propagator. The contribution is of stochastic nature and implies the level broadening. In order that a tunneling description make sense, this frictional level broadening should not exceed the bare interdoublet level spacing, i.e., $\gamma \ll \omega_0$. This condition is not really restrictive because friction strengths of the order of the oscillator frequency, i.e., $\gamma \approx \omega_0$, would indeed strongly suppress quantum effects.

V. THE GENERALIZED MASTER EQUATION IN THE DISCRETE VARIABLE REPRESENTATION

A. *General Derivation*

First, we address the non-driven case. We start by observing that every path which begins and ends in a diagonal state can be seen as a sequence of p clusters punctuated by sojourns. For paths starting out at an off-diagonal and ending in a diagonal state, also the initial semi-cluster appears. Within the gNICA prescription, it is now straightforward to see that the integrations over the sojourn times in Eq. (33) *appear as convolutions*! To use this property effectively, we switch to the Laplace transform $\rho_{\mu_N\mu_N}(\lambda)$. It then follows that the integration over each sojourn contributes a factor λ^{-1}, while each cluster yields a factor which depends on the number of charges and on their configuration inside that particular cluster according to Eq. (33). This very point is elucidated with an example in Appendix D; there, we present in detail the contribution of one specific path to the full path sum. In a second step, we generalize this idea.

We consider transitions from the initial state (μ_0, ν_0) at time t_0 to the final state (μ_N, μ_N) at time t_N. In doing so, we must distinguish between two cases: (i) the initial state is a diagonal state, i.e., $\mu_0 = \nu_0$ and (ii) the initial state is an off-diagonal state, i.e., $\mu_0 \neq \nu_0$. We separate the contributions

to the path sum and obtain then for the Laplace transform $\rho_{\mu_N\mu_N}(\lambda) = \int_0^\infty dt e^{-\lambda t}\rho_{\mu_N\mu_N}(t)$ the expression

$$\rho_{\mu_N\mu_N}(\lambda) = \sum_{\mu_0=1}^{M} \rho_{\mu_0\mu_0}\rho_{\mu_N\mu_N,\mathrm{D}}(\lambda) + \sum_{\substack{\mu_0,\nu_0=1 \\ \mu_0\neq\nu_0}}^{M} \rho_{\mu_0\nu_0}\rho_{\mu_N\mu_N,\mathrm{O}}(\lambda), \tag{44}$$

where $\rho_{\mu_N\mu_N,\mathrm{D}}$ ($\rho_{\mu_N\mu_N,\mathrm{O}}$) denotes the contribution of the diagonal (off-diagonal) initial part, respectively.

To proceed, we need to consider an arbitrary cluster which begins in the diagonal state (μ_i, $\nu_i = \mu_i$) at time t_i and ends in the diagonal state (μ_j, $\nu_j = \mu_j$) at time t_j. We sum over *all* the path configurations and denote this collected contribution the *cluster function* $h_{\mu_j\mu_i}(\lambda)$. Proceeding as in Appendix D yields for the cluster function

$$\begin{aligned} h_{\mu_j\mu_i}(\lambda) = &\sum_{m=|i-j|}^{\infty} \int_0^\infty d\tau_1 \cdots \int_0^\infty d\tau_{m-1} \exp\{-\lambda(\tau_1 + \cdots + \tau_{m-1})\} \\ &\times \sum_{\substack{\{\mu_k\nu_k\} \\ \mu_k\neq\nu_k}} \exp\left\{ i \sum_{k=1}^{m-1} \int_{\sum_{l=1}^{k}\tau_l}^{\sum_{l=1}^{k+1}\tau_l} dt' \left[E_{\mu_{k+i}}(t') - E_{\nu_{k+i}}(t')\right] \right\} \prod_{k=0}^{m} (-1)^{\delta_k} \left(\frac{i}{2}\right)^m \Delta_{k+i} \\ &\times \exp\left\{ \sum_{l=2}^{m}\sum_{k=1}^{l-1} \xi_{l+i} S\left(\sum_{n=k}^{l-1}\tau_n\right)\xi_{k+i} + i \sum_{l=2}^{m}\sum_{k=1}^{l-1} \xi_{l+i} R\left(\sum_{n=k}^{l-1}\tau_n\right)\chi_{k+i} \right\}, \end{aligned} \tag{45}$$

with the difference times $\tau_k = t_k - t_{k-1}$ and with the conventions and notations taken from Eq. (33).

Each contribution to $\rho_{\mu_N\mu_N,\mathrm{D}}(\lambda)$ can be viewed as a sequence of sojourns punctuated by clusters. Thus, in the first case (i), we sum up the contributions of *all* paths which start in (μ_0, $\nu_0 = \mu_0$) and end in (μ_N, $\nu_N = \mu_N$) and which contain p clusters starting in some intermediate diagonal states (σ_k, σ_k) and ending in (σ_{k+1}, σ_{k+1}), i.e.,

$$\rho^{(p)}_{\mu_N\mu_N,\mathrm{D}}(\lambda) = \sum_{\sigma_1,\sigma_2,\ldots,\sigma_p} \frac{1}{\lambda} h_{\sigma_1,\mu_0}(\lambda) \frac{1}{\lambda} h_{\sigma_2,\sigma_1}(\lambda) \cdots h_{\mu_N,\sigma_p}(\lambda) \frac{1}{\lambda}, \tag{46}$$

where the sum runs over all possible intermediate diagonal states $\sigma = 1, \ldots, M$. The factors $1/\lambda$ are the results of the integration over the sojourns, see Appendix D.

In the second case (ii), where the initial state is an off-diagonal state, we assume that the path travels among off-diagonal ones and hits after d transitions *for the first time* a diagonal state (κ_d, κ_d) at time t_d. This part of the path is termed a *semi-cluster* and the interaction with all the other clusters is neglected according to the gNICA. The sum of all such semi-clusters that start in (μ_0, ν_0) and end in (κ_d, κ_d) results in a semi-cluster function $f_{\kappa_d\kappa_d,\mu_0\nu_0}(\lambda)$. From time t_d on, the formalism from (i) is applied. Summing over all possible diagonal states $\kappa_d = 1, \ldots, M$ yields the contribution to the path sum

$$\rho^{(p)}_{\mu_N\mu_N,\mathrm{O}}(\lambda) = \sum_{\kappa_d=1}^{M} \left\{ f_{\kappa_d\kappa_d,\mu_0\nu_0}(\lambda) \sum_{\sigma_1,\sigma_2,\ldots,\sigma_p} \frac{1}{\lambda} h_{\sigma_1,\kappa_d}(\lambda) \frac{1}{\lambda} h_{\sigma_2,\sigma_1}(\lambda) \cdots h_{\mu_N,\sigma_p}(\lambda) \frac{1}{\lambda} \right\}, \tag{47}$$

where the semi-cluster function is given as

$$f_{\kappa_d\kappa_d,\mu_0\nu_0}(\lambda) = \sum_{m=1}^{\infty}\int_0^{\infty} d\tau_1\cdots\int_0^{\infty} d\tau_{m-1}\,\exp\{-\lambda(\tau_1+\cdots+\tau_{m-1})\}$$
$$\times\sum_{\substack{\{\mu_k\nu_k\}\\ \mu_k\neq\nu_k}}\exp\left\{i\sum_{k=1}^{m-1}\int_{\sum_{l=1}^{k}\tau_l}^{\sum_{l=1}^{k+1}\tau_l} dt'\left[E_{\mu_k}(t')-E_{\nu_k}(t')\right]\right\}\prod_{k=1}^{m}(-1)^{\delta_k}\left(\frac{i}{2}\right)^m\Delta_k$$
$$\times\exp\left\{\sum_{l=2}^{m}\sum_{k=1}^{l-1}\xi_l S\left(\sum_{n=k}^{l-1}\tau_n\right)\xi_k + i\sum_{l=2}^{m}\sum_{k=1}^{l}\xi_l R\left(\sum_{n=k}^{l-1}\tau_n\right)\chi_k\right\}. \tag{48}$$

Defining the *cluster matrix* $\mathcal{H}(\lambda)$ with the matrix elements $h_{\mu_j\mu_i}(\lambda)$, we can rewrite Eq. (46) and the inner sum in Eq. (47) as a matrix product, i.e.,

$$\rho^{(p)}_{\mu_N\mu_N,\mathrm{D}}(\lambda) = \frac{1}{\lambda}\left\{\left[\frac{\mathcal{H}(\lambda)}{\lambda}\right]^p\right\}_{\mu_N\mu_0}, \tag{49}$$

$$\rho^{(p)}_{\mu_N\mu_N,\mathrm{O}}(\lambda) = \sum_{\kappa_d=1}^{M}\left\{f_{\kappa_d\kappa_d,\mu_0\nu_0}(\lambda)\frac{1}{\lambda}\left\{\left[\frac{\mathcal{H}(\lambda)}{\lambda}\right]^p\right\}_{\mu_N\kappa_d}\right\}. \tag{50}$$

In a last step, the summation over all possible numbers p of clusters within a path has to be performed. This last sum can be formally recast, yielding

$$\rho_{\mu_N\mu_N,\mathrm{D}}(\lambda) = \left\{\frac{1}{\lambda-\mathcal{H}(\lambda)}\right\}_{\mu_N\mu_0}, \tag{51}$$

$$\rho_{\mu_N\mu_N,\mathrm{O}}(\lambda) = \sum_{\kappa_d=1}^{M}\left\{f_{\kappa_d\kappa_d,\mu_0\nu_0}(\lambda)\left\{\frac{1}{\lambda-\mathcal{H}(\lambda)}\right\}_{\mu_N\kappa_d}\right\}. \tag{52}$$

We insert this result into Eq. (44), exchange the order of summation in the second term of the r.h.s., and end up with

$$\rho_{\mu_N\mu_N}(\lambda) = \sum_{\mu_0=1}^{M}\rho_{\mu_0\mu_0}\left\{\frac{1}{\lambda-\mathcal{H}(\lambda)}\right\}_{\mu_N\mu_0} + \sum_{\kappa_d=1}^{M}\left\{\frac{1}{\lambda-\mathcal{H}(\lambda)}\right\}_{\mu_N\kappa_d} i_{\kappa_d\kappa_d}(\lambda) \tag{53}$$

with

$$i_{\kappa_d\kappa_d}(\lambda) = \sum_{\substack{\mu_0,\nu_0=1\\ \mu_0\neq\nu_0}}^{M}\rho_{\mu_0\nu_0}f_{\kappa_d\kappa_d,\mu_0\nu_0}(\lambda). \tag{54}$$

Equation (53) can be viewed as a vector equation with two vector-matrix products on the r.h.s. For convenience we introduce a vector-matrix notation. $\rho_{\mu_N\mu_N}(\lambda)$ then appear as elements of a vector $\vec{\rho}(\lambda)$. The initial populations $\rho_{\mu_0\mu_0}$ are arranged in the vector $\vec{\rho}_0$ and the initial off-diagonal elements are contained in the vector $\vec{I}(\lambda)$ with the elements $i_{\kappa_d\kappa_d}(\lambda)$. In this notation, Eq. (53) reads

$$\vec{\rho}(\lambda) = \frac{1}{\lambda-\mathcal{H}(\lambda)}\vec{\rho}_0 + \frac{1}{\lambda-\mathcal{H}(\lambda)}\vec{I}(\lambda). \tag{55}$$

Multiplying Eq. (55) with the inverse of the matrix $\frac{1}{\lambda-\mathcal{H}(\lambda)}$ and rearranging the equation, we find

$$\lambda\vec{\rho}(\lambda) - \vec{\rho}_0 = \mathcal{H}(\lambda)\vec{\rho}(\lambda) + \vec{I}(\lambda). \tag{56}$$

Finally, we perform the inverse Laplace transform and end up with the equation

$$\dot{\vec{\rho}}(t) = \int_{t_0}^{t} dt' \mathcal{H}(t-t')\vec{\rho}(t') + \vec{I}(t-t_0) \tag{57}$$

or in the original notation for the single components

$$\dot{\rho}_{\mu\mu}(t) = \sum_{\nu=1}^{M} \int_{t_0}^{t} dt' \mathcal{H}_{\mu\nu}(t-t')\rho_{\nu\nu}(t') + I_\mu(t-t_0), \qquad \mu = 1, \ldots, M. \tag{58}$$

The overdot denotes the derivative with respect to time t. The initial conditions for Eq. (58) are $\rho_{\mu\nu}(t_0) = \rho_{\mu_0\nu_0}$. Equations (57) and (58) are of convolutive form since a time-*in*dependent Hamiltonian was assumed. A similar, although technically more involved, line of reasoning must be used for the *driven* case. We find equations similar to Eqs. (57) and (58) with $\mathcal{H}_{\mu\nu}(t-t') \curvearrowright \mathcal{H}_{\mu\nu}(t,t')$ and $I_\mu(t-t_0) \curvearrowright I_\mu(t,t_0)$. To be explicit, the elements of the rate matrix $\mathcal{H}_{\mu\nu}(t,t')$ are in the general time-dependent case given as

$$\begin{aligned}\mathcal{H}_{\mu\nu}(t,t') = \sum_{N=2}^{\infty} \int_{t'}^{t} \mathcal{D}\{t_j\} \sum_{\substack{\{\mu_j\nu_j\} \\ \nu_j\neq\nu_j}} \exp\left\{ i \sum_{j=0}^{N-1} \int_{t_j}^{t_{j+1}} dt'' \left[E_{\mu_j}(t'') - E_{\nu_j}(t'')\right] \right\} \prod_{j=0}^{N-1} (-1)^{\delta_j} \left(\frac{i}{2}\right)^N \Delta_j \\ \times \exp\left\{ \sum_{l=1}^{N} \sum_{j=0}^{l-1} \xi_l S(t_l - t_j)\xi_j + i \sum_{l=1}^{N} \sum_{j=0}^{l-1} \xi_l R(t_l - t_j)\chi_j \right\}.\end{aligned} \tag{59}$$

The inhomogeneity $I_\mu(t,t_0)$ arises because of the contributions of the non-diagonal initial states; its explicit form reads

$$\begin{aligned} I_\mu(t,t_0) &= \sum_{\substack{\mu_0,\nu_0=1 \\ \mu_0\neq\nu_0}}^{M} \rho_{\mu_0\nu_0} f_{\mu_0\nu_0,\mu\mu}(t,t_0) \\ &= \sum_{\substack{\mu_0,\nu_0=1 \\ \mu_0\neq\nu_0}}^{M} \rho_{\mu_0\nu_0} \sum_{m=1}^{\infty} \int_{t_0}^{t} \mathcal{D}\{t_j\} \sum_{\substack{\{\mu_j\nu_j\} \\ \mu_j\neq\nu_j}} \exp\left\{ i \sum_{j=0}^{m-1} \int_{t_j}^{t_{j+1}} dt'' \left[E_{\mu_j}(t'') - E_{\nu_j}(t'')\right] \right\} \\ &\quad \times \prod_{j=0}^{m-1} (-1)^{\delta_j} \left(\frac{i}{2}\right)^m \Delta_j \exp\left\{ \sum_{l=1}^{m} \sum_{j=0}^{l-1} \xi_l S(t_l - t_j)\xi_j + i \sum_{l=1}^{m} \sum_{j=0}^{l-1} \xi_l R(t_l - t_j)\chi_j \right\}. \end{aligned} \tag{60}$$

The integro-differential equation (58) is called the *generalized master equation (GME)*; it constitutes one *central result* of this work.

In the following, we will see that the inhomogeneity in Eq. (60) plays an important role at short times. However, it will become exponentially suppressed at long times reflecting the fact that the asymptotic state is independent of the initial preparation.

We note that this integro-differential equation (58) is represented in the DVR-basis for the diagonal elements of the reduced density matrix $\boldsymbol{\rho}(t)$. For all practical calculations, the kernels in Eq. (59) and the inhomogeneities in Eq. (60) have to be determined up to a certain order $\mathcal{O}(\Delta^N)$. In practice, this means that $N = \infty$ as the upper limit of the summations has to be replaced by a finite value.

Some comments to elucidate the physical content of the GME (58) are in order: The transformation of the problem from the localized basis to the DVR-basis maps the dynamics of the particle in the spatially continuous potential onto a hopping process of the particle on a spatially discrete grid. The grid points are the discrete positions characterized by the eigenvalues q_κ, $\kappa = 1, \ldots, M$, of the position operator $\mathbf{q}$, according to Eq. (12).

Next, we consider the example of the double-doublet system which has already been introduced in Section III.D. We give the explicit expressions for the kernels in Eq. (59) in the GME up to second order in Δ_j and illustrate the damping mechanism further.

B. *The Leading Order Approximation*

In this section we investigate the GME, Eq. (58), with the kernels in Eq. (59) and the inhomogeneities in Eq. (60) derived to lowest order in the Hamiltonian matrix elements Δ_j. To illustrate the general scheme, we describe the method for the case of the double-doublet system with $M = 4$ levels.

As we want to evaluate the relaxation rate of an initially localized wave packet in one of the wells, say, the left well, we prepare the system in an equally weighted superposition of symmetric and antisymmetric wave function belonging to the *lowest* doublet, i.e.,

$$\boldsymbol{\rho}(t_0) = |L_1\rangle\langle L_1|, \tag{61}$$

where $|L_1\rangle = (1/\sqrt{2})(|1\rangle - |2\rangle)$ and $|n\rangle$, $n = 1, 2$ are the nearly degenerate energy eigenstates of the static, symmetric Hamiltonian $\mathbf{H}_0$ (cf. Eq. (2) and Eqs. (34)). Transforming this initial state to the DVR-basis via Eq. (37), we find

$$\boldsymbol{\rho}(t_0) = v^2(|\alpha_1\rangle\,\langle\alpha_1| + u^2|\alpha_2\rangle\,\langle\alpha_2| + u|\alpha_1\rangle\,\langle\alpha_2| + u|\alpha_2\rangle\,\langle\alpha_1|) \tag{62}$$

with the parameters u and v defined below Eq. (37). We note that the initially prepared localized state is characterized by a *nondiagonal* density matrix in the DVR basis. The diagonal elements in Eq. (62) enter as initial conditions for the first part of the r.h.s. of Eq. (58), while the off-diagonal elements determine the inhomogeneity.

To first order, i.e., with one jump, no transition from an initial diagonal state to a final diagonal state is possible. To achieve this, at least two jumps are necessary. However, transitions starting in an off-diagonal state and ending in a diagonal state are possible within one jump. This means that a first order contribution appears only in the inhomogeneity of Eq. (58). The relevant transitions are the jumps ending in the diagonal state (α_1, α_1), i.e., $(\alpha_1, \alpha_2) \to (\alpha_1, \alpha_1)$ and $(\alpha_2, \alpha_1) \to (\alpha_1, \alpha_1)$, and the jumps ending in (α_2, α_2), i.e., $(\alpha_1, \alpha_2) \to (\alpha_2, \alpha_2)$ and $(\alpha_2, \alpha_1) \to (\alpha_2, \alpha_2)$, respectively. From Eq. (33), it follows that each path traveling "above" the diagonal has a corresponding mirror path traveling "below" the diagonal. The mirror path yields a contribution to the path sum being the complex conjugate of the upper path. Using this feature and the fact that $\rho_{\alpha_1\alpha_2}(t_0) = \rho^*_{\alpha_2\alpha_1}(t_0) = uv^2$, we obtain for the inhomogeneity the following first-order expression

$$\begin{aligned} I^{(1)}_\mu(t, t_0) = {} & \big(\delta_{\mu\alpha_1} - \delta_{\mu\alpha_2}\big)uv^2\Delta_{\alpha_1\alpha_2}\exp\big\{-\big(q_{\alpha_1} - q_{\alpha_2}\big)^2 S(t - t_0)\big\} \\ & \times \sin\left\{\int_{t_0}^{t} dt'\big[E_{\alpha_2}(t') - E_{\alpha_1}(t')\big] - \big(q_{\alpha_1} - q_{\alpha_2}\big)^2 R(t - t_0)\right\}. \end{aligned} \tag{63}$$

Here, $\Delta_{\mu\nu} = \langle\mu|\mathbf{H}^{\mathrm{DVR}}_{\mathrm{DDS}}|\nu\rangle$, $\mu \neq \nu$, are the off-diagonal matrix elements of the system Hamiltonian

in Eq. (41); see also Eq. (40). Note that *only* vibrational transitions *within* the initially populated well contribute in Eq. (63). Moreover, the $q_\kappa(\kappa = \alpha_1, \alpha_2)$ denote the position eigenvalues, see Eq. (38), and $E_\kappa(t') = F_\kappa - q_\kappa s \sin(\Omega t')$ are the time-dependent diagonal elements of the system Hamiltonian; see Eqs. (42), (41), and (30). The influence of the bath enters via the real and imaginary part of the twice integrated bath correlation function, i.e., $S(t)$ and $R(t)$, respectively; see Eq. (11) and Appendix B. The conservation of probability is reflected with the opposite signs of the Kronecker symbols $\delta_{\nu\kappa}$. From Eq. (63) it clearly follows that the contribution of the initial off-diagonal states are damped exponentially on a time scale determined by the damping constant γ and the temperature T. We recall that the lowest order of the contribution of the integral part of the GME, Eq. (58), is of second order. This implies that the contribution of second order to the inhomogeneity should also be taken into account for a consistent treatment. However, we refrain from writing down the complicated second order term which would yield only minor physical insight. It can be neglected anyhow when investigating the long-time dynamics in the following sections.

The lowest order for the kernels in the integral part of the GME (58) is the second order, because at least two jumps are required starting in a diagonal state to end again in a diagonal state. We use once more the feature that each path traveling above the diagonal has a mirror path traveling below the diagonal, yielding the complex conjugate of the upper path contribution. We then obtain for the GME kernels the leading order results

$$\mathcal{H}^{(2)}_{\mu\nu}(t,t') = \frac{\Delta^2_{\mu\nu}}{2} \exp\{-(q_\mu - q_\nu)^2 S(t-t')\} \times \cos\left\{\int_{t'}^{t} dt''[E_\nu(t'') - E_\mu(t'')] - (q_\mu - q_\nu)^2 R(t-t')\right\}, \qquad \mu \neq \nu. \tag{64}$$

The conservation of probability implies for the diagonal kernels the condition

$$\mathcal{H}^{(2)}_{\nu\nu}(t,t') = -\sum_{\substack{\kappa=1 \\ \kappa\neq\nu}}^{M} \mathcal{H}^{(2)}_{\kappa\nu}(t,t'). \tag{65}$$

We emphasize here that the lowest-order expression in Eq. (64) is applicable to a *general* number M of levels. The explicit example of the system double-doublet with $M = 4$ is used for illustrative purpose only.

Note that the $\mathcal{H}^{(2)}_{\mu\nu}$ represents the transition probability for a path starting in the diagonal state (ν, ν), then jumping to the off-diagonal state $(\nu, \mu)/(\mu, \nu)$, and finally ending in the diagonal state (μ, μ). In clear contrast to Eq. (63), now tunneling and vibrational relaxation both contribute in Eq. (64).

The structure of the GME with the kernels $\mathcal{H}^{(2)}_{\mu\nu}$ restricted to leading, i.e., second, order is similar to that one obtained for the driven spin-boson system within the non-interacting blip approximation (NIBA) [1, 3, 5], and to that one for the dissipative tight-binding model within the non-interacting cluster approximation (NICA) performed to lowest order [61]. The main difference to these GMEs is that in our case the factors $(q_\mu - q_\nu)^2$ enter as *prefactors* for the damping constant γ in $S(t)$ and $R(t)$, respectively. Since they arise from *non-nearest neighbor hopping* on a non-equally spaced grid of DVR eigenvalues, they are *not equal* for all transitions. This means that transitions between far away lying DVR-states are stronger damped and therefore less probable compared to those lying close to each other. This insight is especially relevant for the tunneling transitions from one well to the adjacent. Then, the main contribution to the dynamics comes from those two DVR-states which lie closest to the barrier within each well.

One remark on the notation should be made: In the following, we use the superscript in the kernels $\mathcal{H}^{(2)}_{\mu\nu}$ when they are utilized in second order. Whenever this superscript is omitted, the respective formula is valid to any order of $\mathcal{H}_{\mu\nu}$.

The generalized master equation (58) is clearly not solvable analytically in closed form, not even with the kernels and the inhomogeneities approximated to lowest order. Thus, in Appendix C, we provide a numerical iteration algorithm to obtain a numerical solution.

C. *Comparison with Numerical ab-initio Path Integral Simulations*

In this subsection we compare the results for $P_{\rm left}(t)$ obtained from the numerical solution of the GME (58) with those of the numerical iterative algorithm using the method of the quasiadiabatic propagator path integral QUAPI of Makri [21]. It is known that the QUAPI technique yields reliable results for time-dependent spatially continuous confining potentials [59]. Hence, we use it here as a reference in order to check the gNICA.

We present results for the double-doublet system $M = 4$. Figure 3 depicts the outcome for $P_{\rm left}(t)$ for the symmetric ($\varepsilon = 0$) and for the asymmetric ($\varepsilon = 0.08$) system. Each figure contains three lines: (i) the results of the full generalized master equation (full line), (ii) findings of the QUAPI algorithm which are used as a reference, and (iii) the outcome of a Markovian master equation which is introduced in the following Section VI. We postpone the discussion of the Markovian results to the following section. We find a very good agreement, both for the symmetric as well as the asymmetric system. We note that for the asymmetric case, the full GME is solved only up to $t = 1000$ due to the necessary choice of a very small $\Delta t = 5 \times 10^{-3}$ (for a detailed discussion see Appendix C). The QUAPI results have been obtained with $K = 4$ (the number of memory time steps, see Refs. [21, 59] for details) and $\Delta t = 0.1$ for the symmetric and $\Delta t = 0.35$ for the asymmetric case.

The same very good agreement is found for the case with resonant driving, i.e., $s = 1.0$, $\Omega = \bar{\omega}_0 = 0.815$ which is depicted in Fig. 4a for $T = 0.1$. The inset reveals that the agreement is satisfactory also on a shorter time scale. The QUAPI-parameters are $K = 4$ and $\Delta t = 0.75$ for the symmetric, and $\Delta t = 0.3$ for the asymmetric case, respectively. Also for a higher temperature $T = 0.2$ the agreement is very good; see Fig. 4b.

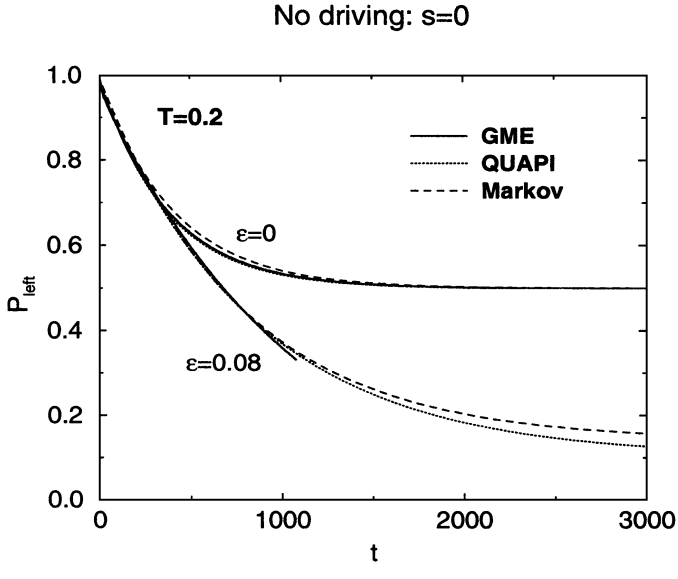

FIG. 3. The probability $P_{\rm left}$ of finding the particle in the left well as a function of time for the symmetric ($\varepsilon = 0$) and the asymmetric ($\varepsilon = 0.08$) case. Considered is the system of two doublets, i.e., $M = 4$. We start from an initially fully localized state in the left well. The barrier height is set to $E_{\rm B} = 1.4$. The temperature is $T = 0.2$, the damping constant is $\gamma = 0.1$, and the cut-off frequency is $\omega_c = 10.0$. For this set of parameters, the dynamics is fully incoherent and the Markov approximation to the GME (58) is rather satisfactory.

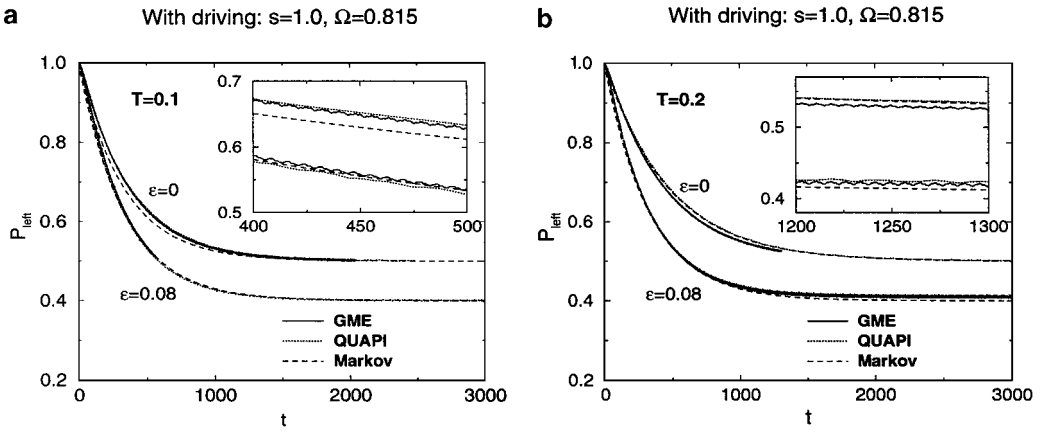

FIG. 4. Same as Fig. 3 in presence of resonant driving $s(t) = s\,\sin(\Omega t)(s = 1.0,\ \Omega = \bar{\omega}_0 = 0.815)$ for $T = 0.1$ (a) and for $T = 0.2$ (b). Insets: enlarged parts of the figures.

All results exhibit a *single exponential decay* at long times. This reveals that the bath parameters have been chosen such that the dynamics is indeed *incoherent* and no quantum coherent oscillations can be observed. In absence of a static asymmetry ($\varepsilon = 0$), the (averaged) asymptotic population of the left well is clearly 0.5. This holds for the undriven ($s = 0$) as well as for the driven case (resonant driving $s = 1.0,\ \Omega = 0.815$). However, in presence of a bias $\varepsilon = 0.08$, the (averaged) asymptotic population of the left well falls below 0.5. The effect of the additional time-dependent driving is to increase the asymptotic population on the left, see Figs. 3 and 4b. The quantum relaxation rate and the asymptotic population of the left well are studied in greater detail in the subsequent Section VI.

VI. THE QUANTUM RELAXATION RATE

The generalized master equation (58) is an integro-differential equation that governs the decay of the population out of one (metastable) well. However, *to extract analytically one single rate*, which rules the interesting dynamics on the largest time scale, requires further approximations. Motivated by the numerical fact that the decay of the population is observed to be exponential with one single exponent (see Section V.C), we proceed by invoking a Markovian approximation for the GME (58). This approximation yields a set of coupled ordinary first-order differential equations. In the absence of external driving, the corresponding coefficients are time-independent. For a driven system, they depend on the actual time variable t. When the frequency of the periodic external driving is of the order of the frequency associated with the interdoublet energy gap or larger, $\Omega \gtrsim \bar{\omega}_0$, the averaging of the dynamics over a full driving period is appropriate. After averaging, the coefficients of the set of coupled first-order differential equations then assume time-independent values. They form the (time-averaged) rate matrix. *The smallest real part of the eigenvalues of this rate matrix* yields the relevant rate, *the quantum relaxation rate*, which rules the dynamics on the largest time scale.

It is this novel expression for the quantum relaxation rate which constitutes a second major result of this work. On one side, we consider shallow barriers $\Delta U \gtrsim \hbar\omega_0$ as well as high barriers $\Delta U \gg \hbar\omega_0$. In the latter case, the condition for the validity of a semiclassical treatment is met. Put differently, since we deal in our approach with discrete energy eigenvalues, the semiclassical limit is reached when the number of levels below the barrier becomes large. In this case, however, the *numerical* solution of the GME becomes intractable. On the other hand, we may consider temperatures $k_{\rm B}T \approx \hbar\omega_0$, such that the higher lying energy doublets cannot be neglected, as well as lower temperatures $k_{\rm B}T \ll \hbar\omega_0$. In fact, our analysis contains the spin-boson solution, being the appropriate limit when $k_{\rm B}T \ll \hbar\omega_0$ and in the absence of strong resonant driving. Finally, we can allow for large driving amplitudes

and interdoublet resonant driving frequencies. In this latter case, both the restriction to a two-level system as well as an equilibrium semiclassical analysis is prohibited.

In the following Section VI.A, we describe the Markov approximation for the generalized master equation. In Section VI.B, the quantum relaxation rate is determined as the smallest real part of the eigenvalues of the rate matrix.

A. *Markovian Approximation*

The starting point is the generalized master equation (58). The inhomogeneities $I_\mu(t, t_0)$ on the r.h.s. do not contribute to the long-time dynamics since they decay exponentially with time on a rather short time scale; see Eq. (63) for the inhomogeneity in the case of the double-doublet system determined within lowest order in Δ_j. Hence, this term can be neglected.

We assume furthermore that the characteristic memory time $\tau_{\rm mem}$ of the kernels of Eq. (58) is the smallest time scale of the problem (*Markovian limit*). This means that we can substitute the argument of $\rho_{\nu\nu}(t')$ under the integral by the time t and draw $\rho_{\nu\nu}(t)$ in front of the integral. Moreover, the upper limit t of the integral can be replaced by ∞. We then obtain the *Markovian approximated generalized master equation*

$$\dot{\rho}_{\mu\mu}(t) = \sum_{\nu=1}^{M} \Gamma_{\mu\nu}(t)\rho_{\nu\nu}(t) \tag{66}$$

with the time-dependent rate coefficients

$$\Gamma_{\mu\nu}(t) = \int_0^\infty d\tau \mathcal{H}_{\mu\nu}(t, t-\tau). \tag{67}$$

The explicit time-dependence of the rate coefficients reflects the explicit time-dependent external forcing. In the case without external driving, the rate coefficients in Eq. (67) become time-independent.

1. Analytic result for the case without driving. To obtain specific results, we investigate the lowest order for the kernels $\mathcal{H}_{\mu\nu}$. The time independent rate coefficients then read, to lowest second order,

$$\Gamma^{(2)}_{\mu\nu} = \frac{\Delta^2_{\mu\nu}}{2} \int_0^\infty d\tau \exp\{-(q_\mu - q_\nu)^2 S(\tau)\} \cos[(F_\nu - F_\mu)\tau - (q_\mu - q_\nu)^2 R(\tau)], \qquad \mu \neq \nu. \tag{68}$$

The used quantities have been introduced in Eqs. (11), (12), (28), (29), and (30). The conservation of probability requires for the diagonal elements of the second order rate coefficients that $\Gamma^{(2)}_{\nu\nu} = -\sum_{\kappa\neq\nu} \Gamma^{(2)}_{\kappa\nu}$. The integral in Eq. (68) can be solved numerically by standard integration routines [62]. However, an analytical solution can also be derived. In the limit $\omega_c t \to \infty$ [3], the correlation functions $S(t)$ and $R(t)$ assume the form in Eq. (B3) for the real part $S(\tau)$, and in Eq. (B6) for the imaginary part $R(\tau)$. After some basic algebra, we obtain for the Markovian approximated rate coefficients the expression

$$\begin{aligned}\Gamma^{(2)}_{\mu\nu} = {} & \frac{\Delta^2_{\mu\nu}}{4\omega_c} \exp\left\{(F_\nu - F_\mu)\frac{\hbar\beta}{2}\right\} \left(\frac{\hbar\beta\omega_c}{2\pi}\right)^{1-(q_\mu-q_\nu)^2\eta/\pi} \\ & \times \frac{|\Gamma[(q_\mu - q_\nu)^2\eta/2\pi + i\hbar\beta(F_\nu - F_\mu)/2\pi]|^2}{\Gamma[(q_\mu - q_\nu)^2\eta/\pi]},\end{aligned} \tag{69}$$

with $\Gamma(z)$ being the Γ-function [63].

2. High-frequency-driving. To extract an average long-time relaxation rate in the case with driving, we choose the external driving frequency Ω to be of the order of the interdoublet level spacing $\bar{\omega}_0 \approx \omega_0$. This assumption is met, for instance, if one wishes to pump population from the lower to the upper doublet by an interdoublet resonant field. A time-average of the time-dependent rates (Krylov–Bogoliubov scheme) in Eq. (67) over the driving period is then appropriate. In general, this averaging procedure is reasonable when the driving frequency is much larger than the time scales related to tunneling, i.e., when $\Omega \gg \Delta_1^{\mathcal{E}}, \Delta_2^{\mathcal{E}}, \ldots$ where the $\Delta_i^{\mathcal{E}}$ are the tunneling splittings of the doublets.

We insert the explicit shape of the periodic driving $s(t) = s\sin(\Omega t)$ in the second order kernels in Eq. (64). The averaging with respect to the driving frequency reads $\langle \Gamma_{\mu\nu}(t)\rangle_\Omega = (\Omega/2\pi)\int_0^{2\pi/\Omega} dt\, \Gamma_{\mu\nu}(t)$. The integration over t can be performed if one represents the sine- and cosine-function in terms of Bessel functions $J_n(x)$ [63]. The only remaining non-zero part is the one which contains the zeroth Bessel function $J_0(x)$. The time-independent averaged Markovian rate matrix elements to second order emerge as

$$\begin{aligned}\Gamma_{\mu\nu}^{\mathrm{av},(2)} &\equiv \left\langle \Gamma_{\mu\nu}^{(2)}(t)\right\rangle_\Omega \\ &= \frac{\Delta_{\mu\nu}^2}{2}\int_0^\infty d\tau\, \exp\{-(q_\mu - q_\nu)^2 S(\tau)\} J_0\left(\frac{2s}{\Omega}(q_\mu - q_\nu)\sin\left(\frac{\Omega}{2}\tau\right)\right) \\ &\quad \times \cos[(F_\nu - F_\mu)\tau - (q_\mu - q_\nu)^2 R(\tau)], \qquad \mu \neq \nu. \end{aligned} \tag{70}$$

Like in the non-Markovian case, the conservation of probability implies for the diagonal matrix elements the condition $\Gamma_{\nu\nu}^{\mathrm{av},(2)} = -\sum_{\kappa\neq\nu}\Gamma_{\kappa\nu}^{\mathrm{av},(2)}$. This expression reveals that the influence of driving is *different* for each pair of DVR-states since the explicit distance $q_\mu - q_\nu$ enters in the argument of the Bessel functions. The averaged rate matrix elements cannot be calculated in closed analytical form as in the undriven case; however, they can be obtained numerically by standard integration routines [62].

B. *The Quantum Relaxation Rate*

Since the diagonal elements $\rho_{\mu\mu}(t)$ obey Eq. (66), the long-time dynamics in this regime is ruled by a *single exponential decay*. In the case without driving, the rate matrix $\Gamma_{\mu\nu}$ is already time-independent, and equivalently for the case of high-frequency driving after the averaging procedure. Both cases reduce to a structure

$$\dot{\rho}_{\mu\mu}(t) = \sum_{\nu=1}^{M}\Gamma_{\mu\nu}^{(\mathrm{av})}\rho_{\nu\nu}(t), \tag{71}$$

where the superscript (av) means that the formula holds for the averaged as well as for the time-independent case. This set of coupled ordinary first-order differential equations can be decoupled via a diagonalization procedure. If one denotes the elements of the transformation matrix by $S_{\mu\nu}$ and the eigenvalues of the (averaged) rate matrix by Λ_μ, the diagonalized (averaged) rate matrix reads

$$\sum_{\kappa_1,\kappa_2=1}^{M}(S^{-1})_{\mu\kappa_1}\Gamma_{\kappa_1\kappa_2}^{(\mathrm{av})}S_{\kappa_2\nu} = \Lambda_\mu\delta_{\mu\nu}. \tag{72}$$

The general solution of the (averaged) Markov approximated GME is obtained to be

$$\rho_{\mu\mu}(t) = \sum_{\nu,\kappa=1}^{M}S_{\mu\nu}(S^{-1})_{\nu\kappa}e^{\Lambda_\nu(t-t_0)}\rho_{\kappa\kappa}(t_0). \tag{73}$$

Since $\Gamma^{(\mathrm{av})}_{\mu\nu}$ is a stochastic matrix, i.e., the diagonal elements of the (averaged) rate matrix are the negative sum of the matrix elements of the corresponding columns, one eigenvalue equals zero, i.e., $\Lambda_1 = 0$ (conservation of probability). Therefore,

$$\rho_{\mu\mu}(t) = \rho^{\infty}_{\mu\mu} + \sum_{\nu=2}^{M}\sum_{\kappa=1}^{M} S_{\mu\nu}(S^{-1})_{\nu\kappa} e^{\Lambda_\nu (t-t_0)} \rho_{\kappa\kappa}(t_0), \tag{74}$$

with $\rho^{\infty}_{\mu\mu} = \sum_{\kappa=1}^{M} S_{\mu,1}(S^{-1})_{1,\kappa}\rho_{\kappa\kappa}(t_0)$ being the asymptotic population of the DVR-state $|q_\mu\rangle$.

The rate which determines the dynamics on the largest time-scale is the smallest non-zero absolute value of the real part of the eigenvalues of the (averaged) rate matrix, i.e.,

$$\Gamma^{(\mathrm{av})} \equiv \min\{|\mathrm{Re}\Lambda_\nu|; \nu = 2, \ldots, M\}. \tag{75}$$

It is called the *quantum relaxation rate*.

Likewise, the asymptotic population $P^{\infty}_{\mathrm{left}}$ of the left well is readily obtained from Eq. (73). It reads

$$P^{\infty}_{\mathrm{left}} = \sum_{\mu=1}^{L} \rho^{\infty}_{\mu\mu}. \tag{76}$$

To compare the predictions of the Markovian approximated master equation (66) with the results of the generalized master equation (58), we recall the outcomes presented in Figs. 3 and 4 of the previous Section V.C. The Markovian results are indicated by the dashed lines. In all investigated parameter combinations, the agreement among the generalized master equation, the predictions of the QUAPI algorithm, and the Markovian master equation is very good apart from minor differences. The rate of the decay is described accurately by $\Gamma^{(\mathrm{av})}$, as well as the asymptotic population of the left well. Also in presence of a time-dependent driving, the averaging yields the correct averaged dynamics. This allows for the conclusion that, in the investigated range of parameters, the driven dissipative multi-level system is adequately described by the Markovian approximated master equation with the eigenvalues determined from second order gNICA.

VII. RESULTS: QUANTUM RELAXATION RATE AND ASYMPTOTIC POPULATIONS

In this section, we present results for the quantum relaxation rate $\Gamma^{(\mathrm{av})}$ and the asymptotic population $P^{\infty}_{\mathrm{left}}$ inside the left well for the (driven) double-well potential, Eq. (2). Throughout the following sections, we choose a set of typical dimensionless parameter values. The corresponding dimensionful values follow from the standard scaling procedure described in Appendix A. The barrier height is consistently chosen to be $E_{\mathrm{B}} = 1.4$. This implies that two doublets lie below the energy barrier and the other energy states lie above the barrier; see Fig. 2. Moreover the lower tunneling splitting is $\Delta_1^{\mathcal{E}} = 3.60 \times 10^{-3}$, the upper tunneling splitting is $\Delta_2^{\mathcal{E}} = 0.121$, and the energy gap between the two doublets is $\bar{\omega}_0 = 0.815$. This choice is mainly motivated by the fact that we explicitly want to investigate the intermediate regime between the two-level approximation and the semiclassical regime. Furthermore, such a shallow barrier height is convenient for numerical reasons. The splitting of the lowest doublet decreases exponentially with increasing barrier height.

In the following subsections, we investigate on the one hand the double-doublet system, i.e., $M = 4$, for the barrier height $E_{\mathrm{B}} = 1.4$. We expect that the results are qualitatively similar for larger barrier heights when more than two doublets lie *below* the barrier because the spectrum is then similar to the double-doublet case. On the other hand, we study the question of *convergence* with

increasing number M of energy levels for the case of $E_B = 1.4$. For $M \to \infty$, the multi-level system is equivalent to the spatially continuous potential.

We consider two typical situations: The *unperturbed* energy spectrum in the symmetric case ($\varepsilon = 0$) exhibits *avoided level crossings*; see Fig. 6a in Section VII.B.1. The second case refers to a tilted potential with $\varepsilon = 0.08$ where the energy levels are rather *strongly separated*; see Fig. 6a.

The parameters for the time-dependent driving are typically chosen in such a way that the regimes of a weak ($s = 0.1$) and a strong ($s = 1.0$) driving amplitude are covered for both. In the first case, the potential stays permanently bistable while in the second case the potential assumes intermediate monostable configurations. With $E_B = 1.4$, the critical amplitude where bistability vanishes is $s_{crit} = 0.64$. The driving frequency is typically chosen either to be in resonance with the interdoublet energy gap, i.e., $\Omega = \bar{\omega}_0 = 0.815$, or off resonance, i.e., $\Omega = 0.2$.

The typical choice for the temperature is $T = 0.1$, being a low to intermediate temperature. We note that the semiclassical expression for the cross-over temperature [2] yields $T_{co} = 0.12$, keeping in mind, however, that our choice of the barrier height does not obey the semiclassical condition.

We use an Ohmic spectral density with an exponential cut-off; see Eq. (5). The damping constant is chosen to be $\gamma = 0.1$; it represents an intermediate damping strength. We note that the dependence of the results on the damping strength and temperature is exponential. The cut-off frequency is always fixed to be $\omega_c = 10.0$.

Finally, we note that in the following symbols such as ● and □ are used to label individual plots in the particular figures. Their number is not related to the number of calculated data points, the latter being much larger.

A. *Absence of External Driving*

We start with the simplest case of the undriven symmetric double-well potential ($s = 0, \varepsilon = 0$) and consider the dependence of the quantum relaxation rate on the number M of energy eigenstates. $M = 4$ denotes the double-doublet system. Figure 5 shows the result for different damping constants γ. A convergence of the rate Γ can be observed for an intermediate damping strength $\gamma = 0.1\,(*)$. We recall that the lowest tunneling splitting is two orders of magnitude smaller than γ and that the upper tunneling splitting is of the same order of magnitude as γ. For a larger damping constant

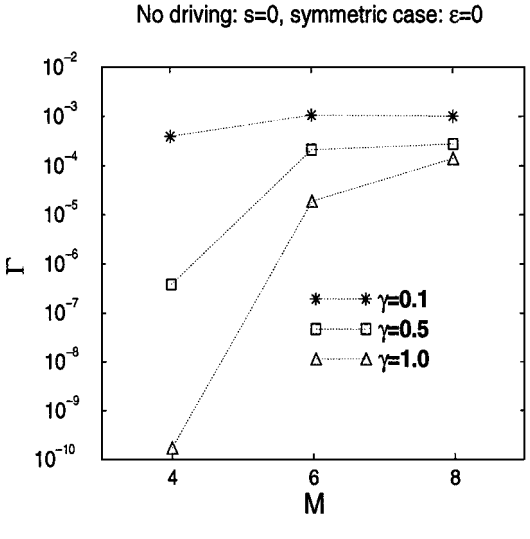

FIG. 5. Quantum relaxation rate Γ for the static symmetric double-well potential with barrier height $E_B = 1.4$ in dependence of the number M of energy eigenstates for the damping constants $\gamma = 0.1\,(*)$, $\gamma = 0.5\,(\square)$, and $\gamma = 1.0\,(\triangle)$. The temperature is chosen to be $T = 0.1$ and the cut-off frequency is $\omega_c = 10.0$.

$\gamma = 0.5$ (□), convergence is also obtained. However, for the case of very strong damping $\gamma = 1.0$ (△), the result for $M = 8$ does not coincide with that for $M = 6$. This fact is due to the following feature: As it can be seen from Eq. (64) for the second order kernels of the generalized master equation, the damping constant γ, which enters via $S(t)$ and $R(t)$, is multiplied by $(q_\mu - q_\nu)^2$ being the square of the tunneling distance between the two involved DVR-states. Upon increasing the number M of energy levels, the DVR-eigenvalues lie more dense in position space. Hence, some distances become small and the multilevel system effectively *flows to weak damping*. The small effective damping is no longer sufficient to suppress long intervals in the off-diagonal states. Thus, the gNICA in *second* order is no longer applicable and contributions of higher orders of the integral kernels in the GME have to be taken into account. A more detailed discussion of the effect of the flow to weak damping is postponed to the Appendix F.

The question of convergence of the quantum relaxation rate with increasing M in the presence of time-dependent driving is investigated in the sections below.

B. *The Influence of External (Time-Dependent) Driving Forces*

In this subsection we investigate the role of external driving. This external perturbation can be either a static potential asymmetry (*bias*) or a time-dependent periodic driving (*ac-driving*), or simultaneously both parts are present.

1. Dependence on a static bias, no ac-driving. Adding a static asymmetry renders one (in our case the left) of the two formerly stable potential minima a metastable minimum. The consequences for the spectrum of the *bare* system are that avoided level crossings occur for particular values of the asymmetry; see Fig. 6a. At such avoided level crossings tunneling is usually enhanced. This effect is known as resonant tunneling. This situation, however, is modified in the presence of a moderate to strong damping. The case of a strong system-bath coupling is considered in Fig. 6b where the relaxation rate shows peaks at particular values of the static bias. Their position strongly depends on temperature. At low temperatures $T = 0.05$ to $T = 0.15$ (full lines), we observe three relative maxima at $\varepsilon = 0$ and around $\varepsilon = 0.12$ and $\varepsilon = 0.25$. First, we emphasize that the quantum relaxation rate *initially decreases* when the bias is increased from zero, i.e., when the effective barrier height is *decreased*. This feature is a typical quantum mechanical footprint. In a classical system, the relaxation rate *grows* when the barrier is *lowered* [2]. Second, we note that the two peaks at nonzero bias values

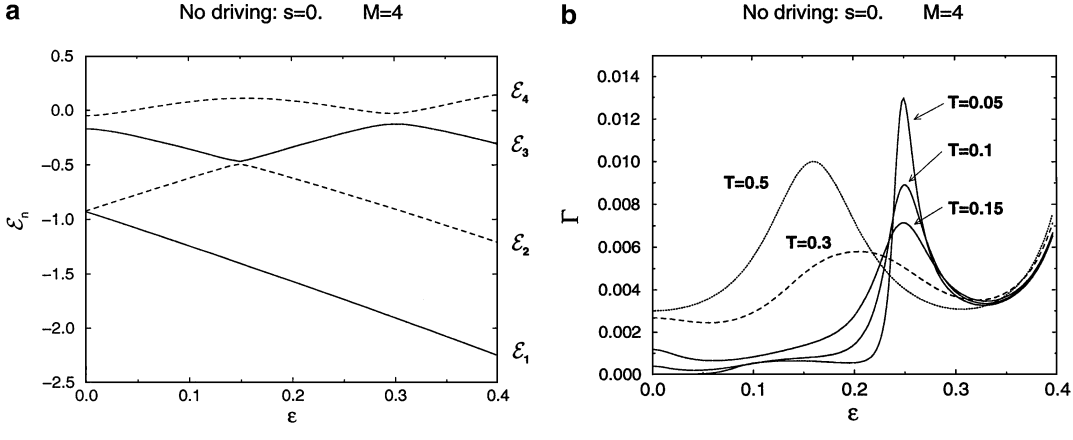

FIG. 6. (a) Spectrum of the unperturbed static ($s = 0$) system Hamiltonian (1) for a barrier height of $E_B = 1.4$ as a function of the static bias ε. (b) Quantum relaxation rate Γ according to Eq. (75) as a function of the static bias ε for different temperatures T. The barrier height is $E_B = 1.4$ and the number of energy levels is $M = 4$. The bath parameters are $\gamma = 0.1$ and $\omega_c = 10.0$.

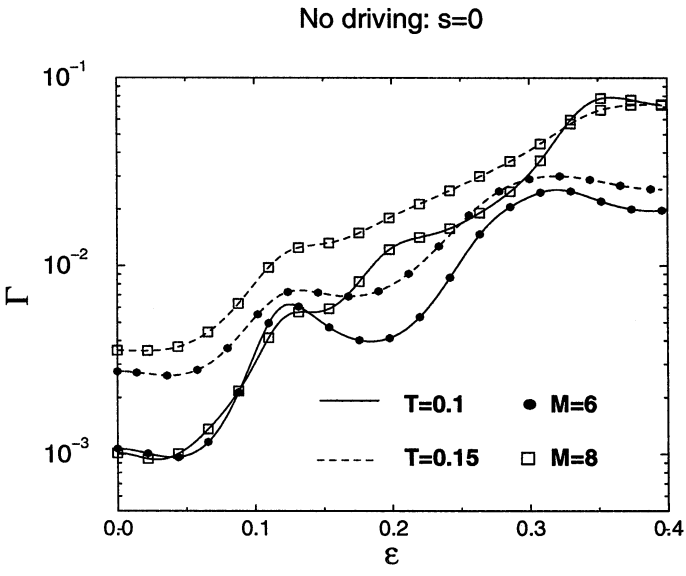

FIG. 7. Quantum relaxation rate Γ as a function of the static bias ε for four different combinations of the number of levels, i.e., $M = 6$ (●) and $M = 8$ (□), and different temperatures, i.e., $T = 0.1$ (solid line) and $T = 0.15$ (dashed line). For the remaining parameters, see Fig. 6.

are shifted to smaller values of the asymmetry compared to those bias strengths where the avoided level crossings occur; see Fig. 6a. This indicates that we are no longer in a weak-coupling regime but encounter already strong incoherent tunneling.

Increasing the temperature results in a decrease of the amplitude of the peak at $\varepsilon = 0.25$. This indicates the enhanced destruction of the resonant tunneling phenomenon. Moreover, the peaks broaden. At an intermediate temperature $T = 0.3$ (dashed line) one characteristic peak occurs at $\varepsilon = 0.2$. Its height is smaller than in the low temperature cases which indicates that tunneling is reduced compared to the low temperature case. This is mainly due to the enhanced environmental level broadening. However, we still observe a clear decrease of Γ when the bias is increased from zero onwards; therefore we conclude that quantum tunneling still occurs. This, however, is no longer observable for the high temperature case $T = 0.5$ (dotted line). A relaxation rate which grows with increasing bias is a signature of classical behavior.

The question of the convergence of the rate with an increasing number M of energy states is addressed with Fig. 7. We show four different cases for $M = 6$ (●) and $M = 8$ (□) and $T = 0.1$ (full line) and $T = 0.15$ (dashed line), respectively. The low temperature case $T = 0.1$ shows a clear convergence when M is increased from $M = 6$ to $M = 8$ for small asymmetries up to $\varepsilon = 0.15$. For larger asymmetries, the two results, however, do not agree. This behavior can be resolved as follows: For large asymmetries, the left well is strongly lifted above the right well. Moreover, the position eigenvalues on the left side move towards each other and are densely located. This means that the tunneling distance of the corresponding transition becomes smaller which in turn reduces the effective damping. Then a *flow to weak damping* occurs and the second order gNICA breaks down. The same explanation holds for the larger temperature $T = 0.15$ where the results for $M = 6$ and $M = 8$ show qualitatively a similar behavior up to $\varepsilon = 0.15$.

We investigate in the following the asymptotic population P_{left}^{∞} of the left well determined in Eq. (76). For the symmetric case, it assumes the value $1/2$. In presence of a positive asymmetry $\varepsilon > 0$, P_{left}^{∞} is smaller than $1/2$ since the left well is energetically higher. Figure 8 shows P_{left}^{∞} as a function of ε for two different temperatures (solid line) for $M = 8$. The damping constant is chosen to be $\gamma = 0.1$. For comparison we additionally show the asymptotic population obtained from a Boltzmann

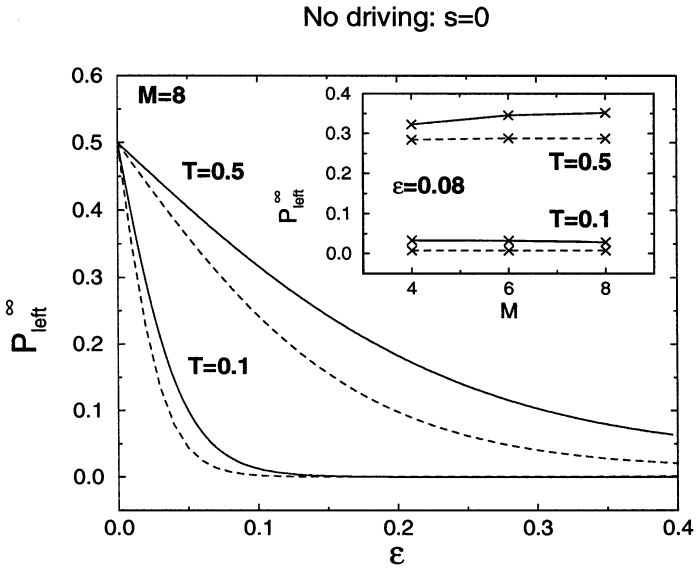

FIG. 8. Asymptotic population $P_{\rm left}^{\infty}$ of the left well in absence of time-dependent driving as a function of the asymmetry ε for two different temperatures (solid line) for $M = 8$. The parameters are $E_{\rm B} = 1.4$, $\gamma = 0.1$, and $\omega_c = 10.0$. The dashed line marks the results obtained from a Boltzmann equilibrium distribution for the same parameters. Inset: $P_{\rm left}^{\infty}$ vs the number M of energy levels for a fixed asymmetry $\varepsilon = 0.08$ (solid line, gNICA in second order; dashed line, with Boltzmann distribution).

equilibrium distribution for the same parameters (dashed line), i.e., $\rho(\infty) = \exp(-\mathbf{H}_0/k_{\rm B}T)$. First, we note that the asymptotic population decreases exponentially with increasing bias. Second, we emphasize that the often made assumption of a Boltzmann equilibrium distribution is only valid for an infinitesimally small coupling of the system to the environment [64]. The depicted results for $M = 8$ have already been converged and are not distinguishable on our scale from the $M = 6$ case. This is indicated in the inset of Fig. 8 for a fixed asymmetry $\varepsilon = 0.08$ for two different temperatures. Convergence is also found for the entire considered parameter range of ε (not shown). The full line again shows the result obtained from gNICA in second order while the dashed line marks the results from a Boltzmann equilibrium distribution.

2. Dependence on the static bias in presence of external ac-driving. The influence of a time-dependent periodic driving on the quantum relaxation rate is elucidated with Figs. 9–11.

For the case of off-resonant driving, Fig. 9 exhibits a non-monotonic dependence of the averaged relaxation rate $\Gamma^{\rm av}$ on the bias. For increasing M the results approach each other. However, a complete convergence as observed in the undriven case (Fig. 7) is not obtained.

Tuning the driving frequency Ω into resonance, the results in Fig. 10 show for a fixed driving strength a characteristic peak, being almost independent of the temperature T. The position of the peak is sensitive to the driving strength. This indicates that the population of the upper doublet is mainly the result of driving and not due to thermal population.

Furthermore, we draw the reader's attention to the strongly ($s = 1.0$) driven symmetric case $\varepsilon = 0$. The low temperature relaxation rate for $T = 0.1$ is larger than for the two other cases with higher temperatures. This is opposite to the situation *without* driving, see Fig. 6b, where Γ is *smaller* for $T = 0.1$ compared to $T = 0.5$. This is a typical footprint of a quantum effect: The resonant driving ($\Omega = 0.815$) in the symmetric potential transfers population to the upper doublet where tunneling is enhanced because the tunneling splitting is large and the temperature is not high enough to destroy coherence completely.

The problem of convergence of the results with increasing M is addressed in Fig. 11 for the resonantly driven case. Shown are four different combinations for $M = 6$ (●) and $M = 8$ (□) for

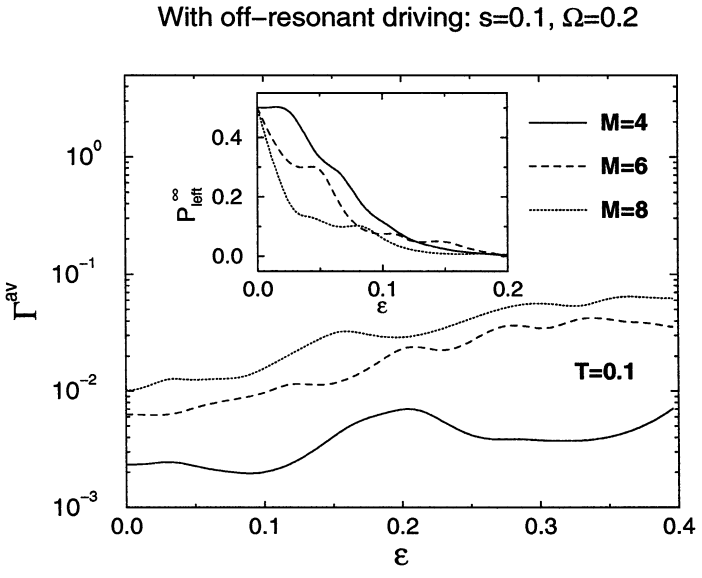

FIG. 9. Averaged quantum relaxation rate $\Gamma^{\rm av}$ as a function of the static bias ε in presence of an off-resonant driving with $s = 0.1$, $\Omega = 0.2$. Shown are the results for three different numbers M of energy levels. The parameters are $E_{\rm B} = 1.4$, $T = 0.1$, $\gamma = 0.1$ and $\omega_c = 10.0$. Inset: The corresponding asymptotic populations $P^{\infty}_{\rm left}$ of the left well as a function of ε.

two temperatures $T = 0.1$ (full line) and $T = 0.15$ (dashed line). We ascertain that no convergence is obtained upon increasing M. The difference between the results for $M = 6$ and $M = 8$ for this large driving frequency is larger than in the case of off-resonant driving; see Fig. 9. Obviously, more than only a few energy eigenstates are necessary to describe the resonantly driven double-well

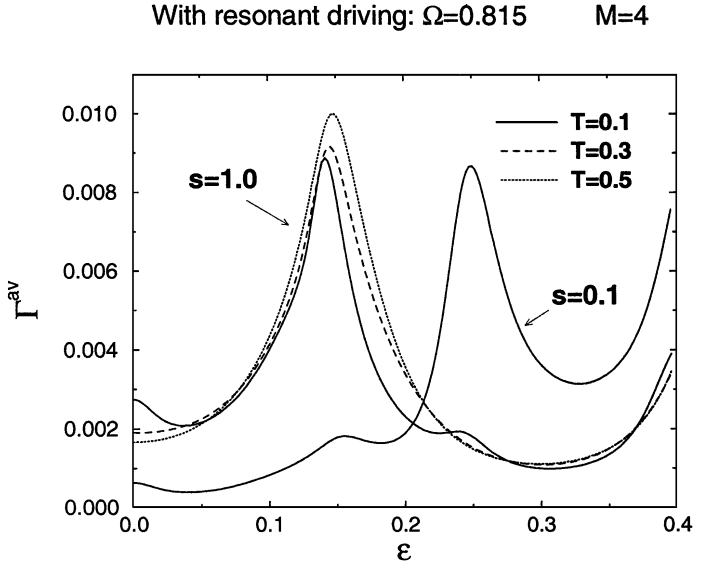

FIG. 10. Averaged quantum relaxation rate $\Gamma^{\rm av}$ as a function of the static bias ε for three different temperatures $T = 0.1$ (solid line), $T = 0.3$ (dashed line), and $T = 0.5$ (dotted line) for the resonantly driven double-doublet system $M = 4$. Shown are the cases of weak driving $s = 0.1$ (for $T = 0.1$ only) and strong driving ($s = 1.0$). For the remaining parameters, cf. Fig. 9.

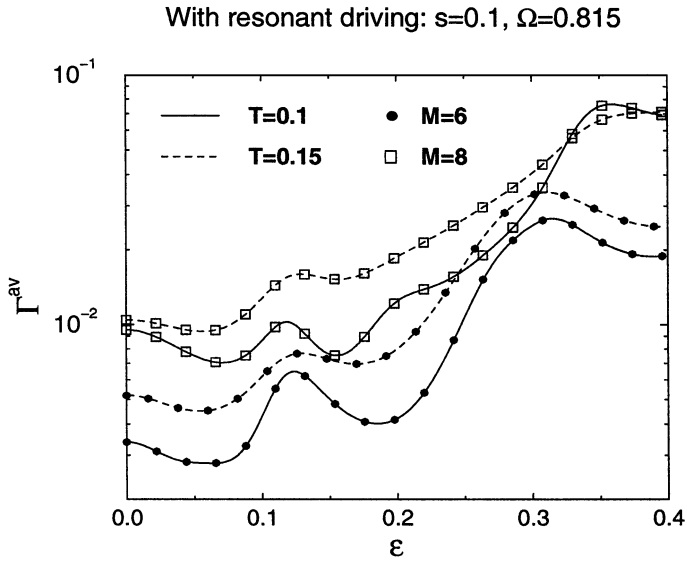

FIG. 11. Γ^{av} as a function of the static bias ε for four different combinations of the number of levels, i.e., $M=6$ (●) and $M=8$ (□), and different temperatures, i.e., $T=0.1$ (solid line) and $T=0.15$ (dashed line). For the remaining parameters, see Fig. 9.

potential accurately. This is not astonishing, however, because the driving frequency is in resonance ($\Omega=0.815$) and many higher energy levels are excited. Moreover, we stress that the results vary *within* the same order of magnitude.

The asymptotic population P_{left}^{∞} of the left well is shown in Fig. 12 as a function of the static bias ε for three different temperatures. The driving frequency is in resonance with the interdoublet

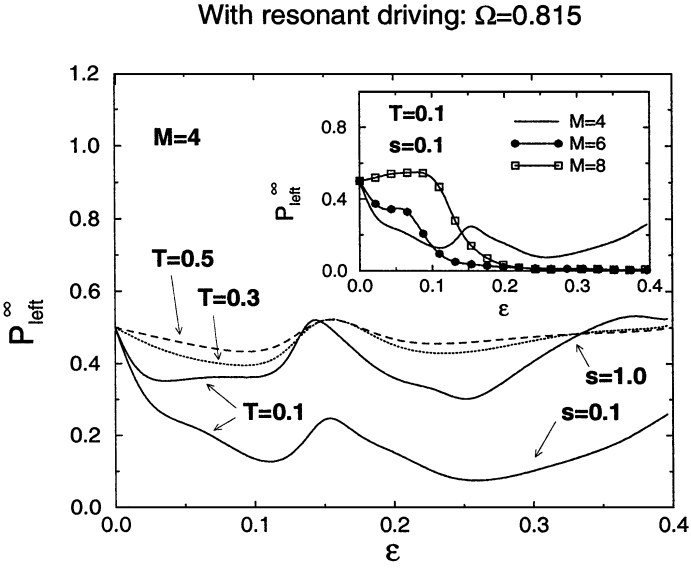

FIG. 12. Asymptotic population P_{left}^{∞} of the left well as a function of the asymmetry ε for the temperatures $T=0.1$ (solid line), $T=0.3$ (dotted line), and $T=0.5$ (dashed line) for the double-doublet system $M=4$. Shown are results for strong driving $s=1.0$ and for weak driving $s=0.1$ (for $T=0.1$ only). For the remaining parameters, see Fig. 9. Inset: P_{left}^{∞} vs the static bias ε for a fixed temperature $T=0.1$ for $M=4$ (solid line), $M=6$ (□), and $M=8$ (●).

energy gap. Compared to the strict monotonic behavior of the undriven case, see Fig. 8, the results with strong driving ($s = 1.0$) show a non-monotonic dependence on the static bias with a distinct maximum at $\varepsilon = 0.15$ being nearly independent of T. This maximum has a value of $P_{\text{left}}^{\infty} \approx 0.5$ indicating an equal population of both the metastable as well as the stable well. The position of this local maximum is invariant under the choice of the driving strength, as indicated by the weak driving result for ($s = 0.1$). We note that a net population inversion can be achieved for the parameter combinations $M = 4$, $T = 0.1$, $s = 1.0$, $\varepsilon = 0.14$. It is interesting to see that convergence of P_{left}^{∞} with increasing M is obtained for asymmetries $\varepsilon > 0.2$; see inset of Fig. 12. For smaller values of the bias the qualitative behavior in the case of $M = 6$ is similar to the case of $M = 8$. However, the local maximum around $\varepsilon = 0.15$ in the double-doublet case $M = 4$ vanishes upon increasing M.

3. Dependence on the driving strength. Figure 13 depicts the averaged rate as a function of the amplitude s of the ac-driving field with resonant driving frequency $\Omega = \bar{\omega}_0 = 0.815$ for the symmetric double-doublet system ($\varepsilon = 0$, $M = 4$). Shown are the results for three different temperatures. The asterisks $*$ mark the results of an exponential fit to QUAPI results (not shown) and confirm the validity of our new analytical approach.

The averaged rate for the case of a high temperature $T = 0.5$ is reduced compared to the undriven situation where $\Gamma^{\text{av}}(\equiv\Gamma)$ has a maximum. Upon decreasing the temperature, the relative maximum at $s \approx 0.9$ grows out to a global maximum for $T = 0.1$. This resonance is useful for practical applications ("Hydrogen subway," see Section 1.A) if one desires to accelerate the transfer of population from the left to the right well. So not only a resonant driving frequency $\Omega = \bar{\omega}_0$ but also a suitably chosen driving strength is important to maximize the transfer. The behavior of Γ^{av} vs the driving amplitude is shown in Fig. 14 for an increasing number M of energy states (note the logarithmic scale). For small driving strengths (up to $s \approx 0.2$), the result for $M = 10$ does not significantly differ from the case for $M = 8$, indicating numerical convergence. For intermediate to strong driving, the differences increase. However, we stress that the results for $M = 8$ and $M = 10$ remain within the same order of magnitude.

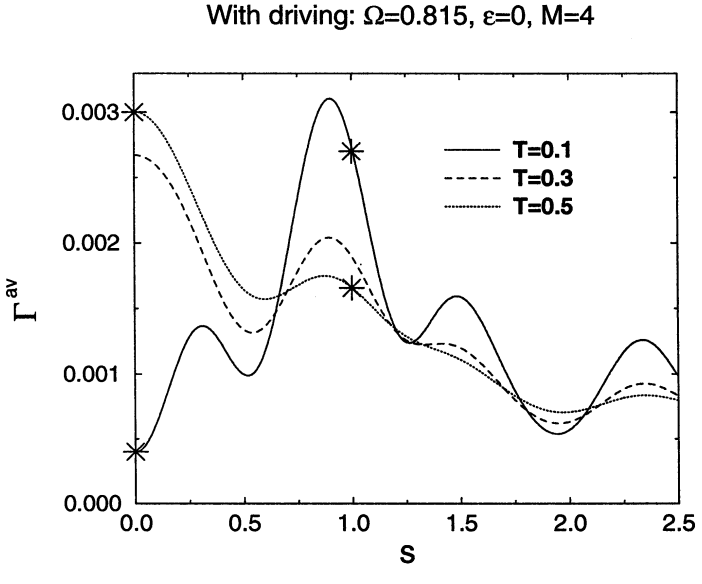

FIG. 13. Averaged quantum relaxation rate Γ^{av} as a function of the driving amplitude s for three different temperatures $T = 0.1$ (solid line), $T = 0.3$ (dashed line), and $T = 0.5$ (dotted line) for the driven symmetric ($\varepsilon = 0$) double-doublet system $M = 4$. The static barrier height is $E_{\text{B}} = 1.4$ and the driving frequency is $\Omega = \bar{\omega}_0 = 0.815$. The bath parameters are $\gamma = 0.1$ and $\omega_c = 10.0$. The asterisks $*$ mark the findings of an exponential fit to QUAPI results (not shown).

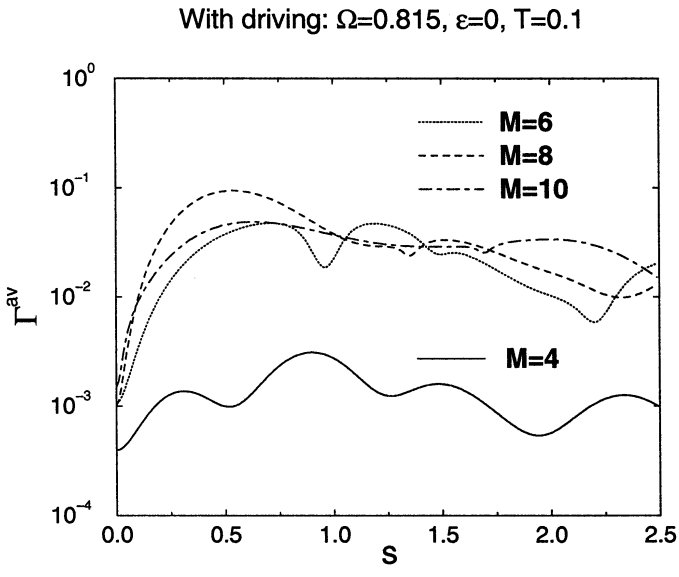

FIG. 14. Γ^{av} as a function of the driving amplitude s for an increasing number of levels. The temperature is fixed to $T = 0.1$. For the remaining parameters, see Fig. 13.

4. Dependence on the driving frequency. The dependence of the averaged relaxation rate on the driving frequency is shown in Fig. 15 for the symmetric and the asymmetric double-doublet system $M = 4$. The results can be viewed as a scan of the spectrum of the driven dissipative double-doublet system. At some values of Ω the transition from the left to the right well is enhanced. The intermediate damping constant $\gamma = 0.1$ leads to a considerable broadening of the energy levels involved in the transitions, as can be deduced from the rather broad resonance lines. The symmetric (asymmetric)

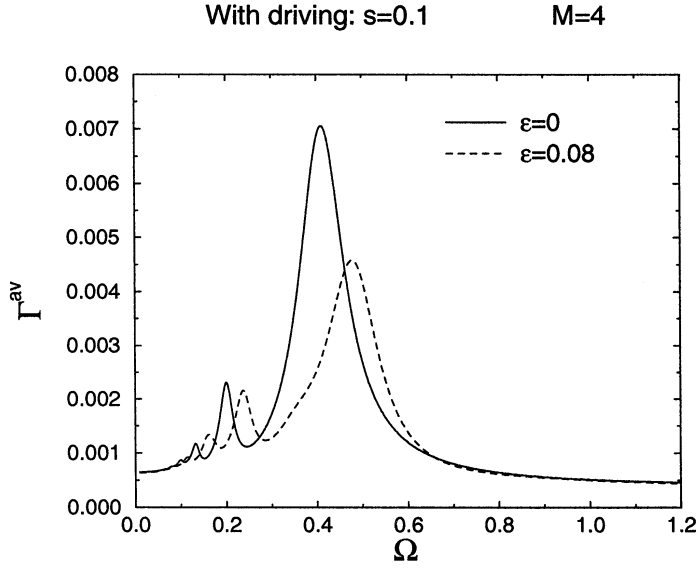

FIG. 15. Averaged quantum relaxation rate Γ^{av} as a function of the driving frequency Ω for the driven symmetric (solid line) and the asymmetric (dashed line) double-doublet system $M = 4$. The static barrier height is $E_B = 1.4$ and the driving strength is $s = 0.1$. The bath parameters are $T = 0.1$, $\gamma = 0.1$, and $\omega_c = 10.0$.

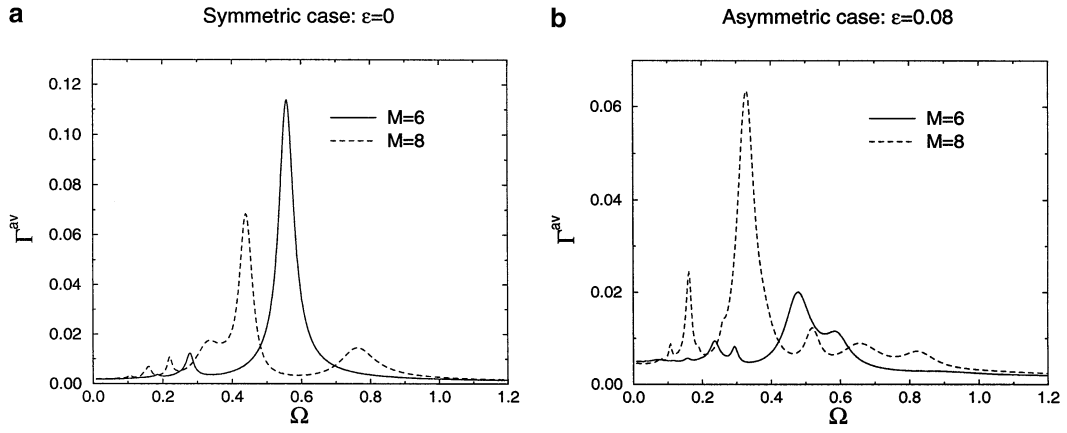

FIG. 16. Γ^{av} as a function of the driving frequency Ω for different numbers M of levels. (a) symmetric case $\varepsilon = 0$, (b) asymmetric case $\varepsilon = 0.08$. The remaining parameters are as in Fig. 15.

case reveals a distinct peak at $\Omega = 0.4$ ($\Omega = 0.5$) together with sidebands at the corresponding fractions of Ω. The behavior of Γ^{av} for an increasing number M of energy levels is depicted in Fig. 16a for the symmetric case and in Fig. 16b for the asymmetric case. It can be seen that the additional energy levels yield additional resonance lines. However, if one chooses the driving frequency sufficiently far from any resonance line, convergence can be achieved.

The asymptotic population $P_{\mathrm{left}}^{\infty}$ of the left well as a function of the driving frequency Ω is depicted in Fig. 17 for an increasing number M of states. Clearly, the results do in general not converge with growing M. This confirms our result that for an accurate description of a strongly driven quantum system more than only a few basis states are required.

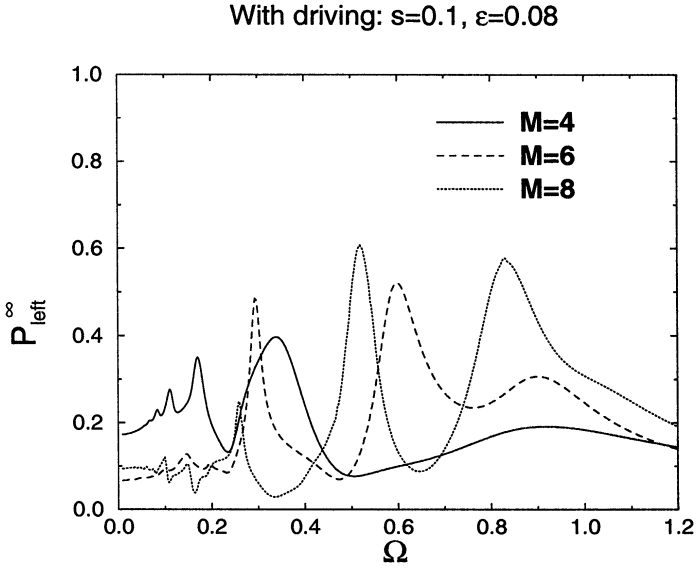

FIG. 17. Asymptotic population $P_{\mathrm{left}}^{\infty}$ of the left well as a function of the driving frequency Ω for an increasing number M of states. The driving amplitude is $s = 0.1$ and the static bias is $\varepsilon = 0.08$. The temperature is fixed at $T = 0.1$, the damping constant is chosen to be $\gamma = 0.1$, and the cut-off is $\omega_c = 10.0$.

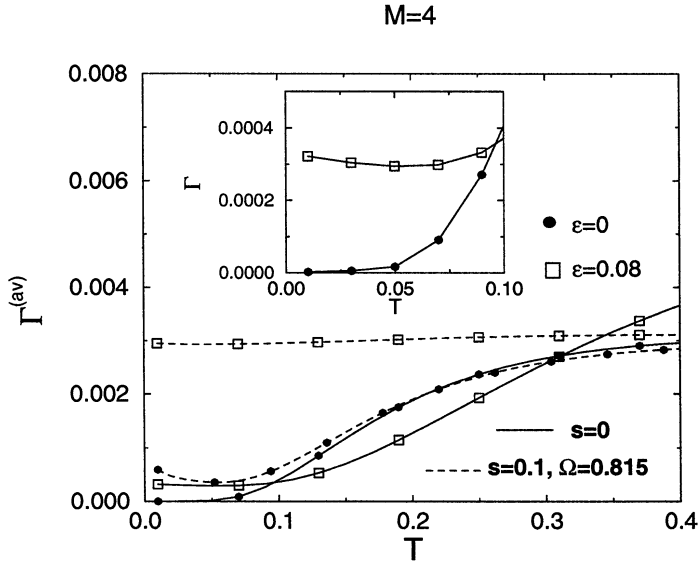

FIG. 18. (Averaged) Quantum relaxation rate $\Gamma^{(\mathrm{av})}$ as a function of temperature T for four different combinations of the undriven ($s=0$) and the resonantly driven ($s=0.1$, $\Omega=0.815$) case without ($\varepsilon=0$) and with ($\varepsilon=0.08$) static bias for the double-doublet system $M=4$. The parameters are $E_{\mathrm{B}}=1.4$, $\gamma=0.1$, and $\omega_c=10.0$. Inset: Enlarged part of the low temperature regime for the undriven case $s=0$.

C. *Dependence on the Bath Parameters*

1. Influence of temperature. The dependence of the quantum relaxation rate on temperature is depicted in Fig. 18 for the case of the double-doublet system $M=4$. Shown are four cases without ac-driving ($s=0$), with resonant ac-driving ($s=0.1$, $\Omega=0.815$), without bias ($\varepsilon=0$), and with bias ($\varepsilon=0.08$). We first concentrate on the undriven case $s=0$ (full line). Interestingly enough, we find in the low temperature regime (see inset of Fig. 18) that the rate first *decreases* when the temperature is *increased* in the presence of a static bias. This is a characteristic quantum feature: In contrast to a classical behavior, the quantum relaxation rate first decreases with increasing temperature due to an enhancement of decoherence. Then, however, the rate starts to increase again as soon as the higher doublet becomes thermally populated. This typical behavior has also been observed experimentally in the context of tunneling of impurities in solids [37–42] (see also Section IA and especially Ref. [39]). For the intermediate temperature regime the comparison between the symmetric and the asymmetric case reveals another interesting characteristic: One could argue that the almost linear increase of the rate with temperature reveals a classical Arrhenius behavior. This, however, is not the case. We are still in a deep quantum regime, since Γ in the asymmetric case is *smaller* than in the symmetric case! This is again a clear sign of quantum mechanics since the symmetric potential with $\varepsilon=0$ corresponds to a resonant tunneling situation. A finite bias of $\varepsilon=0.08$ implies a non-resonant tunneling situation. There, the transfer via resonant tunneling is suppressed and the rate becomes smaller. In the regime of intermediate to high temperatures, this behavior is inverted, i.e., the rate for the asymmetric case with reduced barrier height is now larger as compared to the symmetric case.

In the presence of a weak resonant ac-driving $s=0.1$, $\Omega=0.815$, the quantum relaxation rate Γ^{av} for the symmetric case $\varepsilon=0$ at low temperature is larger than the corresponding undriven relaxation rate. Coherent excitations to the upper doublet where tunneling is enhanced dominate at low temperature. The presence of an additional static bias $\varepsilon=0.08$ renders the averaged relaxation rate Γ^{av} almost independent of temperature.

The question of convergence of the rate with increasing the number M of energy eigenstates is addressed in Fig. 19a for the undriven case $s=0$ and in Fig. 19b for the off-resonantly driven case

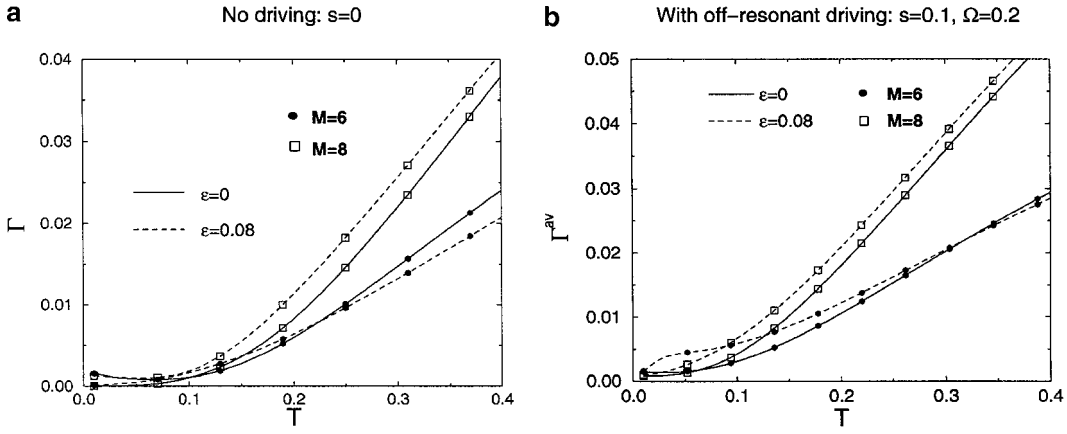

FIG. 19. $\Gamma^{(av)}$ as a function of temperature T for different numbers M of levels. (a) No ac-driving $s = 0$, (b) with weak off-resonant ac-driving $s = 0.1$, $\Omega = 0.2$. The remaining parameters are as in Fig. 18.

$s = 0.1$, $\Omega = 0.2$. In absence of ac-driving, a satisfactory convergence between the cases $M = 6$ and $M = 8$ is achieved in the low temperature regime for both the symmetric and the asymmetric potential. Clearly for higher temperatures the agreement is worse because now the higher lying energy states are not negligible. Also in presence of an off-resonant ac-driving, convergence is achieved at low temperatures.

The asymptotic population P_{left}^{∞} of the left well as a function of the temperature T is shown in Fig. 20 for an increasing number M of states. The results for the undriven case $s = 0$ reveal a satisfactory convergence over the entire temperature regime. For comparison, we also depict the asymptotic population stemming from the assumption of a Boltzmann equilibrium distribution. A similar argumentation as in Section VII.B.I (see Fig. 8) holds to explain the disagreement.

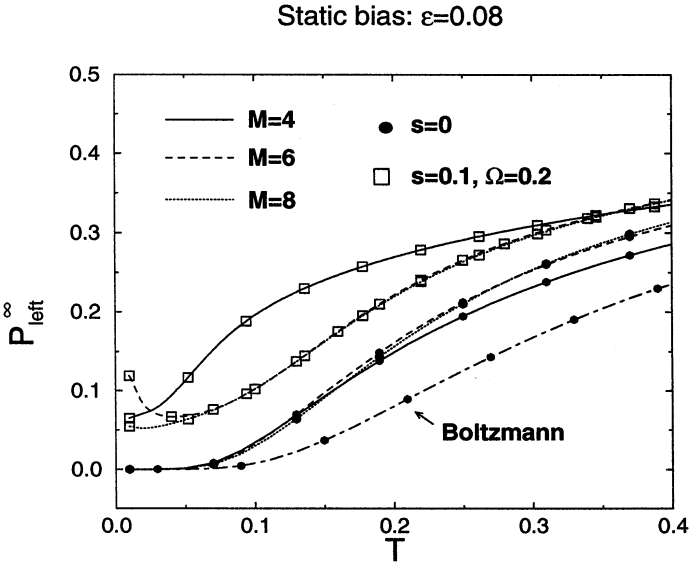

FIG. 20. Asymptotic population P_{left}^{∞} of the left well as a function of temperature T for an increasing number M of states. The static bias is $\varepsilon = 0.08$. Shown are the case without ac-driving $s = 0$ together with the results obtained from a Boltzmann equilibrium distribution (dashed-dotted line) and the case with off-resonant ac-driving $s = 0.1$, $\Omega = 0.2$. The remaining parameters are as in Fig. 18.

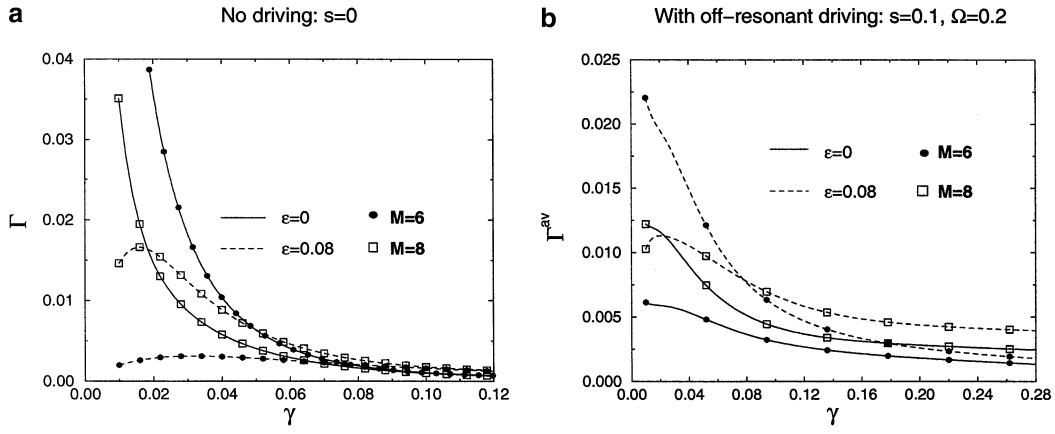

FIG. 21. (Averaged) Quantum relaxation rate $\Gamma^{(\mathrm{av})}$, respectively, as a function of the damping strength γ for different numbers M of levels. (a) No ac-driving $s = 0$, (b) with off-resonant ac-driving $s = 0.1$, $\Omega = 0.2$. Shown are the results for the cases without ($\varepsilon = 0$) and with ($\varepsilon = 0.08$) static bias. The parameters are $E_{\mathrm{B}} = 1.4$, $T = 0.1$, and $\omega_c = 10.0$.

2. Influence of damping. Figure 21 depicts the (averaged) rate vs γ for an increasing number M of states. We find for the undriven case $s = 0$ in Fig. 21a convergence for $\gamma \geq 0.08$ for both the symmetric and the asymmetric potential. However, for smaller γ notable differences occur which indicate that the gNICA to second order is not reliable because the effective damping becomes too weak (effect of flow to weak damping, see discussion in Appendix F). The situation is similar in the presence of an off-resonant ac-driving $s = 0.1$, $\Omega = 0.2$; see Fig. 21b. The results for the case of a resonant driving $\Omega = \bar{\omega}_0$ are qualitatively similar (not shown).

VIII. CONCLUSIONS AND OUTLOOK

A *novel* scheme to investigate analytically as well as numerically tunneling and vibrational relaxation in a strongly driven bistable potential was presented. A necessary first step in our approach is the reduction of the system dynamics to the Hilbert space spanned by the M lowest energy eigenstates of the static bistable potential. Because the coupling to the heat bath is bilinear in the system and bath coordinates, the convenient basis to perform calculations consists of the eigenbasis of the position operator, i.e., the so-termed discrete variable representation (DVR). It is this DVR basis which permitted us to derive a set of non-Markovian generalized master equations (GME) for the diagonal elements of the reduced density matrix. In the studied regime of temperature and damping, the Markovian approximation to the GME yields novel analytical results. They agree well, both with those of the full GME and of precise *ab-initio* numerical path integral calculations. In turn, the *quantum relaxation rate* could be extracted from the Markovian rate matrix. The dependence of the quantum relaxation on the five most relevant model parameters, namely bias strength ε, driving strength s, driving frequency Ω, temperature T, and damping γ, was outlined in detail.

We have identified several quantum mechanical footprints in this strongly damped system. The four most pronounced quantum features are:

(i) In absence of ac-driving we find resonant incoherent tunneling. This is demonstrated by striking resonances in the relaxation rate at distinct values of the dc-bias.

(ii) We observe a decrease of the relaxation rate as the effective barrier is lowered by a static bias. This finding is due to a reduction of tunneling since the energy gaps forming the tunneling doublets increase with increasing asymmetry. In contrast, the relaxation rate in a classical system always increases for a reduced barrier.

(iii) The ac-driven quantum system shows distinct resonances of the relaxation rate for particular values of the driving amplitude. Especially at low temperature, the relaxation rate is enhanced by driving as compared to the undriven case.

(iv) A *non-monotonic* dependence of the relaxation rate on temperature is observed. Increasing the temperature in a classical system always increases the rate. However, in a quantum system, a higher temperature induces a larger population of the energetically higher lying doublets, where tunneling is favored. Increasing temperature further renders the quantum system more incoherent and the relaxation via tunneling is again hampered. The rate therefore decreases before it grows again due to thermal hopping.

Our analysis furthermore permits us to determine the asymptotic population of the left metastable well. We have shown explicitly that a Boltzmann equilibrium distribution (both in absence and in presence of an ac-field) is *not* attained for the chosen set of parameters.

The GME in Eq. (58) and its time-inhomogeneous Markov approximation in Eq. (66) treat the external driving field *exactly* and are reliable for moderate temperatures and/or moderate damping strengths. Indeed, the equations become exact for Ohmic dissipation at high temperatures. Thus, our approach complements a Redfield-type analysis being appropriate for weak damping. In contrast to semiclassical calculations we can consider shallow potential barriers substaining only a few doublets below the barrier. Moreover, in contrast to semiclassical imaginary-time rate calculations, we are not limited by the requirement of thermal equilibrium at adiabatically varying external fields.

A major restriction of the presented method is that the generalized non-interacting cluster approximation (gNICA) that we used to obtain the GME turns out to be useful *in praxi* for numerical purposes only when (i) the number M of levels remains moderately small ($M \leq 10$), and when (ii) the truncation of the gNICA kernels in Eq. (59) to lowest order in $\Delta_{\mu\nu}^2$ is appropriate; see Eq. (64). Clearly, the number M of levels involved in the dynamics increases with increasing temperature and/or for large driving strengths s, and/or for resonant driving frequencies Ω.

Taking into account a larger number M of basis states implies that the position eigenvalues lie more dense in position space (in the limit of infinitely many energy eigenstates the distance between neighboring DVR-points is infinitesimally small). However, we have observed in the preceding sections that the square of the distance between two DVR-points enters as a prefactor for the twice integrated bath autocorrelation function $S(t) + iR(t)$ in the second order kernels in Eq. (64) of the generalized master equation. This implies that upon increasing M the effective damping of each transition is reduced and the multi-level system effectively *flows to weak damping*. For small effective damping the noise action does no longer suppress long intervals in the off-diagonal states (clusters) and higher than second order transitions start to contribute.

To deal with this effective weak coupling situation (which occurs for large M even when the global coupling constant $\gamma = \eta/\mathcal{M}$ is not small), a procedure similar to the one used by Zwerger [65] and Grabert *et al*. [66] to investigate transport in Josephson junctions can be used; see Appendix F.

Due to its very general nature, the newly developed analytical technique contains a large potential for applications to specific experimental situations. Several possible applications for experimental systems have been discussed in Section I.A.

A prominent question for future work refers to the behavior of the crossover to the classical regime. Our results should merge into those of the quantum Kramers rate [2] for semiclassical barrier heights, i.e., $\Delta U/(\hbar\omega_0) = E_{\rm B} \gg 1$, in the case without ac-driving. Once this regime is explored, the method can be generalized to time-dependent semiclassical quantum systems. However, one has to be aware that for the driven system a chaotic dynamics generally occur [68]. We expect that the dynamics in the semiclassical regime involves an increasing number M of DVR states. Then the effect of the flow to weak damping occurs. The analysis in Appendix F represents the starting point for future investigations towards this challenge.

APPENDIX A

Scaling to Dimensionless Quantities

For the specific calculations, we introduce in this Appendix dimensionless quantities. They are obtained by scaling the Hamiltonian in Eqs. (1) and (2) and the environmental parameters specified in the Eqs. (5) and (6). The relations read

$$\tilde{t} = \omega_0 t, \qquad \tilde{q}(\tilde{t}) = \sqrt{\mathcal{M}\omega_0/\hbar}\, q \left(t = \frac{\tilde{t}}{\omega_0}\right), \qquad E_{\mathrm{B}} = \Delta U/\hbar\omega_0,$$
$$\tilde{\varepsilon} = \varepsilon\sqrt{\mathcal{M}\omega_0/\hbar}\,/\hbar\omega_0, \qquad \tilde{s} = s\sqrt{\mathcal{M}\omega_0/\hbar}\,/\hbar\omega_0, \qquad \tilde{\Omega} = \Omega/\omega_0, \tag{A1}$$
$$\tilde{\gamma} = \gamma/\omega_0, \qquad \tilde{T} = \frac{k_B}{\hbar\omega_0} T, \qquad \tilde{\omega}_c = \omega_c/\omega_0.$$

We omit all the tildes for the sake of better readability.

APPENDIX B

The Bath Correlation Function

In this Appendix we give the explicit expressions for the twice integrated bath correlation function $Q(t) = S(t) + i\,R(t)$ of Eq. (11) with an Ohmic spectral density of Eq. (5); see also [3]. The real part $S(t)$ can be evaluated analytically by solving the integral in terms of the ψ-function. One arrives after some algebra at the exact expression

$$S(t) = \frac{\eta}{\pi}\left\{-\ln\left|\frac{\Gamma(1+1/\hbar\beta\omega_c + it/\hbar\beta)}{\Gamma(1+1/\hbar\beta\omega_c)}\right|^2 + \frac{1}{2}\ln\bigl(1+\omega_c^2 t^2\bigr)\right\}. \tag{B1}$$

For finite temperatures $k_{\mathrm{B}}T \ll \hbar\omega_c$(*scaling limit*), we obtain with $\Gamma(1+iy)\Gamma(1-iy) = \pi y/\sinh(\pi y)$ the expression

$$S_{\mathrm{s.l.}}(t) = \frac{\eta}{\pi}\left\{-\ln\left[\frac{\pi t}{\hbar\beta\sinh(\pi t/\hbar\beta)}\right] + \frac{1}{2}\ln\bigl(1+\omega_c^2 t^2\bigr)\right\}. \tag{B2}$$

At long times $\omega_c t \to \infty$ the function $S_{\mathrm{s.l.}}(t)$ behaves like

$$S_{\mathrm{s.l}}(t) \xrightarrow{\omega_c t\to\infty} \frac{\eta}{\pi}\ln\left(\frac{\hbar\beta\omega_c}{\pi}\sinh\frac{\pi t}{\hbar\beta}\right) \tag{B3}$$
$$\approx \frac{\eta}{\pi}\left\{\frac{\pi t}{\hbar\beta} + \ln\left(\frac{\hbar\beta\omega_c}{2\pi}\right)\right\}, \qquad k_{\mathrm{B}}T \ll \hbar\omega_c. \tag{B4}$$

This illustrates that the correlations between the paths are damped out exponentially at long times for a low temperature Ohmic bath. The temperature-independent imaginary part $R(t)$ in Eq. (11) can be determined exactly. We obtain after the integration over ω

$$R(t) = \frac{\eta}{\pi}\arctan(\omega_c t). \tag{B5}$$

For long times $\omega_c t \to \infty$, the arctan-function approaches the Heaviside function, i.e.,

$$R(t) \xrightarrow{\omega_c t \to \infty} \frac{\eta}{2}\Theta(t), \tag{B6}$$

so that the imaginary part $R(t)$ becomes a constant function for all times t.

APPENDIX C

Numerical Iteration Scheme for Solving the Generalized Master Equation

The generalized master equation (58) is a *set of M coupled integro-differential equations with inhomogeneities.* For the one-dimensional case $M = 1$, the GME would be of Volterra type. For this case, several standard techniques for a numerical treatment are known [62, 67] and common numerical libraries [62] supply codes. The general M-dimensional case is far from being standard and we are not aware of available algorithms in the literature. The non-locality in time detains us from diagonalizing the kernel rate matrix and thereby decoupling the equations. We develop in this Appendix a rather simple numerical algorithm for solving the general set of M coupled inhomogeneous integro-differential equations.

We start by formally integrating the GME (58) once and choose the integration constants such that the initial conditions are fulfilled. After interchanging the order of integration, we obtain

$$\rho_{\mu\mu}(t) = \sum_{\nu=1}^{M} \int_{t_0}^{t} dt' \mathcal{K}_{\mu\nu}(t, t')\rho_{\nu\nu}(t') + \int_{t_0}^{t} dt' I_\mu(t', t_0) + \rho_{\mu\mu}(t_0), \tag{C1}$$

where we have defined the integrated kernels

$$\mathcal{K}_{\mu\nu}(t, t') \equiv \int_{t'}^{t} dt'' \mathcal{H}_{\mu\nu}(t'', t'). \tag{C2}$$

In the next step, we iterate the integrated GME from time t to time $t + \Delta t$ and split the integrals to obtain

$$\begin{aligned}
\rho_{\mu\mu}(t+\Delta t) &= \sum_{\nu=1}^{M} \int_{t_0}^{t+\Delta t} dt' \mathcal{K}_{\mu\nu}(t+\Delta t, t')\rho_{\nu\nu}(t') + \int_{t_0}^{t+\Delta t} dt' I_\mu(t', t_0) + \rho_{\mu\mu}(t_0) \\
&= \sum_{\nu=1}^{M} \int_{t_0}^{t} dt' \int_{t'}^{t} dt'' \mathcal{H}_{\mu\nu}(t'', t')\rho_{\nu\nu}(t') + \int_{t_0}^{t} dt' I_\mu(t', t_0) + \rho_{\mu\mu}(t_0) \\
&\quad + \sum_{\nu=1}^{M} \int_{t_0}^{t} dt' \int_{t}^{t+\Delta t} dt'' \mathcal{H}_{\mu\nu}(t'', t')\rho_{\nu\nu}(t') \\
&\quad + \int_{t}^{t+\Delta t} dt' I_\mu(t', t_0) + \sum_{\nu=1}^{M} \int_{t}^{t+\Delta t} dt' \mathcal{K}_{\mu\nu}(t+\Delta t, t')\rho_{\nu\nu}(t') \\
&= \rho_{\mu\mu}(t) + \sum_{\nu=1}^{M} \int_{t_0}^{t} dt' \rho_{\nu\nu}(t') \int_{t}^{t+\Delta t} dt'' \mathcal{H}_{\mu\nu}(t'', t') \\
&\quad + \int_{t}^{t+\Delta t} dt' I_\mu(t', t_0) + \sum_{\nu=1}^{M} \int_{t}^{t+\Delta t} dt' \mathcal{K}_{\mu\nu}(t+\Delta t, t')\rho_{\nu\nu}(t').
\end{aligned} \tag{C3}$$

So far, every manipulation was an exact transformation. To proceed, we have to invoke an approximation for the last term in Eq. (C3), i.e., that one involving $\mathcal{K}_{\mu\nu}(t+\Delta t, t')$. It is this term only which requires the knowledge of $\rho_{\nu\nu}(t')$ in the time interval $[t, t+\Delta t]$. All the other terms only need $\rho_{\nu\nu}(t')$ up to time t which are known. For that reason, we use in a third step the simplest approximation rule for the integral, i.e., the Simpson trapezoid rule, to obtain

$$\sum_{\nu=1}^{M} \int_{t}^{t+\Delta t} dt' \mathcal{K}_{\mu\nu}(t+\Delta t, t')\rho_{\nu\nu}(t') \approx \sum_{\nu=1}^{M} \frac{\Delta t}{2}\{\mathcal{K}_{\mu\nu}(t+\Delta t, t)\rho_{\nu\nu}(t) + \mathcal{K}_{\mu\nu}(t+\Delta t, t+\Delta t)\rho_{\nu\nu}(t+\Delta t)\}. \tag{C4}$$

The corrections are of the order of Δt^3. With Eq. (C2), it follows that $\mathcal{K}_{\mu\nu}(t+\Delta t, t+\Delta t) = 0$ and we arrive at the final iteration scheme

$$\rho_{\mu\mu}(t+\Delta t) = \sum_{\nu=1}^{M} \rho_{\nu\nu}(t)\left\{\delta_{\mu\nu} + \frac{\Delta t}{2}\mathcal{K}_{\mu\nu}(t+\Delta t, t)\right\} + \sum_{\nu=1}^{M} \int_{t}^{t+\Delta t} dt'' \int_{t_0}^{t} dt' \mathcal{H}_{\mu\nu}(t'', t')\rho_{\nu\nu}(t') + \int_{t}^{t+\Delta t} dt' I_{\mu}(t', t_0), \tag{C5}$$

where the $\delta_{\mu\nu}$ is the Kronecker symbol. We note that this iterative procedure requires the knowledge of $\rho_{\nu\nu}(t')$ in the time interval $t' \in [t_0, t]$ when propagating from time t to time $t+\Delta t$. Furthermore, we remark that this iterative algorithm is not restricted to the lowest order for the kernels $\mathcal{H}_{\mu\nu}(t, t')$ and the inhomogeneities $I_{\mu}(t, t_0)$. Finally, we observe that the integrations from t to $t+\Delta t$ for each step can be performed numerically to a very high precision such that the only relevant numerical error arises from the splitting in Eq. (C4). Practical calculations reveal that the time step Δt has to be chosen rather small since the problem is similar to a stiff differential equation. In praxi, this means a value of the order of $\Delta t = 10^{-2}$ or smaller. This rather small value for Δt restricts the applicability of this very simple and straightforward iteration scheme to problems where the decay is not too slow. More refined numerical algorithms are imaginable which could circumvent this problem.

Because we are interested in the long-time dynamics, iterations up to times $t = 5000$ can be necessary. Since the kernel matrix elements contain exponentials with asymptotically linearly growing exponents (see Eqs. (11) and (B4) in Appendix B), the memory ranging from time t backwards to time t_0 can be cut-off after some fixed time span τ_r. Then the memory is only relevant over the time interval $t - \tau_r$ and all exponentially small contributions from the time interval $[t_0, t-\tau_r]$ can be neglected. This accelerates the iteration considerably and avoids too large arrays for the storage of the intermediate values of $\rho_{\nu\nu}(t')$. However, lowering the temperature demands an increasing memory range τ_r.

Once the diagonal elements $\rho_{\mu\mu}(t)$ are known, the population of the left well $P_{\text{left}}(t)$ can be evaluated according to Eq. (24).

APPENDIX D

Example: A Single Path Subject to Dissipation

The purpose of this Appendix is to illustrate the general derivation of the cluster function, Eq. (45), within the gNICA scheme introduced in Section IV. This approximation scheme is the basis for the derivation of the generalized master equation presented in Section V. For simplicity, we pick one

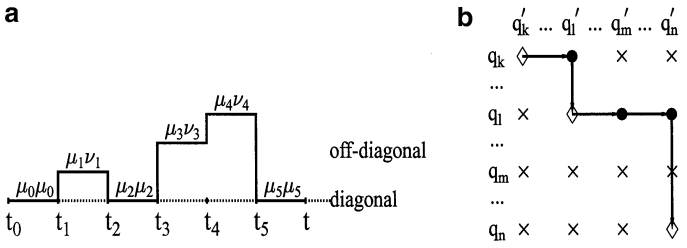

FIG. 22. Example of one path consisting of three sojourns and two clusters (see text). (a) Time-resolved representation of the path jumping between diagonal (dashed line) and off-diagonal states. (b) The same path illustrated in the (q, q')-plane of the reduced density matrix. The labels q_k, q'_k of the reduced density matrix are not specified further. Diamonds $\diamond$ mark the visited diagonal states and filled circles $\bullet$ mark the visited off-diagonal states.

single path subject to dissipation and starting in the diagonal state $(\mu_0, \mu_0) = (q_\kappa, q'_\kappa = q_\kappa)$ and ending after $N = 5$ jumps in the diagonal state $(\mu_5, \mu_5) = (q_n, q'_n = q_n)$. The full path is illustrated in Fig. 22a in a time-resolved picture and in Fig. 22b as a path jumping between the states of the reduced density matrix in the (q, q')-plane. The path is characterized by the sequence of index pairs

$$\begin{aligned}(\mu_0, \mu_0) &\to (\mu_1, \nu_1) \to (\mu_2, \mu_2) \to (\mu_3, \nu_3) \to (\mu_4, \nu_4) \to (\mu_5, \mu_5) \\ &\equiv (q_k, q_k) \to (q_k, q'_l) \to (q_l, q_l) \to (q_l, q'_m) \to (q_l, q'_n) \to (q_n, q_n). \end{aligned} \tag{D1}$$

It contains three sojourns (from t_0 to t_1, from t_2 to t_3 and from t_5 to t), cf. Fig. 22a. Moreover, the path contains two clusters (from t_1 to t_2 and from t_3 to t_5). The details of the visited states are illustrated in Fig. 22b: The diagonal states are marked by diamonds $\diamond$ and the visited off-diagonal states by filled circles $\bullet$. For our purpose here, it is only important to distinguish between diagonal and off-diagonal states. The specific indices of the states are irrelevant.

We evaluate now the contribution $\mathcal{I}(t)$ of this specific path to the full path sum in Eq. (33). The product of the factors Δ_j in Eq. (33) yields a proportionality factor which we omit for the moment for simplicity. For further convenience, we consider the time-*in*dependent system, implying that the diagonal elements E_{μ_j}, see Eq. (30), in the Hamiltonian $\mathbf{H}_{\mathrm{S}}^{\mathrm{DVR}}$ are constant in time. The generalization to time-dependent systems is discussed in Section V.A. Therefore, we introduce the short-hand notation in Eq. (33) according to

$$\begin{aligned}\Delta E_j &= E_{\mu_j} - E_{\nu_j}, \\ \mathcal{F}_{lj}(t_l - t_j) &= \exp\{\xi_l S(t_l - t_j)\xi_j + i\xi_l R(t_l - t_j)\chi_j\}. \end{aligned} \tag{D2}$$

The contribution of the specific path to the path sum follows from Eq. (33) as

$$\begin{aligned}\mathcal{I}(t) = \int_{t_0}^{t} dt_5 \int_{t_0}^{t_5} dt_4 \int_{t_0}^{t_4} dt_3 \int_{t_0}^{t_3} dt_2 \int_{t_0}^{t_2} dt_1 \exp\{i[\Delta E_1(t_2 - t_1) + \Delta E_3(t_4 - t_3) \\ + \Delta E_4(t_5 - t_4)]\} \mathcal{F}_{1,0}(t_1 - t_0)\mathcal{F}_{2,0}(t_2 - t_0)\mathcal{F}_{2,1}(t_2 - t_1)\mathcal{F}_{3,0}(t_3 - t_0) \\ \times \mathcal{F}_{3,1}(t_3 - t_1)\mathcal{F}_{3,2}(t_3 - t_2)\mathcal{F}_{4,0}(t_4 - t_0)\mathcal{F}_{4,1}(t_4 - t_1)\mathcal{F}_{4,2}(t_4 - t_2) \\ \times \mathcal{F}_{4,3}(t_4 - t_3)\mathcal{F}_{5,0}(t_5 - t_0)\mathcal{F}_{5,1}(t_5 - t_1)\mathcal{F}_{5,2}(t_5 - t_2)\mathcal{F}_{5,3}(t_5 - t_3)\mathcal{F}_{5,4}(t_5 - t_4). \end{aligned} \tag{D3}$$

Equation (D3) is still exact. We apply then the generalized non-interacting cluster approximation gNICA in different steps.

(i) Neglect of the intercluster correlations. Let us consider the product

$$\mathcal{P}_1 \equiv \mathcal{F}_{3,1}(t_3-t_1)\mathcal{F}_{3,2}(t_3-t_2)\mathcal{F}_{4,1}(t_4-t_1)\mathcal{F}_{4,2}(t_4-t_2)\mathcal{F}_{5,1}(t_5-t_1)\mathcal{F}_{5,2}(t_5-t_2). \tag{D4}$$

If we assume a very large cut-off frequency, i.e., $\omega_c \to \infty$, we can approximate the real part $S(t_i-t_j)$ of the bath correlation function by its linearized form, Eq. (B4), and the imaginary part $R(t_i-t_j)$ by the constant value $\eta/2$; see Eq. (B6). Then, $\mathcal{P}_1$ can easily be brought into the form

$$\begin{aligned}\mathcal{P}_1 \approx \exp\Bigg\{&[\xi_3+\xi_4+\xi_5]\left[\frac{\eta}{\hbar\beta}(t_3-t_1)\xi_1+\frac{\eta}{\hbar\beta}(t_3-t_2)\xi_2+\frac{\eta}{\pi}\ln\left(\frac{\hbar\beta\omega_c}{2\pi}\right)(\xi_1+\xi_2)\right]\\ &+\left[\xi_4\frac{\eta}{\hbar\beta}(t_4-t_3)+\xi_5\frac{\eta}{\hbar\beta}(t_5-t_3)\right][\xi_1+\xi_2]\Bigg\}=1.\end{aligned} \tag{D5}$$

In the last step, we have used the neutrality of each cluster, i.e., $\xi_1+\xi_2=0$ and $\xi_3+\xi_4+\xi_5=0$. The overall result is that we can set in the influence functional the product with all the couplings between different clusters equal to 1; i.e., we disregard intercluster correlations.

(ii) Neglect of cluster-sojourn correlations. Consider the product

$$\begin{aligned}\mathcal{P}_2 &\equiv \mathcal{F}_{3,0}(t_3-t_0)\mathcal{F}_{4,0}(t_4-t_0)\mathcal{F}_{5,0}(t_5-t_0)\\ &= \exp\{\xi_3 S(t_3-t_0)\xi_0+\xi_4 S(t_4-t_0)\xi_0+\xi_5 S(t_5-t_0)\xi_0\\ &\quad + i[\xi_3 R(t_3-t_0)\chi_0+\xi_4 R(t_4-t_0)\chi_0+\xi_5 R(t_5-t_0)\chi_0]\}\end{aligned} \tag{D6}$$

describing the interaction of the clusters with the initial state characterized by (χ_0,ξ_0). Since we start in a diagonal state, it follows that $\xi_0=0$. Moreover, we apply the same argumentation like in (i) for the imaginary part $R(t)$ and obtain

$$\mathcal{P}_2 \approx \exp\left\{i[\xi_3+\xi_4+\xi_5]\frac{\eta}{2}\chi_0\right\}=1. \tag{D7}$$

The corresponding argumentation holds for the third product $\mathcal{F}_{2,0}(t_2-t_0)\mathcal{F}_{1,0}(t_1-t_0)$.

Steps (i) and (ii) contain all the correlations disregarded within gNICA. In contrast, we entirely keep the *intra*cluster interaction $\mathcal{F}_{5,4}(t_5-t_4)$ as well as the interactions of the particular clusters with the directly preceding sojourn, i.e., $\mathcal{F}_{4,3}(t_4-t_3)$, $\mathcal{F}_{5,3}(t_5-t_3)$, and $\mathcal{F}_{2,1}(t_2-t_1)$. After reordering the integrals we obtain

$$\begin{aligned}\mathcal{I}^{\mathrm{gNICA}}(t) = \int_{t_0}^{t}dt_5\int_{t_0}^{t_5}dt_4\int_{t_0}^{t_4}dt_3\exp\{i[\Delta E_3(t_4-t_3)+\Delta E_4(t_5-t_4)]\}\,\mathcal{F}_{4,3}(t_4-t_3)\mathcal{F}_{5,3}(t_5-t_3)\\ \times\mathcal{F}_{5,4}(t_5-t_4)\int_{t_0}^{t_3}dt_2\int_{t_0}^{t_2}dt_1\exp[i\Delta E_1(t_2-t_1)]\mathcal{F}_{2,1}(t_2-t_1).\end{aligned} \tag{D8}$$

This expression can be treated more conveniently after a Laplace transformation to $\mathcal{I}(\lambda)=\mathcal{L}_t\{\mathcal{I}(t)\}=\int_0^\infty dt\exp(-\lambda t)\mathcal{I}(t)$. Using the property $\mathcal{L}_t\{\int_0^t dt_5 f(t_5-t_0)\}=\frac{1}{\lambda}\mathcal{L}_{\tilde{t}}\{f(\tilde{t})\}$ the integration over t_5 yields the factor $1/\lambda$. The remaining function $f(\tilde{t})$ to be Laplace transformed can be recast into the convolutive form $f(\tilde{t})=\int_{t_0}^{\tilde{t}}dt_3 g(\tilde{t}-t_3)h(t_3)$ with $g(\tilde{t}-t_3)=\int_{t_3}^{\tilde{t}}dt_4\exp\{i[\Delta E_3(t_4-t_3)+\Delta E_4(\tilde{t}-t_4)]\}\mathcal{F}_{4,3}(t_4-t_3)\mathcal{F}_{5,3}(\tilde{t}-t_3)\mathcal{F}_{5,4}(\tilde{t}-t_4)$ and with $h(t_3)=\int_{t_0}^{t_3}dt_2\int_{t_0}^{t_2}dt_1\exp[i\Delta E_1(t_2-t_1)]\mathcal{F}_{2,1}(t_2-t_1)$. By application of the convolution theorem $\mathcal{L}_{\tilde{t}}\{\int_{t_0}^{\tilde{t}}dt_3 g(\tilde{t}-t_3)h(t_3)\}=\mathcal{L}_{\tilde{t}}\{g(\tilde{t})\}\mathcal{L}_{\tilde{t}}\{h(\tilde{t})\}$ and by

performing the integration over t_2, we obtain the product

$$\begin{aligned}\mathcal{I}^{\mathrm{gNICA}}(\lambda) &= \mathcal{L}_t\{\mathcal{I}^{\mathrm{gNICA}}(t)\} \\ &= \frac{1}{\lambda}\mathcal{L}_{\tilde{t}}\Big\{\int_{t_0}^{\tilde{t}} dt_4 \int_{t_0}^{t_4} dt_3 \exp\{i[\Delta E_3(t_4-t_3)+\Delta E_4(\tilde{t}-t_4)]\}\mathcal{F}_{4,3}(t_4-t_3)\mathcal{F}_{5,3}(\tilde{t}-t_3) \\ &\quad \times \mathcal{F}_{5,4}(\tilde{t}-t_4)\Big\}\frac{1}{\lambda}\mathcal{L}_{\tilde{t}}\Big\{\int_{t_0}^{\tilde{t}} dt_1 \exp[i\Delta E_1(\tilde{t}-t_1)]\mathcal{F}_{2,1}(\tilde{t}-t_1)\Big\}. \qquad \text{(D9)}\end{aligned}$$

The Laplace transforms are the contributions of the full intracluster interactions of the two clusters. Performing the Laplace transforms and transforming to the time differences $\tau_j = t_{j+1} - t_j$, we finally arrive at the expression

$$\begin{aligned}\mathcal{I}^{\mathrm{gNICA}}(\lambda) &= \frac{1}{\lambda}\int_0^\infty d\tau_4 \int_0^\infty d\tau_3 \exp\{-\lambda(\tau_3+\tau_4)\}\exp\{i(\Delta E_3\tau_3+\Delta E_4\tau_4)\} \\ &\quad \times \mathcal{F}_{4,3}(\tau_3)\mathcal{F}_{5,3}(\tau_3+\tau_4)\mathcal{F}_{5,4}(\tau_4)\frac{1}{\lambda}\int_0^\infty d\tau_1 \exp\{-\lambda\tau_1\}\exp\{i\Delta E_1\tau_1\}\mathcal{F}_{2,1}(\tau_1)\frac{1}{\lambda}, \qquad \text{(D10)}\end{aligned}$$

where the last factor $1/\lambda$ appears after the integration over the first sojourn $t_1 - t_0$. Equation (D10) is an example of a contribution of one specific path to the total path sum in Eq. (45).

APPENDIX E

Harmonic Well Approximation

In this Appendix we give explicit results for an approximation for the energy eigenstates in the wells of the double-well potential (2) without external forces, i.e., $\varepsilon = 0$ and $s = 0$. The scaling of this Hamiltonian is performed according to the standard procedure described in the previous Appendix A; see Eq. (A1). In the literature [50], often the assumption is made that the energy eigenvalues and the localized states in the two wells can be approximated by those of a harmonic oscillator potential whose minimum coincides with the single well minimum. The localized states of the double-well potential are linear combinations of the symmetric and the antisymmetric energy eigenstate corresponding to one doublet. They have been introduced in Section III.D, Eq. (34) for the case of the double-doublet system and a generalization to more than two doublets is straightforward.

The eigenenergies and the energy eigenstates of a spatially shifted harmonic potential are given in dimensionless units by

$$\mathcal{E}_n = n + 1/2, \qquad n = 0, 1, \ldots, \qquad \text{(E1)}$$

and

$$\psi_n(q) = \langle n \mid q\rangle = (2^n n!\sqrt{\pi})^{-1/2}\exp\left\{-\frac{1}{2}(q-q_0)^2\right\} H_n(q-q_0), \qquad n = 0, 1, \ldots, \qquad \text{(E2)}$$

where $q_0 = \pm\sqrt{8E_{\mathrm{B}}}$ is the position of the minima of the double-well potential with barrier height E_{B} and $H_n(q)$ are the Hermite polynomials.

Figure 23 shows the results of this approximation for two cases of a barrier height E_{B} in the deep quantum regime, i.e., $E_{\mathrm{B}} = 1.4$ (Fig. 23a) with two doublets below the barrier and $E_{\mathrm{B}} = 2.5$ (Fig. 23b) with three doublets below the barrier. For comparison the exact (numerically obtained)

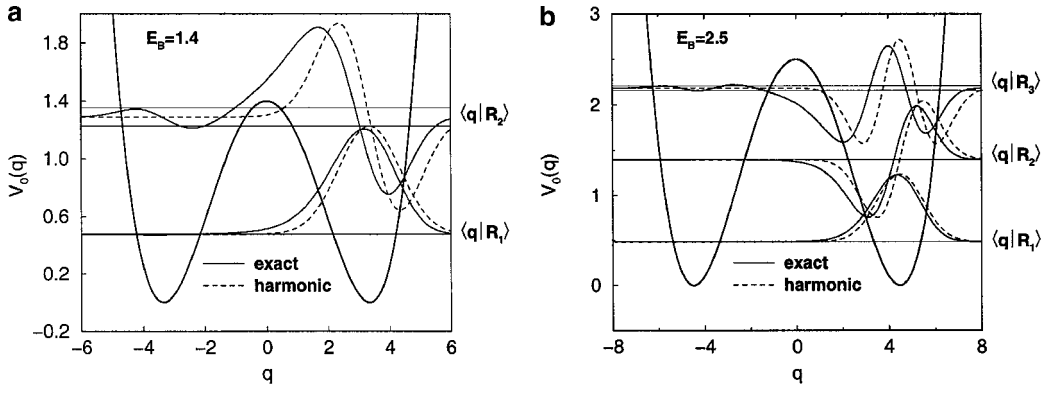

FIG. 23. (a) Exact localized states $\langle q \mid R_1\rangle$ and $\langle q \mid R_2\rangle$ (full lines) of the unperturbed system Hamiltonian (2) in position representation for a barrier height of $E_B = 1.4$. The dashed lines depict the results of the harmonic well approximation. The horizontal lines mark the exact eigenenergies of the double-well potential occurring always in pairs (doublets, the intradoublet spacing between the lower lying states is not visible on this scale). Note that the harmonic states are energetically shifted to the position of the exact localized states for graphical reasons. (b) Same for a barrier height $E_B = 2.5$.

wave functions are depicted. In both cases, the agreement is not convincing, as expected. Increasing the barrier height improves the agreement for the lower lying states. The states lying closed to the barrier top show a noticeable disagreement. Especially the part of the wave function which penetrates the barrier and which is in turn associated with tunneling is underestimated.

We note that for graphical reasons, the harmonic states are positioned at the *exact* eigenenergies of the double-well potential. However, in the approximation the harmonic eigenenergies are also shifted compared to the exact one (cf. scaling on the ordinate). To be specific, the interdoublet energy gap in the case of $E_B = 1.4$ is $\bar{\omega}_0 = 0.815$ in contrast to $\bar{\omega}_0 = \omega_0 = 1$ for the corresponding harmonic potential. For the case of $E_B = 2.5$ the lower interdoublet splitting is $\bar{\omega}_{0,1} = 0.892$ and the upper interdoublet splitting is $\bar{\omega}_{0,2} = 0.805$. These values have also to be compared with $\bar{\omega}_0 = \omega_0 = 1$ for the corresponding harmonic potential.

The deviations up to 20% are certainly not astonishing since the condition for the applicability of the harmonic well approximation is a rather high barrier, i.e., $E_B \gg 1$. This is also the relevant condition where semiclassical methods are applicable to calculate quantum relaxation rates [2]. They are rather simple compared to existing approaches [50]. For barrier heights of the order of the interdoublet spacing, this approximative treatment of the eigenenergies and the wave functions is not applicable.

APPENDIX F

Flow to Weak Damping

In this Appendix we describe the main steps of a proposal of how to deal with the effect of the flow to weak damping. A detailed investigation is still in progress. This part is to be viewed as a starting point for future work (see Section VIII) and should only point out that this behavior can also be treated *within* the formalism of real-time path integrals.

To deal with this effective weak-coupling situation, the twice integrated bath autocorrelation function $S(t)+i\,R(t)$ in the asymptotic limit of the scaling limit, i.e., Eqs. (B4) and (B6) of Appendix B, may be used. The deviations from the exact form of the autocorrelation function are small for high temperatures and/or weak damping. We use these approximative expressions in the kernels in Eq. (59)

for the generalized master equation and obtain for the discrete influence phase (see also Eq. (23))

$$\begin{aligned}\phi_{\mathrm{FV}}[\chi,\xi] &= -\sum_{l=1}^{N}\sum_{j=0}^{l-1}\xi_l S(t_l-t_j)\xi_j - i\sum_{l=1}^{N}\sum_{j=0}^{l-1}\xi_l R(t_l-t_j)\chi_j \\ &= -\frac{\eta}{\hbar\beta}\sum_{l=1}^{N}\sum_{j=0}^{l-1}\xi_l(t_l-t_j)\xi_j - \frac{\eta}{\pi}\ln\!\left(\frac{\hbar\beta\omega_c}{2\pi}\right)\sum_{l=1}^{N}\sum_{j=0}^{l-1}\xi_l\xi_j - i\frac{\eta}{2}\sum_{l=1}^{N}\sum_{j=0}^{l-1}\xi_l\chi_j. \quad \text{(F1)}\end{aligned}$$

We define

$$p_j \equiv \sum_{l=1}^{j}\xi_l, \quad \text{(F2)}$$

and note that each cluster has a cumulative path weight of zero, see Eq. (43), i.e., $p_N = 0$. This allows for an elementary rearrangement of the double sums in order to obtain with $\tau_j = t_j - t_{j-1}$ the expressions

$$\sum_{l=1}^{N}\sum_{j=0}^{l-1}\xi_l(t_l-t_j)\xi_j = \sum_{j=1}^{N}\tau_j p_j^2, \quad \sum_{l=1}^{N}\sum_{j=0}^{l-1}\xi_l\xi_j = -\frac{1}{2}\sum_{j=1}^{N}\xi_j^2, \quad \sum_{l=1}^{N}\sum_{j=0}^{l-1}\xi_l\chi_j = -\sum_{j=1}^{N-1}\chi_j p_j. \quad \text{(F3)}$$

Inserting these equations into the kernels, Eq. (59), it follows that

$$\begin{aligned}\mathcal{H}_{\mu\nu}(t,t') = \sum_{N=2}^{\infty}\sum_{\substack{\{\mu_j\nu_j\}\\ \mu_j\neq\nu_j}}\prod_{j=1}^{N}(-1)^{\delta_j}\left(\frac{i}{2}\right)^N\Delta_{j-1}\left(\frac{2\pi}{\hbar\beta\omega_c}\right)^{\xi_j^2\eta/2\pi\hbar} \\ \times\exp\!\left(-i\frac{\eta}{2\hbar}(-1)^{\delta_j}\xi_j p_j\right)\int_{t'}^{t}dt_N\int_{t'}^{t_N}dt_{N-1}\cdots\int_{t'}^{t_2}dt_1 \\ \times\exp\!\left\{i\sum_{j=0}^{N-1}\left\{\int_{t_j}^{t_{j+1}}dt''\big[E_{\mu_j}(t'')-E_{\nu_j}(t'')\big]-\frac{\eta}{\hbar\beta}p_{j+1}^2\tau_{j+1}\right\}\right\}, \quad \text{(F4)}\end{aligned}$$

where $\delta_j = 0\,(1)$ for a vertical (horizontal) jump.

In order to evaluate the series of integrals in Eq. (F4), we use the following technique: The upper limit t of the first integral is replaced by ∞ and for compensation the step function $\Theta(t-t_N)$ is added to the integrand. Then, the order of integration is interchanged and the integrals are transformed to difference coordinates $\tau_j = t_j - t_{j-1}$. Like in the previous sections, it is assumed that the driving frequency Ω is large and averaging over the driving period is appropriate. In a final step, the Θ-function in the integrand is represented as a complex integral according to

$$\Theta(t-t_N) = \frac{1}{2\pi i}\int_{-i\infty-\varepsilon}^{+i\infty-\varepsilon}d\lambda\frac{1}{\lambda}\exp\!\left[\lambda\left(t-\sum_{j=0}^{N-1}\tau_{j+1}-t'\right)\right]. \quad \text{(F5)}$$

The complex integration over λ can afterwards be carried out with the help of the calculus of residues for the residue at $\lambda = 0$. After this tedious but straightforward procedure, one arrives at the final result

for the averaged Markovian approximated rate matrix elements

$$\Gamma_{\mu\nu}^{\mathrm{av}} = \sum_{N=2}^{\infty} \sum_{\substack{\{\mu_j \nu_j\} \\ \mu_j \neq \nu_j}} \prod_{j=1}^{N} (-1)^{\delta_j} \left(\frac{i}{2}\right)^N \Delta_{j-1} \left(\frac{2\pi}{\hbar\beta\omega_c}\right)^{\xi_j^2 \eta / 2\pi\hbar} \exp\left(-i\frac{\eta}{2\hbar}(-1)^{\delta_j}\xi_j p_j\right)$$
$$\times \int_0^{\infty} d\tau J_0\left(p_j \frac{2s}{\Omega} \sin\left(\frac{\Omega\tau}{2}\right)\right) \exp\left\{-\left(i\left[F_{\mu_j} - F_{\nu_j}\right] - \frac{\eta}{\hbar\beta} p_j^2\right)\tau\right\}, \qquad \text{(F6)}$$

where $J_0(x)$ is the zeroth Bessel function.

It is not possible to treat this complicated expression analytically. If one has to determine explicit results, the help of the computer is needed to evaluate the sum over all configurations $\{\mu_j \nu_j\}$. Then, in a first step, all paths belonging to a fixed order N are created numerically by means of recursive programming. In the next step the sum over all the occurring paths has to be evaluated before one has to go to the next order by increasing N. Finally, convergence with respect to N has to be obtained.

We summarize this Appendix by concluding that also the effect of the flow to weak damping can be treated by real-time path integrals although the expressions become much more involved. Equation (F6) constitutes the starting point for the study of the cross-over to the classical regime. One has to be aware, however, that the driven problem is far from being trivial since even a chaotic dynamics may occur.

ACKNOWLEDGMENTS

We thank Professor M. Morillo and Dr. I. Goychuk for most helpful discussions. This work has been supported by the Deutsche Forschungsgemeinschaft Grant HA 1517/19-1 (P.H., M.T.), in part by the Sonderforschungsbereich 486 of the Deutsche Forschungsgemeinschaft (P.H), and by the DFG-Graduiertenkolleg 283.

REFERENCES

1. A. O. Caldeira and A. J. Leggett, *Phys. Rev. Lett.* **46** (1981), 211; A. J. Leggett, S. Chakravarty, A. T. Dorsey, M. Fisher, A. Garg, and W. Zwerger, *Rev. Mod. Phys.* **59** (1987), 1; **67** (1995), 725 (E).
2. P. Hänggi, P. Talkner, and M. Borkovec, *Rev. Mod. Phys.* **62** (1990), 251.
3. U. Weiss, "Quantum Dissipative Systems," World Scientific, Singapore, 1993; 2nd ed., 1999.
4. Th. Dittrich, P. Hänggi, G.-L. Ingold, B. Kramer, G. Schön, and W. Zwerger, "Quantum Transport and Dissipation," Wiley-VCH, Weinheim, 1998.
5. M. Grifoni and P. Hänggi, *Phys. Rep.* **304** (1998), 230.
6. F. Grossmann, T. Dittrich, P. Jung, and P. Hänggi, *Phys. Rev. Lett.* **67** (1991), 516.
7. Th. Dittrich, B. Oelschlägel, and P. Hänggi, *Europhys. Lett.* **22** (1993), 5.
8. R. Löfstedt and S. N. Coppersmith, *Phys. Rev. Lett.* **72** (1994), 1947; *Phys. Rev. E* **49** (1994), 4821.
9. D. E. Makarov and N. Makri, *Phys. Rev. B* **52** (1995), R2257; *Phys. Rev. E* **52** (1995), 5863.
10. M. Grifoni and P. Hänggi, *Phys. Rev. Lett.* **76** (1996), 1611; M. Grifoni, L. Hartmann, S. Berchtold, and P. Hänggi, *Phys. Rev. E* **53** (1996), 5890; M. Grifoni and P. Hänggi, *Phys. Rev. E* **54** (1996), 1390.
11. M. Thorwart and P. Jung, *Phys. Rev. Lett.* **78** (1997), 2503.
12. T. P. Pareek, M. C. Mahato, and A. M. Jayannavar, *Phys. Rev. B* **55** (1997), 9318.
13. M. Thorwart, P. Reimann, P. Jung, and R. F. Fox, *Chem. Phys.* **235** (1998), 61.
14. L. Gammaitoni, P. Hänggi, P. Jung, and F. Marchesoni, *Rev. Mod. Phys.* **70** (1998), 223.
15. I. Goychuk and P. Hänggi, *Phys. Rev. E* **59** (1999), 5137; I. Goychuk and P. Hänggi, *New J. Phys.* **1** (1999), 14.1.
16. Th. Wellens and A. Buchleitner, *Phys. Rev. Lett.* **84** (2000), 5118.
17. M. Thorwart, P. Reimann, P. Jung, and R. F. Fox, *Phys. Lett. A* **239** (1998), 233.
18. "Dynamics of Driven Quantum Systems," Special issue of Chemical Physics (W. Domcke, P. Hänggi, and D. Tannor, Eds.), *Chem. Phys.* **217** (2,3) (1997), 117.
19. L. Viola, E. Knill, and S. Lloyd, *Phys. Rev. Lett.* **82** (1999), 2417.

20. M. Thorwart, L. Hartmann, I. Goychuk, and P. Hänggi, *J. Mod. Opt.* **47** (2000), 2905.
21. N. Makri, *in* "Time-Dependent Quantum Molecular Dynamics," Proceedings of a NATO Advanced Research Workshop, Snowbird, UT, 1992 (J. Broeckhove and L. Lathouwers, Eds.), NATO ASI Ser. B Phys., Vol. 299, Plenum, New York, 1992; D. E. Makarov and N. Makri, *Chem. Phys. Lett.* **221** (1994), 482; N. Makri, *J. Math. Phys.* **36** (1995), 2430; N. Makri and D. E. Makarov, *J. Chem. Phys.* **102** (1995), 4600; **102** (1995), 4611.
22. M. Thorwart, M. Grifoni, and P. Hänggi, *Phys. Rev. Lett.* **85** (2000), 860.
23. "Quantum Tunneling of Magnetization," Proceedings of the NATO Advanced Research Workshop, Grenoble, France, 1994 (L. Gunther and B. Barbara, Eds.), NATO ASI Ser. E Appl. Sci., Vol. 301, Kluwer Academic, Dordrecht, 1995.
24. J. L. van Hemmen and A. Sütő, *Europhys. Lett.* **1** (1986), 481; *Phys. B* **141** (1986), 37.
25. J. R. Friedman, M. P. Sarachik, J. Tejada, and R. Ziolo, *Phys. Rev. Lett.* **76** (1996), 3830; J. M. Hernández, X. X. Zhang, F. Luis, J. Bartolomé, J. Tejada, and R. Ziolo, *Europhys. Lett.* **35** (1996), 301; L. Thomas, F. Lionti, R. Ballou, D. Gatteschi, R. Sessoli, and B. Barbara, *Nature* **383** (1996), 145; E. M. Chudnovsky, *Science* **274** (1996), 938; J. M. Hernández, X. X. Zhang, F. Luis, J. Tejada, J. R. Friedman, M. P. Sarachik, and R. Ziolo, *Phys. Rev. B* **55** (1997), 5858; J. A. A. J. Perenboom, J. S. Brooks, S. Hill, T. Hathaway, and N. S. Dalal, *Phys. Rev. Lett.* **58** (1998), 330; G. Bellessa, N. Vernier, B. Barbara, and D. Gatteschi, *Phys. Rev. Lett.* **83** (1999), 416; W. Wernsdorfer, R. Sessoli, and D. Gatteschi, *Europhys. Lett.* **42** (1999), 254.
26. C. Sangregorio, T. Ohm, C. Paulsen, R. Sessoli, and D. Gatteschi, *Phys. Rev. Lett.* **78** (1997), 4645; J. Tejada, X. X. Zhang, E. del Barco, J. M. Hernández, and E. M. Chudnovsky, *Phys. Rev. Lett.* **79** (1997), 1754; W. Wernsdorfer and R. Sessoli, *Science* **284** (1999), 133; W. Wernsdorfer, T. Ohm, C. Sangregorio, R. Sessoli, D. Mailly, and C. Paulsen, *Phys. Rev. Lett.* **82** (1999), 3903; W. Wernsdorfer, I. Chiorescu, R. Sessoli, D. Gatteschi, and D. Mailly, *Phys. B* **284**–**288** (2000), 1231.
27. W. Wernsdorfer, R. Sessoli, A. Caneschi, D. Gatteschi, and A. Cornia, *Europhys. Lett.* **50**(4) (2000), 552.
28. J. Clarke, A. N. Cleland, M. H. Devoret, D. Estève, and J. M. Martinis, *Science* **239** (1988), 992.
29. S. Han, J. Lapointe, and J. E. Lukens, *Phys. Rev. Lett.* **66** (1991), 810.
30. R. Rouse, S. Han, J. E. Lukens, *Phys. Rev. Lett.* **75** (1995), 1614.
31. S. Han, R. Rouse, and J. E. Lukens, *Phys. Rev. Lett.* **76** (1996), 3404.
32. P. Silvestrini, V. G. Palmieri, B. Ruggiero, and M. Russo, *Phys. Rev. Lett.* **79** (1997), 3046.
33. S. Han, R. Rouse, and J. E. Lukens, *Phys. Rev. Lett.* **84** (2000), 1300.
34. J. R. Friedmann, V. Patel, W. Chen, S. K. Tolpygo, and J. E. Lukens, *Nature* **406** (2000) 43; G. Blatter, *Nature* **406** (2000), 25.
35. J. E. Mooij, T. P. Orlando, L. Levitov, L. Tian, C. H. van der Wal, and S. Lloyd, *Science* **285** (1999), 1036.
36. C. H. van der Wal, A. C. ter Haar, F. K. Wilhelm, R. N. Schouten, C. J. P. M. Harmans, T. P. Orlando, S. Lloyd, and J. E. Mooij, *Science* **290** (2000), 773.
37. A. Würger, "From Coherent Tunneling to Relaxation: Dissipative Quantum Dynamics of Interacting Defects," Springer-Verlag, Berlin, 1997; P. Esquinazi (Ed.), "Tunneling Systems in Amorphous and Crystalline Solids," Springer-Verlag, Berlin, 1998.
38. B. Golding, N. M. Zimmerman, and S. N. Coppersmith, *Phys. Rev. Lett.* **68** (1992), 998.
39. K. Chun and N. O. Birge, *Phys. Rev. B* **48** (1993), R11500.
40. R. I. Cukier, M. Morillo, K. Chun, and N. O. Birge, *Phys. Rev. B* **51** (1995), 13767.
41. J. C. Noya, C. P. Herrero, and R. Ramõrez,*Phys. Rev. Lett.* **79** (1997), 111.
42. C. Enss and S. Hunklinger, *Phys. Rev. Lett.* **79** (1997), 2831.
43. B. H. Meier, F. Graf, and R. R. Ernst, *J. Chem. Phys.* **76** (1982), 767; S. Nagaoka, T. Terao, F. Imashiro, A. Saika, and N. Hirota, *J. Chem. Phys.* **79** (1983), 4694; A. Stoeckli, A. Furrer, Ch. Schoenenberger, B. H. Meier, R. R. Ernst, and I. Anderson, *Phys. B* **136** (1986), 161; A. Stöckli, B. H. Meier, R. Kreis, R. Meyer, and R. R. Ernst, *J. Chem. Phys.* **93** (1990), 1502; A. J. Horsewill, P. J. McDonald, and D. Vijayaraghavan, *J. Chem. Phys.* **100** (1994), 1889; A. J. Horsewill and A. Ikram, *Phys. B* **226** (1996), 202.
44. N. Došlić, O. Kühn, J. Manz, and K. Sundermann, *J. Phys. Chem. A* **102** (1998), 9645.
45. H. Naundorf, K. Sundermann, and O. Kühn, *Chem. Phys.* **240** (1999), 163.
46. W. H. Louisell, "Quantum Statistical Properties of Radiation," Wiley, New York, 1973; F. Haake, *in* "Quantum Statistics in Optics and Solid-State Physics," Springer Tracts in Modern Physics (G. Höhler, Ed.), Vol. 66, Springer-Verlag, Berlin, 1973.
47. S. Kohler, Th. Dittrich, and P. Hänggi, *Phys. Rev. E* **55** (1997), 300.
48. P. E. Parris and R. Silbey, *J. Chem. Phys.* **83** (1985), 5619; D. R. Reichman and R. J. Silbey, *J. Phys. Chem.* **99** (1995), 2777.
49. M. Morillo and R. I. Cukier, *Phys. Rev. B* **54** (1996), 13962; M. Morillo, C. Denk, and R. I. Cukier, *Chem. Phys.* **212** (1996), 157; R. I. Cukier, C. Denk, and M. Morillo, *Chem. Phys.* **217** (1997), 179.
50. H. Dekker, *Phys. Rev. A* **44** (1991), 2314; *Phys. A* **175** (1991), 485; **176** (1991), 220; **178** (1991), 289; **179** (1991), 81; **210** (1994), 507 (E).
51. A. I. Larkin and Yu. N. Ovchinnikov, *Zh. Eksp. Teor. Fiz.* **91** (1986), 318; *Sov. Phys. JETP* **64** (1986), 185.
52. A. I. Larkin, Yu. N. Ovchinnikov, and A. Schmid, *Phys. B* **152** (1988), 266.

53. Yu. N. Ovchinnikov and A. Schmid, *Phys. Rev. B* **50** (1994), 6332.
54. P. Silvestrini, Yu. N. Ovchinnikov, and R. Cristiano, *Phys. Rev. B* **41** (1990), 7341.
55. P. Silvestrini, B. Ruggiero, and Yu. N. Ovchinnikov, *Phys. Rev. B* **53** (1996), 67.
56. P. Silvestrini, B. Ruggiero, and Yu. N. Ovchinnikov, *Phys. Rev. B* **54** (1996), 1246.
57. R. P. Feynman and F. L. Vernon, Jr., *Ann. Phys. (N.Y.)* **24** (1963), 118.
58. D. O. Harris, G. G. Engerholm, and W. D. Gwinn, *J. Chem. Phys.* **43** (1965), 1515.
59. M. Thorwart, P. Reimann, and P. Hänggi, *Phys. Rev. E* **62** (2000), 5808.
60. M. Winterstetter and U. Weiss, *Chem. Phys.* **217** (1997), 155.
61. R. Egger, C. H. Mak, and U. Weiss, *Phys. Rev. E* **50** (1994), R655.
62. "The NAG Fortran Library, Mark: 18A, Implementation IBM RISC System/6000 AIX, Precision: Double," NAG, Oxford, 1999; W. H. Press, S. A. Teukolsky, W. T. Vetterling, and B. P. Flannery, "Numerical Recipes in FORTRAN," 2nd ed., Cambridge Univ. Press, Cambridge, UK, 1992.
63. I. S. Gradshteyn and I. M. Ryzhik, "Tables of Integrals, Series and Products," Academic Press, London, 1965.
64. R. Kubo, M. Toda, and N. Hashitsume, "Statistical Physics II," Springer Series in Solid-State Sciences, Vol. 31, Springer-Verlag, Berlin, 1985.
65. W. Zwerger, *Phys. Rev. B* **35** (1987), 4737.
66. H. Grabert, G.-L. Ingold, and B. Paul, *Europhys. Lett.* **44** (1998), 360.
67. S. Kohler, R. Utermann, P. Hänggi, and Th. Dittrich, *Phys. Rev. E* **58** (1998), 7219; P. Hänggi, S. Kohler, and Th. Dittrich, *in* "Statistical and Dynamical Aspects of Mesoscopic Systems" (D. Reguera, G. Platero, L. L. Bonilla, and J. M. Rubõ, Eds.), Lecture Notes in Physics, Vol. 547, Springer-Verlag, Berlin, 2000.
68. H. Brunner and P. J. van der Houwen, "The Numerical Solution of Volterra Equations," CWI Monograph 3, North-Holland, Amsterdam, 1985; M. A. Goldberg (Ed.), "Solution Methods for Integral Equations," Plenum, New York, 1979.